Efficient Subspace based Techniques for Processing Single Channel Electroencephalogram Signals

A
Thesis Submitted
in Partial Fulfillment of the Requirements
for the Degree of
DOCTOR OF PHILOSOPHY
By

Ajay Kumar Maddirala
*Roll No:*11610217

Under the Supervision of
Dr. Shaik Rafi Ahamed

Department of Electronics and Electrical Engineering
Indian Institute of Technology Guwahati
North Guwahati, Assam, India 781039
March, 2017

Declaration

This is to certify that the thesis entitled "**Efficient Subspace based Techniques for Processing Single Channel Electroencephalogram Signals**", submitted by me to the *Indian Institute of Technology Guwahati*, for the award of the degree of Doctor of Philosophy, is a bonafide work carried out by me under the supervision of Dr. Shaik Rafi Ahamed. The content of this thesis, in full or in parts, have not been submitted to any other University or Institute for the award of any degree or diploma.

Signed: _____

Ajay Kumar Maddirala
Department of Electronics and Electrical Engineering,
Indian Institute of Technology Guwahati,
Guwahati-781039, Assam, India.

Date: _____

Dedicated
to My Parents and My Wife for their sacrifices .....

Certificate

This is to certify that the thesis entitled "**Efficient Subspace based Techniques for Processing Single Channel Electroencephalogram Signals**", submitted by Ajay Kumar Maddirala (11610217), a research scholar in the *Department of Electronics and Electrical Engineering*, *Indian Institute of Technology Guwahati*, for the award of the degree of Doctor of Philosophy, is a record of an original research work carried out by him under my supervision and guidance. The thesis has fulfilled all requirements as per the regulations of the institute and in my opinion has reached the standard needed for submission. The results embodied in this thesis have not been submitted to any other University or Institute for the award of any degree or diploma.

Signed: _____

Supervisor: Dr. Shaik Rafi Ahamed
Department of Electronics and Electrical Engineering,
Indian Institute of Technology Guwahati,
Guwahati-781039, Assam, India.

Date: _____

Acknowledgements

Sincere thanks and gratitude to my Lord and Savior *Jesus Christ* for his constant grace up on me since my childhood.

Words cannot be expressed how grateful I am to my mother and father for all of the sacrifices they have made on my behalf.

I thank the LORD for selecting the beautiful and humble wife for me. During this time she carry my family needs and take my kid Aman Kumar M. Bangarutally, without you it is not possible. I also thank my brother Syam Kumar Maddirala and his wife Roji for their love on my child during my absence.

I take this opportunity to thank the supervisor of my work, **Dr. Shaik Rafi Ahamed**, whose constant encouragement during the course of this research has helped me in several ways. I am deeply indebted to him for his insightful guidance at various stages of this distortion.

I am grateful to my doctoral scrutiny committee members **Prof. Samarendra Dandapat**, **Prof. S. R. Mahadeva Prasanna** and **Prof. Rohit Sinha** for their invaluable comments towards the betterment of this work.

I am grateful to all the faculty members, scientific officers and staff in the department of EEE. Special thank to our lab scientific officer Misses Josephine J for her help during my research period.

I am also grateful to all Lab mates Dr. Surya Prakash. M, Mr. Harikrishna V, Mr. Karam Singh M, Ms. Babita Jajodia, Mr. Mohammad Tasleem Khan, Mr. Indrajit and Ms. Jinti Hazarika for providing a motivating research environment within advanced digital signal processing (ADSP) lab, Indian Institute of Technology Guwahati.

I am also grateful to all my friends in IITG for their help during my Ph.D. Special thank to Dr. Kannan Thirugnanam, Dr. Anil Kumar Deepati, Mr. Ravi Chandra Rao, Bhaskar Naik, Mr. Bheemraj, Dr. Suresh Vasimalla, Mr. Shivarama Krishna N, Mr. Venkata Ramana Kasi, Mr. Ramesh Bhukya, Mr. Balaji Rao, Mr. Ujzwal, Mr. Rama Krishna M, Mr. Bhagat, for sharing my thoughts and funny discussions during this period.

Special thanks to my M-Tech supervisor Dr. Mohammad Zia Ur Rahman for his valuable motivation and suggestions in doing Ph.D.

I am very thankful to my cousin brother Mr. G. Shanti Kumar and his wife Anjali, who stays near to my institute, for their support during my Ph. D. I am very thankful to my uncles, aunties, brothers, sisters, sister-in-laws and brother-in-laws.

I am very thankful to my badminton team members, Dr. Bimlesh Kumar, Dr. Ajay Kalamdhad, Dr. Sisir Kumar Nayak, Dr. M.K. Bhuyan, Dr. Sachin D. Kore, Dr. Soumitra Nandi and Dr. Tapan Mishra for their invaluable suggestion to my carrier.

I am grateful to Prof. Roy Paily Palathinkal, Misses Josephine J, Dr. P. D. Pamu, Mr. T. T. Haokip and Paster. Thangkholal Haokip, and Church members for their valuable contribution in my spiritual growth.

Last but not least I thank you my big father Mr. Yesu Bhaktha Maddirala for his valuable contribution in my carrier. His contributions were unforgettable as he traveled with me where ever I am having the interviews to join into higher studies. Thank you very much PEDANANA..... for your contribution in life.

Sincerely
Ajay Kumar Maddirala

Abstract

In recent years, the use of portable/wearable EEG systems in health care applications has been increased due its low-power consumption, easy to operate and minimum instrumentation complexity, and reduces the cumbersome to the subject under test. In general, the EEG signals often measured in ambulatory situations, hence, they were contaminated by several artifacts. The presence of these artifacts will degrade the performance of EEG based detection systems. Since the portable EEG devices comprise single or few (at most four) EEG channels, traditional artifact removal techniques, such as blind source separation (BSS), cannot be applied to remove these artifacts. Hence, in this thesis, various subspace based artifact removal techniques for single channel EEG signals were proposed.

Singular spectrum analysis (SSA) is a subspace based technique used in this thesis to remove artifacts from single channel EEG signals. Using the frame work of SSA, first, we proposed new grouping criteria to identify the desired signal (EEG signal) subspace. In this criterion, the local mobility of the eigenvectors is considered and employed for removing the motion artifacts from single channel EEG signals. In addition, SSA is combined with ANC to remove the eye blink artifact in EEG epochs recorded for BCI application.

In general, the measured EEG signal is a mixer of statistically independent source signals. As SSA uses second order statistics (SOS) of the data, the extracted sources are not statistically uncorrelated. Independent component analysis (ICA) is widely used as BSS technique to extract the statistically independent source signals from the mixed EEG data. In order to use ICA in the source separation problem, the number of measured signals should more than or equal to the number of sources to be extracted. Due to this limitation, direct adaptation of ICA on single channel EEG signals is not possible. We investigated this problem and proposed a new scheme such that ICA can be used to process single channel EEG signals. Further, we have also further investigated the performance of the seizure detection algorithm by employing SSA based muscle artifact removal technique as preprocessing step. From the results it is noticed that the adaptation of SSA based muscle artifact removal technique reduces the false positive rate of the seizure detection algorithm.

Contents

List of Figures

List of Tables

1

Introduction

This thesis explored several artifact removal techniques for single channel electroencephalogram (EEG) signals using a subspace-based technique, also called singular spectrum analysis (SSA). First, the background theory of EEG signals and its artifact components were discussed to understand the results presented in the subsequent chapters. Next, we discussed the major issues in SSA and adaptive noise canceler (ANC) to process the single channel EEG signals. In addition to that the limitations of independent component analysis to single channel EEG signals is discussed in this chapter. Finally, the contribution of this thesis chapter-by-chapter is outlined.

1.1 Basics of Electroencephalogram (EEG) Signals

Physiological signals measured from the brain are highly complex signals, and they carry the information related to the brain state and the disorder. In general, these physiological signals were measured from the brain using a recorder called electroencephalogram (EEG). Basically, it measures the electrical potentials in the brain by keeping electrodes over the scalp. The electrical potentials so obtained are called EEG signals. In late 1800,

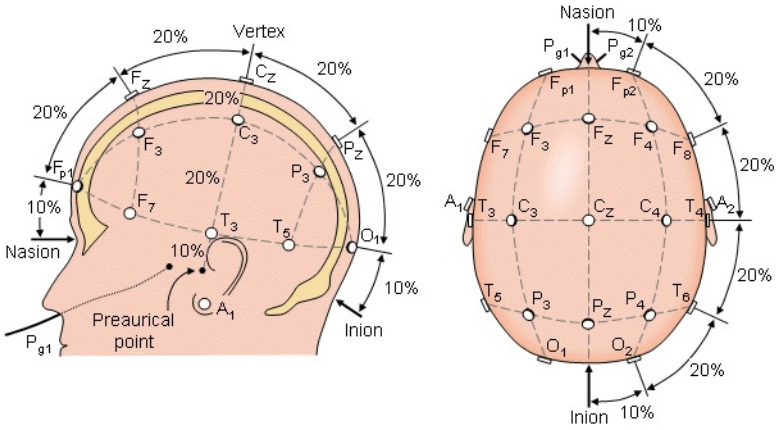

FIGURE 1.1: The international 10-20 system of electrodes placement looking from (a) left and (b) above the head. Notations: F_p-Frontal polar, F-frontal, C-central, T-temporal, P-parietal, O-occipital and A-ear lobe, [1].

Richard Caton recorded brain signals from rabbits. After that, in 1929, Hans Berger explored the electrical signals from human brain [7]. The placement of electrodes to record EEG signals from the scalp is shown in Fig. 1.1. However, in 1921, the electrodes names in the mid-temporal and the posterior temporal has been changed by American Clinical Neurophysiology Society (ACNS). The names of the electrodes in the mid-temporal T_3 and T_4 are replaced by T_7 and T_8 and the posterior temporal electrodes T_5 and T_6 are renamed by P_7 and P_8. There are three basic electrode montages often used to measure the EEG signals from the scalp: bipolar, unipolar and common average reference [2]. The electrode montage is a pattern of placing the electrodes over the scalp to record the EEG signals. To measure the electrical potential of the brain over the scalp, in bipolar electrode montage, each channel is connected between the two electrodes. In case of unipolar montage, each EEG channel is derived using an active electrode and an electrode common to all the channels. In case of common average reference montage, each EEG channel is derived using an active electrode and an average reference electrode, derived by connecting the all active electrodes through a resistor. Fig. 1.2 shows the commonly used three electrode montages to record EEG signals. Fig. 1.3 shows a typical 10 s multichannel EEG data recorded from pediatric subjects with intractable seizures and downloaded from *CHB-MIT Scalp EEG Database* and is contributed to physio bank [3]. More details of EEG data is discussed in [8].

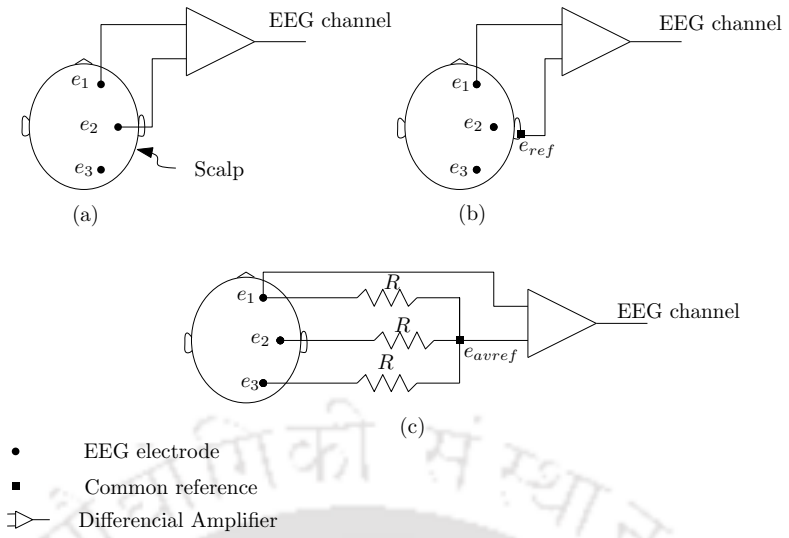

FIGURE 1.2: Commonly used electrode montages (a) bipolar, (b) unipolar and (c) average reference, respectively. Modified from [2]. Note e_x electrode x.

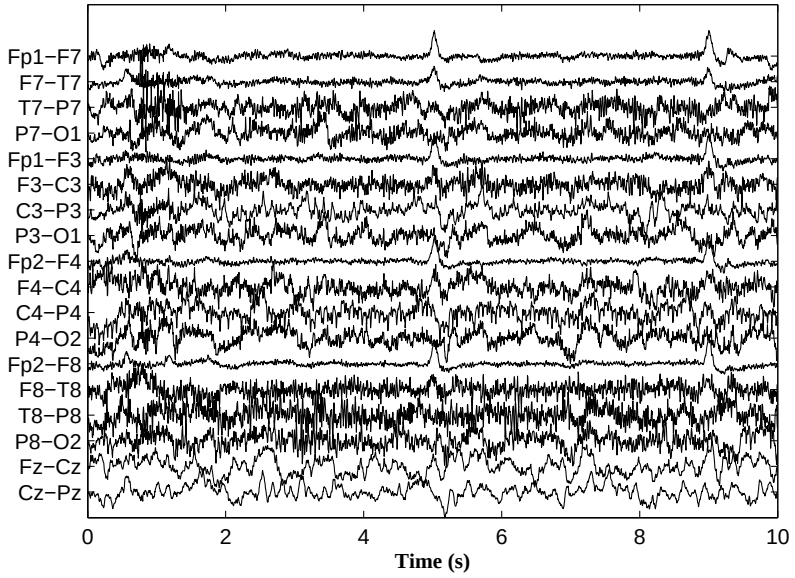

FIGURE 1.3: A typical 10 s multichannel EEG data [3].

1.1.1 Rhythmic Components of EEG Signals

The EEG signal is a complex nature and constitute several rhythmic patterns, shown in Fig. 1.4. The commonly present rhythmic components in the EEG signals are:

- **Gamma rhythms** (γ) : They are fastest brain waves and they were become popular after the cellular level experiments [9, 10]. The bandwidth of *gamma* rhythm is $32 - 100\,Hz$.

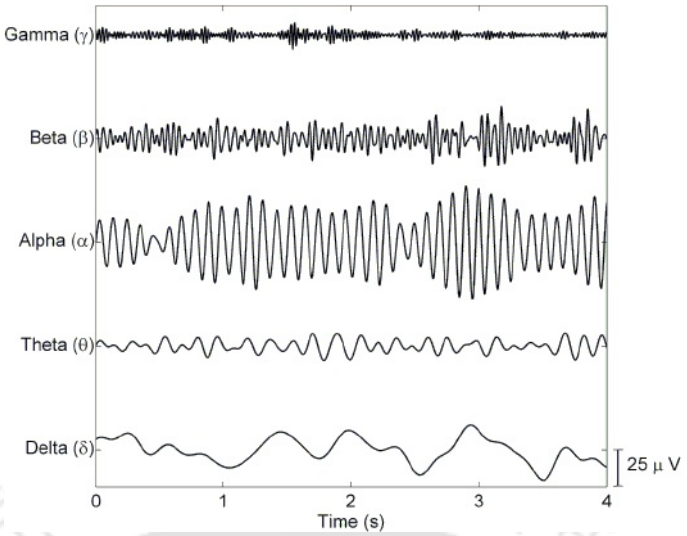

FIGURE 1.4: EEG components extracted from typical EEG signal recorded during rest state with eyes closed [4].

- **Beta rhythms** (β): They are characteristics of second fastest activity of the brain, will be generated when the person brain is engaged in decision making, judgement and in focused mental activity.These rhythms are more prominent in frontal and central regions. The bandwidth of β rhythms is $12 - 30\,Hz$.

- **Alpha rhythms** (α) : These rhythmic components results in adults during relaxation condition with closed eyes and they were attenuated when eyes were opened. Moreover, they are very prominent in occipital region and look like oscillating components in the frequency band $8 - 12\,Hz$.

- **Theta rhythms** (θ) : Usually they are boosted during sleep and play significant role during childhood and infancy. The presence of high θ rhythms in awake adults would be considered as brain disorder. The bandwidth of θ rhythms is $4 - 8\,Hz$.

- **Delta rhythms** (δ) : They are low-frequency rhythmic signals and usually generated in dreamless or deep sleep. However, the presence of these rhythms in adult during awake would be considered as abnormal. The bandwidth of these rhythms is $0.5 - 4\,Hz$.

1.1.2 Artifacts in EEG Signals

When recording EEG signals, they were often contaminated by electrooculogram (EOG), Electromyogram (EMG), electrocardiogram (ECG) and motion artifacts. These artifacts

are non-cerebral signals, as these signals were not produced from the brain.

- **Electrooculogram** : The EOG artifact is a representation of standing electrical potential exist between the front and the back of the human eye ball. This artifact is often present in the recorded EEG signal like spike-type signal with large magnitude. The EOG signals usually having wide frequency spectrum and the most of the energy is below $5\,Hz$ [11]. The contribution of EOG artifact is more predominant in frontal EEG channels ($F_{p_1} - F_7$ and $F_{p_2} - F_8$) and is evident from Fig. 1.3.

- **Electromyogram** : Another artifact very commonly appeared in the EEG signals is EMG artifact, also called muscle artifact. The muscle artifacts are present in the EEG signal due to the activation of muscles associated to face and jaw. Since the muscle artifacts having wide spectral distribution, its presence obscures the visual inspection of the EEG components and complicates the interpretation of EEG signals [12]. These artifacts were more predominant in the EEG signals obtained from the temporal channels ($T_7 - P_7$ and $T_8 - P_8$) which is evident from Fig. 1.3.

- **Electrocardiogram** : ECG signal is the large magnitude physiological signal and is propagated throughout the body and appears like a spike in the recorded EEG signals. In most of the patients, the electrical field distribution of heart is uniform over the scalp and hence the remanent of ECG will be canceled out in the recorded EEG signal using bipolar montage. But, in case of patients with short-neck the ECG artifact often appear in the EEG signal when bipolar montage is used. Whereas the ECG artifact could be seen clearly in the EEG signal when unipolar montage is used and is clear from Fig. 1.5. In case of common average reference montage the remanent of ECG is minimum [2].

- **Motion artifact** : This type of artifact is most appears in EEG signals recorded in ambulatory conditions. They were resulted due to motion of the subject under test as well as movement of the recording electrode, that result devastating disturbances in baseline of the EEG signals. Fig. 1.6 shows a lengthy EEG signal contaminated by motion artifact.

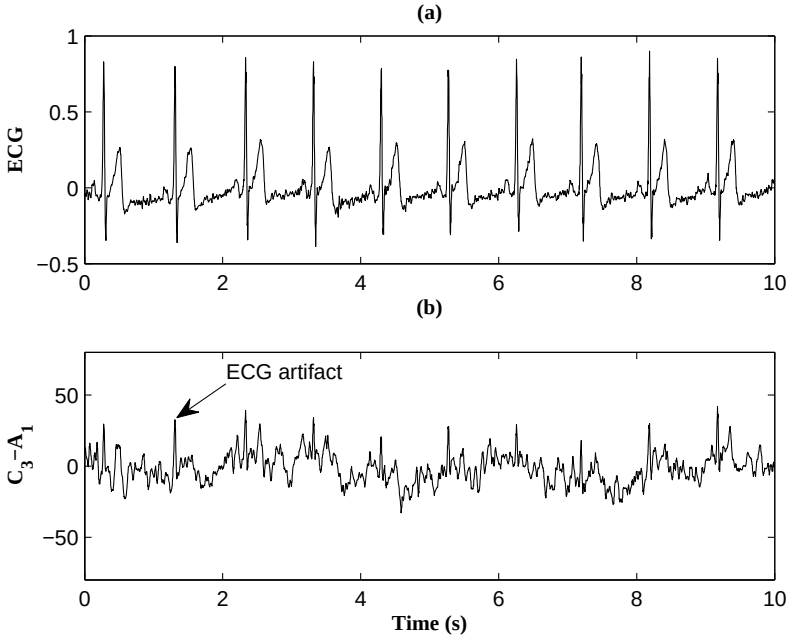

FIGURE 1.5: Parallel recording of (a) ECG signal and (b) the EEG signal in unipolar montage.

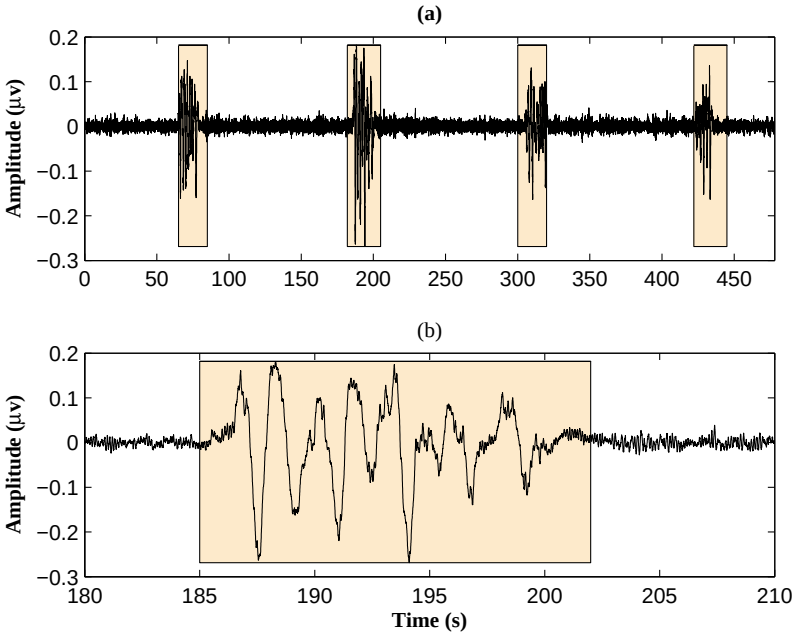

FIGURE 1.6: (a) A lengthy EEG signal contaminated by motion artifact and (b) zoomed version of above plot between the time interval $180 - 210\,s$ [3, 5].

1.1.3 Applications of EEG signals

EEG signals are widely used to study the disorders associated to epilepsy and sleep as well as in brain computer interface (BCI).

- **Seizure detection/prediction** : Epilepsy is a neurological disorder that results epileptic seizures. Basically, seizure is a condition where group of neural cells in the brain synchronously active and causes high amplitude rhythmic pattern in the measured EEG signal. In general the neurologist or physician manually look for such rhythmic patterns in the measured EEG signals to identify what type of seizure the patient is suffering with. However, manual looking of such lengthy EEG records is time consuming. Hence, use of an automatic seizure detection algorithm can reduce the volume of data to be observed by the physician.

  Seizure detection is binary class problem, where one class corresponding to normal EEG and other correspond to presence of seizure. In seizure detection algorithm, the features of EEG signals associated to seizure and non-seizure EEG were extracted to built a classifier. Later, the trained classifier is used to detect automatically the presence of seizure pattern in the lengthy EEG records.

- **Brain computer interface**: The use of EEG signals has been extended to the application like brain computer interface (BCI). Basically, BCI establishes a communication channel between the users brain and output devices such as computer. Here, the user (subject) performs motor imagery task based on the given protocols. As a result, the features of corresponding EEG signals were used as a control signal to the output device [13, 14]. In all BCI applications, the motor imagery has been used as a major approach [15, 16].

It is reported in several studies that the performance of seizure detection and BCI algorithms were degraded due to the presence of these artifacts. Hence, removal of these artifacts plays an important role in EEG signal processing.

1.2 Literature Review on Artifact Removal Techniques

Recently, the use of portable EEG devices both in medical and entertainment applications has been increased due to their low power consumption and comfort to the subject

under test. Moreover, it also facilitates the longer time recording of EEG signals. The traditional diagnostic monitoring for inpatients the EEG test is conducted for 20 to $30min$, therefore epilepsy misdiagnosis rate will be increased. The longer durations tests enhance misdiagnosis rate [17]. Moreover, these devices reduces the cost to 50% when compared to the inpatient monitoring and clinically efficient in 70% of patients [18]. Therefore, the use of portable/wearable EEG devices has been increased both in medical and entertainment applications [19–26]. However, the quality of the measured EEG signals is degraded due to the presence of EOG and EMG artifacts. The effect of EOG and EMG artifact in EEG based seizure detection and BCI systems is discussed in [27–31]. In [32], spectral and topographical characteristics of EMG in BCI application is studied. This study also considered the weak contraction of muscles associated to frontails and temporalis and reported that EMG can obscure μ and β components. Moreover, the presence of these artifacts increase the false positive rate (FPR) and as a results the overall performance of detection systems will be degraded [30, 33]. Therefore, the removal of EOG/EMG artifacts is very important in EEG signals processing. Several techniques has been reported in the literature for the removal of artifacts from both multichannel and single channel EEG signals. The details of these techniques are discussed in the following sections.

1.2.1 Multichannel EEG signals

The blind source separation (BSS) technique often used to remove artifacts from EEG signals [34–37]. Independent component analysis (ICA) is a special case of BSS technique, widely used to remove several artifacts from mixed multichannel EEG data [38–44]. Particularly, this technique more effective in removing the EOG artifact from the multichannel EEG signals [38–41]. Basically, ICA finds de-mixing matrix to estimate the source signals which are statistically independent components (ICs). To compute the de-mixing matrix, ICA uses the non-Gaussianity of the sources as measure and can be computed based on the higher order statistics (HOS) [45–48], mutual information [49, 50] or joint approximate diagonalization [51, 52] of the data. However, for efficient separation, the number of measured signals should be greater than or equal to the the sources to be extracted [53].

The canonical correlation analysis (CCA) [54] is another class of BSS technique, firstly applied on the multichannel EEG data to remove muscle artifacts [55]. Basically CCA finds the source which are maximally autocorrelated and mutually uncorrelated. The major difference between CCA and ICA is that the former estimates the sources based on the second order statistics (SOS), whereas later uses HOS of the data. In [55], it is also reported that the performance of CCA in removing muscle artifacts is better than the ICA. However, BSS techniques are not applicable to process single channel EEG signals. This issue can be addressed by first mapping single channel EEG signal into multivariate data using decomposition techniques described in the following subsection.

1.2.2 Single Channel EEG signals

In [56], Devis. et al. has proposed single channel ICA (SCICA) technique and employed on univariate signal by imposing the following two conditions on the source signals of interest: (i) the source signals to be extract should be disjoint in their spectral domain, (ii) they should be stationary signals. However, these conditions may not hold for EEG signals, which results in poor source separation. To adapt ICA on single channel EEG signal, first the target signal has to be mapped into multivariate data. After that ICA can be used to extract the source signals from the multivariate data. Any decomposition techniques, such as discrete wavelet transform (DWT) and ensemble empirical mode decomposition (EEMD) [57] techniques could be used to map the single channel signal into multivariate data. DWT and EEMD techniques are used in seizure detection algorithms to represent the given signal into band of components [58–64]. Unlike DWT, EEMD decomposes the signal into intrinsic mode function without prior knowledge about the signal of interest. In [65, 66], ICA is employed on the single channel physiological signals by combining with DWT/EEMD, where DWT/EEMD were used to map the single channel signal into multivariate data. However, the performance of combined use of DWT and ICA shortly named as w-ICA mainly depends on the signal morphology. Whereas in case of EEMD-ICA technique the performance depends on the tuning parameters such as noise parameter np and the number of ensembles ne. Moreover, the tuning of these parameters for better performance is difficult, as the EEMD consumes with high computational time.

Singular spectrum analysis (SSA) [67, 68] is another class of decomposition technique for single channel/multichannel signals. Unlike DWT technique, the parameter of SSA technique is independent to the morphology of signal of interest and the tuning of SSA parameters is easy as compared with the EEMD. SSA has been widely used in processing single climatic time series data [67]. Recently, it has been applied to the physiological signals such as EEG, ECG and EMG [69–76]. However, the overall performance of the SSA technique mainly depends on grouping step and the window length. Moreover, as SSA accounts the covariance of the data, therefore, the decomposed components are statistically uncorrelated. The way of grouping the components and combining with BSS technique to extract the statistically independent signals are the highlights of the thesis. In addition to that the performance effect of SSA parameters were also addressed.

The adaptive noise canceler (ANC) [77] has been applied to process single channel biomedical signals [78–81]. Unlike regression based technique [82, 83], where the filter coefficients were pre-computed, the ANC adapts its filter coefficients based the input signal applied to its reference input. However, the main requirement is that the reference EOG signal has to be recorded separately. In general, the reference EOG signal is recorded from the eye by using additional electrode. In BCI applications, the additional electrode over the eye may create discomfort to the subject. Moreover, the electrode which is placed over the eye to record the EOG signal for ANC is also pick the EEG components. In ANC, as the reference signal is subtracted from the contaminated EEG signal, this may result loss of useful information in the corrected EEG signal. In special cases, for example, in Epilepsy Monitoring Unit (EMU), the EOG signal is not recorded, as it causes discomfort to the patient [84]. Recently, in [85], DWT and ANC techniques were combined to address this problem, where, the reference signal for ANC is estimated from the contaminated EEG signal using DWT. However, in this technique, the user has to select the mother wavelet function based on EOG signal morphology. In fact, the morphology of EOG signal will be changed due to non-linear eyelid blink/movements. To overcome this limitation, in this thesis, we proposed efficient technique by replacing DWT with SSA. Moreover, as SSA is data-driven technique the performance is independent to the morphology of the EOG artifact.

1.3 Outline of the Thesis

Based on the background discussed above, the salient contributions made by this thesis are presented as follows:

- **Chapter 1** : The introductory chapter provides brief description of EEG signals and also the provides the artifact removal technique available for multi/single channel EEG signals in the literature. The need for the artifact removal techniques for single channel EEG single channel EEG signals.
- **Chapter 2** : In this chapter, first, the mathematical background of existing techniques for both multichannel as well as for single channel EEG signals were introduced. In addition, mathematical background of SSA technique which is used throughout this thesis is also presented.
- **Chapter 3** : The grouping step in SSA is a critical step and shows an impact in the final result. However, in traditional SSA technique, this step will be performed based on the magnitude of the eigenvalues of a covariance matrix. In this chapter, a semi-automatic grouping step is introduced to identify the eigenvectors corresponding to the desired signal. The effectiveness of the new grouping criteria on real EEG signals contaminated by motion artifacts is evaluated. In addition, the computational complexity of SSA is evaluated and compared with the existing techniques.
- **Chapter 4** : As it was discussed earlier that ANC need a reference signal which is some how correlated with the artifact (EOG) to be removed from the contaminated EEG signal. In application like BCI, a separate electrode place over the eye to record the reference signal for ANC, which will be inconvenient to the subject under study. Hence, in this chapter, we introduced a method in which the reference signal (EOG) for ANC is extracted from the contaminated EEG signal using SSA and applied to the reference input of ANC. Such technique could reduce the need for extra electrode used to record the EOG signal.
- **Chapter 5** : ICA often used to separate the sources from the mixed EEG data. Basically, it assumes the sources to extracted are statistically independent components. However, the direct adaptation of ICA on single channel EEG signals is

not possible, as ICA demands that the number of channels should be more than or equal to the number of sources to be extracted. In this chapter, a scheme to adapt ICA on single channel EEG signals is presented, where, first, SSA is employed to map single channel EEG into multivariate data needed for ICA. After that ICA is employed on the multivariate data to extract the statistically independent sources.

- **Chapter 6** : Muscle artifact is a non-cerebral signal often contaminates the EEG data. The presence of this artifact usually obscure the valuable inspection of the EEG signals and also degrade the performance of seizure detection/predection or BCI systems. In this chapter, a subspace based decomposition technique is proposed to remove muscle artifact from single channel EEG signal and compared with the discrete wavelet transform (DWT) and ensemble empirical mode decomposition techniques. In addition, the performance of the seizure detection algorithm is evaluated when our muscle artifact removal technique is used as preprocessing step.

- **Chapter 7** : Finally, summary of each chapter and future scope of the work is discussed in this chapter.

2

Mathematical Preliminaries of Artifact Removal Techniques

In this chapter, the mathematical framework of existing artifact removal techniques for multi and single channel EEG signals is presented. In addition, the mathematical formulation of the subspace based technique called singular spectrum analysis (SSA) is also outlined. Moreover, the open problem i.e. the existing grouping step and its limitations in traditional SSA technique is also be discussed..

2.1 Methods for Processing Multichannel EEG signals

In real-life, the measured signals are always consists of mixture of designed and undesired components. In EEG recordings, the undesired signals encountered are EOG and EMG signals. The separation of these components will always necessitates the further analysis EEG signals using the following techniques.

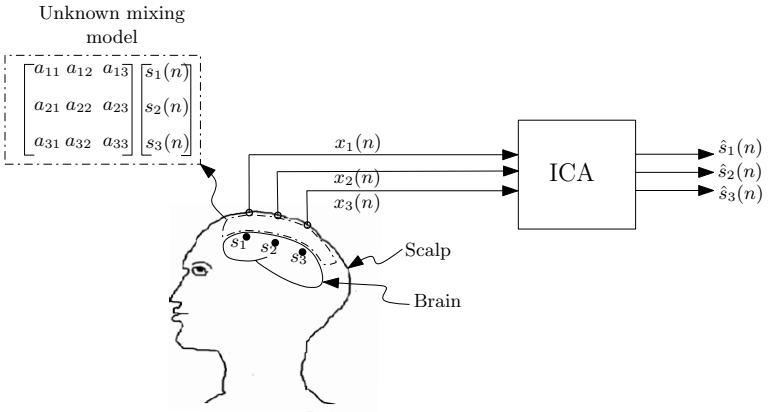

FIGURE 2.1: Application of ICA model to EEG.

2.1.1 Independent Component Analysis

Independent component analysis (ICA) is a class of blind source separation (BSS) technique often used to decompose the mixed data into statistically independent components (ICs). It is applied in many fields like biomedical signal processing [38–41], audio processing [86, 87], and image processing [88]. The cocktail party problem is a classical example of ICA technique, where, the underlying speech signals were recovered from the mixed speech data emitted by the group of people in a room. Consider the signals $x_1(n)$, $x_2(n)$ and $x_3(n)$ are measured from three microphones and they were weighted summation of speech signals $s_1(n)$, $s_2(n)$ and $s_3(n)$ emitted by the three persons. Then, the ICA model for cocktail party problem is given by

$$\begin{aligned} x_1(n) &= a_{11}s_1(n) + a_{12}s_2(n) + a_{13}s_3(n) \\ x_2(n) &= a_{21}s_1(n) + a_{22}s_2(n) + a_{23}s_3(n) \\ x_3(n) &= a_{31}s_1(n) + a_{32}s_2(n) + a_{33}s_3(n) \end{aligned} \tag{2.1}$$

Fig. 2.1 shows the application of the cocktail party problem to EEG, where, $s_1(n)$, $s_3(n)$ and $s_3(n)$ are the brain signals emitted by the sources s_1, s_2 and s_3 in the brain. Then the measured EEG signals are the weighted summation of brain signals. The equations in (2.1) can be represented as matrix vector multiplication and given by

$$\mathbf{x} = \mathbf{A}\mathbf{s} \tag{2.2}$$

where, $\mathbf{A}$ is mixing matrix and its elements are mixing coefficients; the random vectors $\mathbf{x}$ and $\mathbf{s}$ represents the observed mixtures and independent components respectively. All

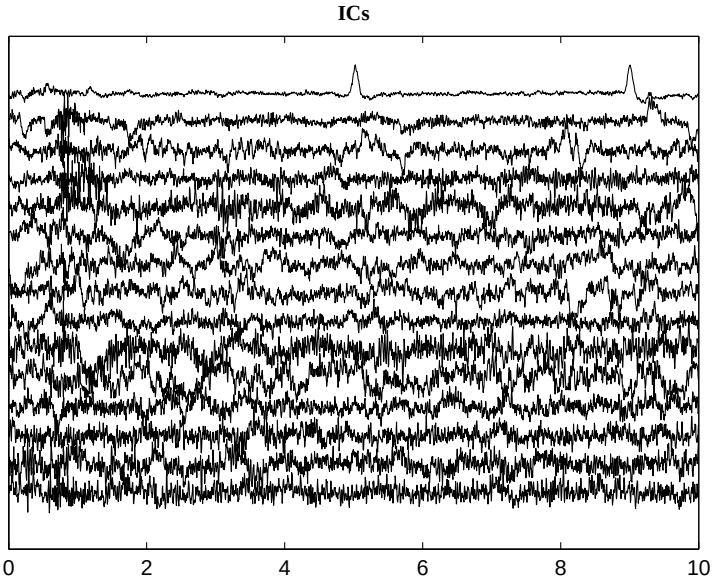

FIGURE 2.2: The extracted ICs from 10 *s* multichannel EEG data as shown in Fig. 1.3.

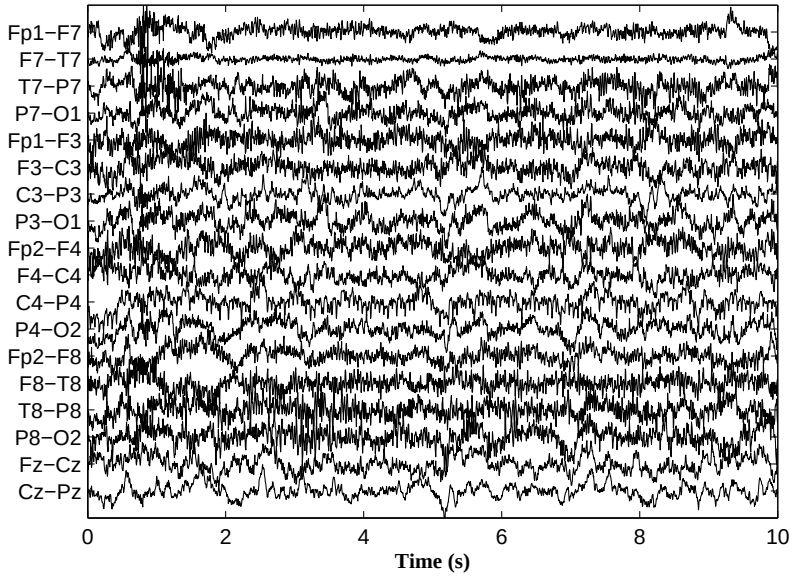

FIGURE 2.3: Corrected EEG signals using ICA from 10 *s* multichannel EEG shown in Fig. 1.3.

ICA algorithms finds the de-mixing $\mathbf{B}$ with elements b_{ij} by considering the statistical independence of the signal. Since the de-mixing matrix $\mathbf{B}$ is derived based on the signal statistics, therefore, multiplying the mixed data onto it results statistically independent components (IC) matrix $\mathbf{S}$ (note that the estimated sources are in ICA domain). To compute the de-mixing matrix $\mathbf{B}$ from the mixed data, several algorithms were proposed in the literature [45–52]. However, in this thesis, FastICA algorithm [45–48, 89] is used to compute the de-mixing matrix $\mathbf{B}$. FastICA algorithm is widely used for blind source separation (BSS) problems as it is computationally efficient. As it estimates the sources one by one requires less memory as compared with entropy based method. Moreover, its performance is quite comparable with the existing methods. This algorithm finds the de-mixing matrix $\mathbf{B}$ based on the non-Gaussianity of the sources to be extracted [90].

Consider 10 s multichannel EEG data as shown in Fig. 1.3, contaminated by EOG. Fig. 2.2 shows the extracted ICs from the multichannel EEG data using FastICA algorithm. To remove EOG artifact, first, the corresponding ICs in $\mathbf{S}$ set to zero. It is clear from Fig. 2.2 it is clear that the first IC is corresponds to the EOG artifact and the corresponding row is set to zero. Finally, the time domain version of source signals shown in Fig. 2.3 are extracted by multiplying $\mathbf{S}$ with the $\mathbf{B}^{-1}$.

2.1.2 Canonical correlation analysis

Another class of BSS technique is CCA, often used to remove artifacts from the multichannel EEG signals [55]. Basically, CCA finds the solution to the BSS problem by imposing the constraint that the sources to be extract are maximally auto-correlated and mutually un-correlated [55]. Consider the mixed data matrix $\mathbf{X}(t)$ with J sources, having N number of samples and let the data matrix $\mathbf{Y}(t)$ is one sample delayed version of $\mathbf{X}(t)$ *i.e.*$\mathbf{Y}(t) = \mathbf{X}(t-1)$. Then, CCA finds the basis vector $\mathbf{w_x}$ and $\mathbf{w_y}$ corresponding to $\mathbf{X}$ and $\mathbf{Y}$ respectively, such that the correlation coefficient ρ between the canonical variables $\mathbf{v} = \mathbf{w}_\mathbf{x}^T\mathbf{X}$ and $\mathbf{u} = \mathbf{w}_\mathbf{y}^T\mathbf{Y}$ is maximized. Then the expression for correlation coefficient ρ is given by

$$\rho = \frac{\mathbf{w}_\mathbf{x}^T\mathbf{C}_{\mathbf{xy}}\mathbf{w}_\mathbf{y}}{\sqrt{(\mathbf{w}_\mathbf{x}^T\mathbf{C}_{\mathbf{xx}}\mathbf{w}_\mathbf{x})(\mathbf{w}_\mathbf{y}^T\mathbf{C}_{\mathbf{yy}}\mathbf{w}_\mathbf{y})}} \tag{2.3}$$

where, $\mathbf{C_{xx}}$ and $\mathbf{C_{yy}}$ are auto-covariance matrices of $\mathbf{X}$ and $\mathbf{Y}$ respectively, and $\mathbf{C_{xy}}$ is the cross-covariance matrix of $\mathbf{X}$ and $\mathbf{Y}$. The maximum value of ρ is obtained by taking the derivative of (2.3) with respect to $\mathbf{w_x}$ and $\mathbf{w_y}$, and equating to zero. The resulting equations following the two eigenvalue problems [91] are

$$\begin{aligned} \mathbf{C}_{xx}^{-1}\mathbf{C}_{xy}\mathbf{C}_{yy}^{-1}\mathbf{C}_{yx}\hat{\mathbf{w}}_x &= \rho^2\hat{\mathbf{w}}_x \\ \mathbf{C}_{yy}^{-1}\mathbf{C}_{yx}\mathbf{C}_{xx}^{-1}\mathbf{C}_{xy}\hat{\mathbf{w}}_y &= \rho^2\hat{\mathbf{w}}_y \end{aligned} \tag{2.4}$$

Since the data matrices $\mathbf{X}(t)$ and $\mathbf{Y}(t)$ differ by one sample, finding the basis vector $\hat{\mathbf{w}}_\mathbf{x}$ is sufficient to extract the source signals.

However, the minimum condition to extract the source signals using CCA from the two data sets $\mathbf{X}$ and $\mathbf{Y}$ as given in [92, 93] can be represented by

$$| \rho_{\mathbf{x},\mathbf{y}}^{(i)} | \neq | \rho_{\mathbf{x},\mathbf{y}}^{(k)} | \qquad 1 \leq i < k \leq J \tag{2.5}$$

where, $| \rho_{\mathbf{x},\mathbf{y}}^{(i)} |$ represents the correlation coefficient between the i^{th} source from the data set $\mathbf{X}$ and $\mathbf{Y}$. To demonstrate the performance of the CCA algorithm, we considered the muscle artifact contaminated multichannel EEG data as shown in Fig. 2.4. The details of this EEG data is outlined in Chapter 5.2.2. Fig. 2.5 and 2.6 shows the extracted canonical components and their correlation coefficient (ρ). As the muscle artifact inherits white noise properties [94], therefore the corresponding correlation coefficients shown in Fig. 2.6, are low. Based on this fact a threshold of 0.99 is set to identify the muscle artifact component (from 7 to 21) and set them to zero. Finally, muscle artifact corrected EEG signals is obtained by multiplying canonical components with the inverse of the de-mixing matrix $\mathbf{W}$, whose columns are the eigenvectors derived using (2.4). It is obvious from Fig. 2.7 that still we could see the remnants of muscle artifacts in the corrected EEG signals.

When looking into the decomposition process of both techniques, CCA uses the SOS of the data, whereas ICA uses HOS of the data. Therefore, the computational complexity of CCA is lower than ICA technique. In [55], it was reported that the performance of CCA in removing the muscle artifact is superior to the ICA. We have also noticed that for lower SNRs the performance of CCA technique is degraded which is evident from Fig. 2.7. However, both ICA and CCA techniques cannot be used to process the single channel EEG signals. In order to extract the source signals from a single channel EEG

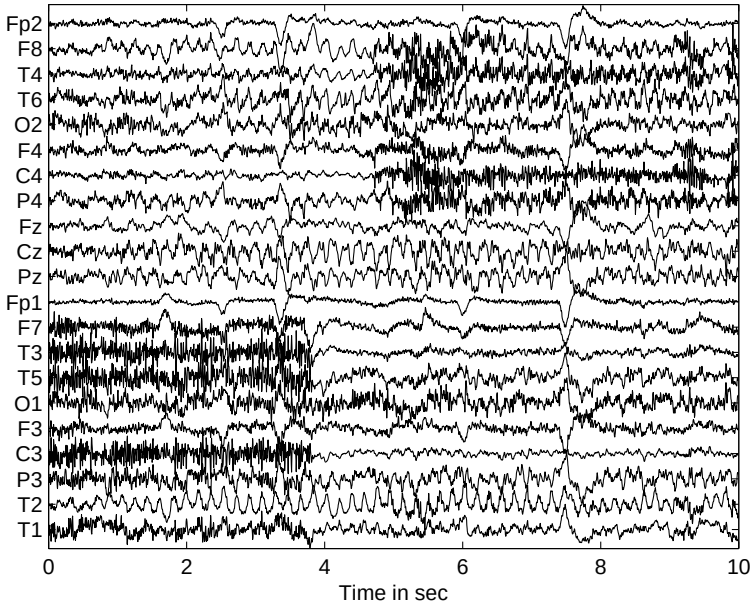

FIGURE 2.4: Ten second multichannel EEG epoch recordings contaminated by muscle artifacts [6]

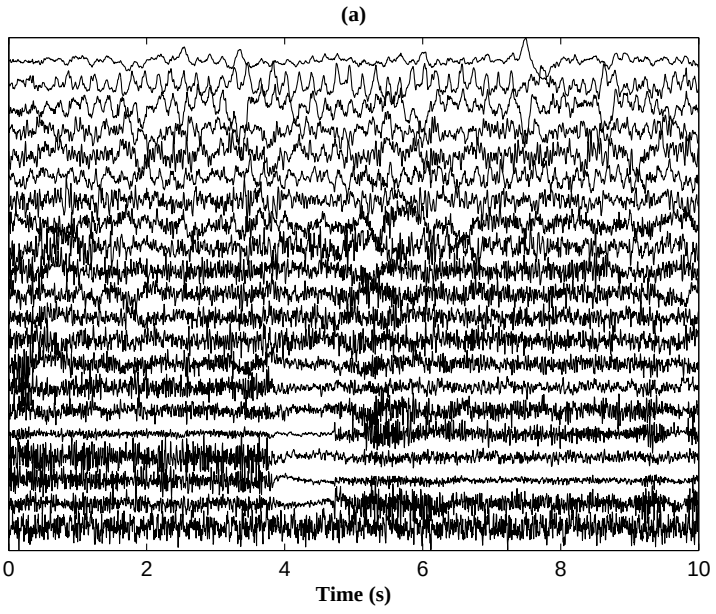

FIGURE 2.5: The extracted canonical components using CCA.

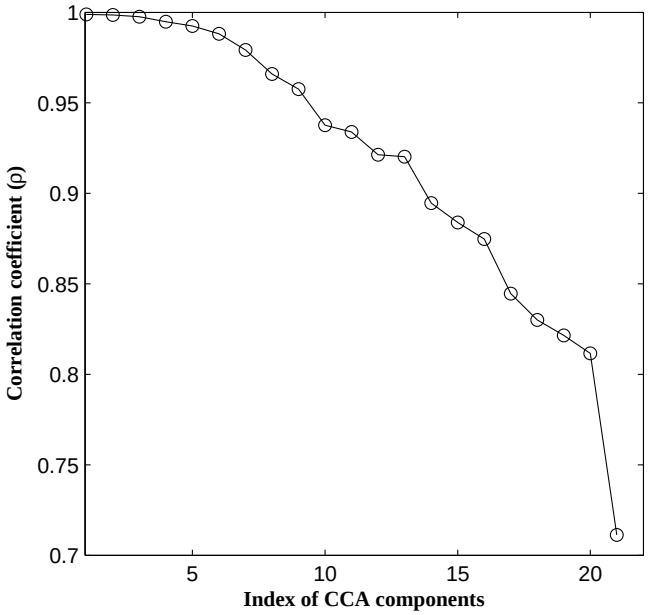

FIGURE 2.6: Correlation coefficient ρ of CCA components in Fig. 2.5.

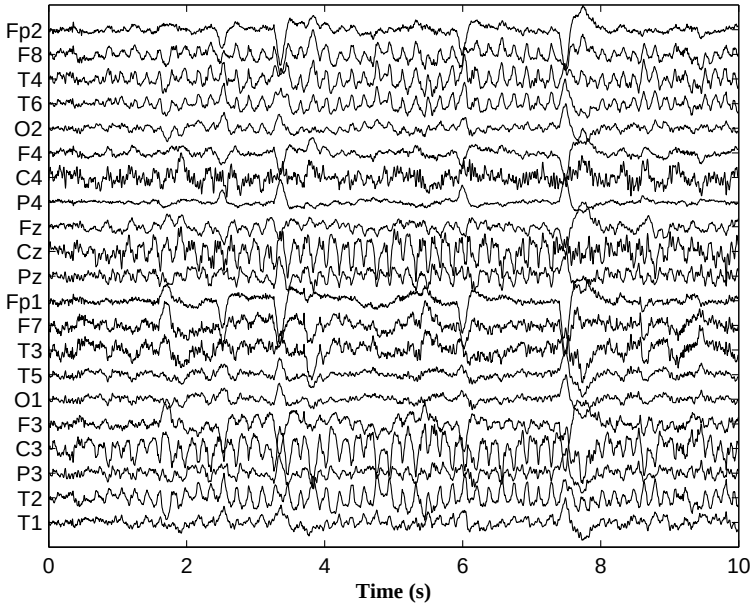

FIGURE 2.7: Muscle artifact corrected EEG signals using CCA technique.

signal, first, it should be mapped into a multivariate data before applying to ICA/CCA. Such conversion from a single channel signal into a multivariate signal can be efficiently performed by using either DWT/EEMD.

2.2 Methods for Processing Single channel EEG signals

The artifact removal techniques discussed in the above section cannot be used for processing single channel EEG signals. By addressing this issue, few technique has been reported in the literature for processing single channel EEG signals.

2.2.1 w-ICA

The discrete wavelet transform (DWT) is a useful tool for analyzing the signals and widely used in seizure detection algorithms [58–63]. The advantage of the wavelet transform is that, it can provide the temporal as well as the spectral information of the signal, which means, it can provide the better temporal resolution for higher frequency components and better frequency resolution for lower frequency components. Hence, the wavelet transform is used for the multi resolution analysis (MRA) of a signal. The given signal $x(t)$ can be represented into wavelet series as follows [95]

$$x(t) = \sum_{m} a_{Pm}\phi_{Pm} + \sum_{l=1}^{P}\sum_{m} d_{lm}\varphi_{lm}(t) \tag{2.6}$$

where a_{Pm} and d_{lm} are the approximate and detail coefficients respectively. For a given level of decomposition, say P, the original signal $x(t)$ can be reconstructed using the approximation and the detail coefficients, as given by

$$x(t) = A_P(t) + \sum_{l=1}^{P} D_l(t) \tag{2.7}$$

As ICA cannot be used to process the single channel EEG signal, the alternating solution is mapping the target signal into multivariate data using decomposition technique. In [65], w-ICA technique is proposed to separate the source components from the single channel physiological signal, In this technique, first wavelet transform is used to represent the univariate signal into multivariate data matrix $\mathbf{X}$. After that, FastICA algorithm

[89, 96] is employed on data matrix $\mathbf{X}$. The FastICA algorithm provides mixing, de-mixing matrices $\mathbf{A}$, $\mathbf{B}$ respectively and an independent component (IC) matrix $\mathbf{S} = \mathbf{BX}$ as output. Unlike basic ICA, where the matrix $\mathbf{A}$ mixes the sources into different channels (see Fig. 2.1), in case of source separation from single channel signals it is assumed that the mixing matrix $\mathbf{A}$ mixes the sources into different decomposed components. In order to extract a particular source signal which is statistically independent, the corresponding column vector of $\mathbf{A}$ should be multiplied with that of the IC of interest, thus results newly derived wavelet components. Finally, the newly derived components are summed together to obtain the desired source signal as single channel signal. However, the over all performance of w-ICA technique mainly depends on the selected wavelet function, consequently, the selection of wavelet function demands the prior knowledge (*i.e.* morphology) of the sources to be extracted.

2.2.2 EEMD-ICA/CCA

The empirical mode decomposition (EMD) [97] is data-driven technique often used to decompose the given N sampled signal vector $\mathbf{x} = [x(1), x(2), ..., x(N)]$ into intrinsic mode functions (IMFs). The IMF components are oscillatory functions and they are orthogonal components. Therefore, the given signal vector $\mathbf{x}$ can be expressed as sum of its IMF components and residue, $\mathbf{x} = \sum_{j=1}^{q} \mathbf{f}_j + \mathbf{e}_q$, where, $\mathbf{f}_j$ is the j^{th} IMF component and $\mathbf{e}_q$ is the residual signal after extraction of q IMF components. However, this technique suffers from the mode mixing problem; which is defined as presence of a component of similar scale residing in different IMFs. To alleviate this problem, ensemble EMD (EEMD) technique has been proposed in [57]. In this technique, firstly, the targeted signal is added with independent identically distributed white noise of that of the same standard deviation (SD). Next, IMF components from the noisy signal were derived using EMD. This process is repeated for a number of ensembles (ne) and the averaged IMF components are derived. Finally, the output of the EEMD algorithm is an average of IMF components obtained after executing the EMD algorithm for finite ensembles and is represented by $\mathbf{X}$. In [66], EEMD-ICA technique is proposed to make use of ICA on single channel EEG signals. In this technique, first, EEMD is used to represent the univariate signal into multivariate data matrix $\mathbf{X}$. Thereafter, FastICA algorithm is then applied on $\mathbf{X}$ and estimate the mixing, de-mixing matrices $\mathbf{A}$, $\mathbf{B}$ respectively and the IC matrix $\mathbf{S} = \mathbf{BX}$ as output. In order to extract a particular source

signal, the corresponding column vector of **A** should be multiplied with that of the IC of interest. Finally, by summing the newly derived IMF components, desired source signal can be reconstructed as a single channel signal.

Like EEMD-ICA technique, another two stage source separation technique called EEMD-CCA is proposed in [98] to remove motion artifact from single channel EEG signal. In order to apply CCA technique on single channel signal, like EEMD-ICA, first, the given signal is mapped into multivariate data and CCA is applied to separate the artifact and EEG components. However, in the process of make use of BSS techniques to single channel EEG signals, EEMD technique used as preprocessor. Thus, the overall computational complexity of EEMD-ICA/CCA is high. Moreover, their performance also depends on the EEMD tuning parameter np and ne, which is very difficult to set.

2.2.3 Adaptive noise canceler

In addition to the BSS technique, digital filters also employed to process the single channel EEG signals. Digital filters are filters are used to extract the desired signal of interest from the noisy corrupted signals. Normally, fixed coefficient digital filters were used to remove the artifacts from the biomedical signals. However, when the statistics of the signal is time varying in nature the digital filters with adaptive coefficients, known as adaptive filter, would be useful [77, 99–102]. As the adaptive filters are able to work in unknown environment as well as ability to track the signal variations, it is extensively used in signal processing and control applications. Moreover, it is widely applied in the fields like biomedical signal processing and communication engineering. The adaptive filter can be operated into four functional modes: (i) system identification, (ii) prediction, (iii) inverse modeling and (iv) noise canceler. In this thesis, we use the adaptive filter as noise canceler.

Fig. 2.8 shows the ANC, consists of two inputs , primary and reference inputs. The filtering and weight updating are the main functional blocks of ANC. In general, the contaminated EEG signal $x(n)$ is applied to the primary input of ANC and a reference signal of artifact which is to be removed from the contaminated EEG signal is applied to the reference input of ANC. By using either least mean square (LMS) or recursive least square (RLS) algorithms [77], the weights of the adaptive filter are updated. In this thesis, RLS algorithm is employed because of its fast convergence property. Let us denote

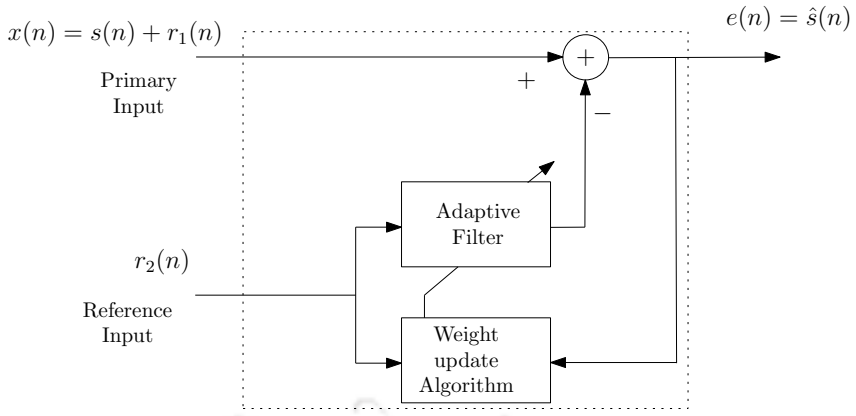

FIGURE 2.8: Block diagram of adaptive noise canceler.

$\mathbf{r}_2(n) = [r_2(n), r_2(n-1), ..., r_2(n-L+1)]^T$ and $\mathbf{w}(n) = [w_1(n), w_2(n), ..., w_L(n)]^T]$, are the input and the weight vectors of L-tap adaptive filter at the time instant n respectively, where, T is transpose operator. Then the equations presented in Algorithm. 1 are computed recursively until the mean square error (MSE) is minimum.

Algorithm 1 RLS Algorithm

Initialize: $\mathbf{w}(1) = \mathbf{0}$ and $\mathbf{B}(1) = \delta^{-1}\mathbf{I}$

η and δ are positive constants.

for $n = 1, 2, ...$

$\mathbf{a}(n) = \frac{\eta^{-1}\mathbf{B}(n)\mathbf{r}_2(n)}{1+\eta^{-1}\mathbf{r}_2^T(n)\mathbf{B}(n)\mathbf{r}_2(n)}$

$\hat{r}_1(n) = \mathbf{w}^T(n)\mathbf{r}_2(n)$

$e(n) = x(n) - \hat{r}_1(n)$

$\mathbf{w}(n+1) = \mathbf{w}(n) + \mathbf{a}(n)e(n)$

$\mathbf{B}(n+1) = \eta^{-1}\mathbf{B}(n) - \eta^{-1}\mathbf{a}(n)\mathbf{r}_2^T(n)\mathbf{B}(n)$

end

2.2.4 Singular spectrum analysis

Singular spectrum analysis (SSA) [67, 68] is a subspace based decomposed technique and represents the signal into trend, oscillating and noise components, respectively. SSA comprises the following steps: embedding, decomposition, grouping and reconstruction. Let us consider the contaminated EEG signal as

$$\mathbf{x} = \mathbf{s} + p\mathbf{a} \tag{2.8}$$

where **s** and **a** be the desired and artifact components and p is a propagation constant. In embedding step N sampled signal vector, $\mathbf{x} = [x(1), x(2), ..., x(N)]$, is mapped into multivariate trajectory matrix $\mathbf{X}$, of size $M \times K$.

$$\mathbf{X} = \begin{bmatrix} x(1) & x(2) & ..... & ..... & x(K) \\ x(2) & x(3) & ..... & ..... & x(K+1) \\ : & : & ..... & ..... & : \\ x(M) & x(M+1) & ..... & ..... & x(N) \end{bmatrix} \tag{2.9}$$

where, M is the window length, selected using the criteria $M > f_s/f$ [69]. Here, f_s is the sampling frequency and f is the minimum frequency signal which to be extracted and $K = N - M + 1$. It is obvious from (2.9) that $\mathbf{X} = \mathbf{S} + \mathbf{A}$, where $\mathbf{S}$ and $\mathbf{A}$ are the trajectory matrices of desired and artifact (noise) components.

In the decomposition step of SSA, first the trajectory matrix is factored using singular value decomposition (SVD). Next, using the singular matrices obtained by SVD operation, trajectory matrix $\mathbf{X}$ is represented into M number of low rank trajectory matrices. SVD of trajectory matrix is given by

$$\mathbf{X} = \mathbf{V}\mathbf{\Sigma}\mathbf{W}^T \tag{2.10}$$

where, $\mathbf{V}$ and $\mathbf{U}$ are the left and right singular matrices and $\mathbf{\Sigma}$ is the diagonal matrix and T is transpose operator. From (2.10), i^{th} trajectory matrix $\mathbf{X}_i$ can be represented as

$$\mathbf{X}_i = \sqrt{\lambda_i}\mathbf{v}_i\mathbf{u}_i^T \quad i = 1, 2, ..., M \tag{2.11}$$

The trajectory matrix of the contaminated signal can be represented as $\mathbf{X} = \mathbf{X}_1 + \mathbf{X}_2 + ... + \mathbf{X}_M$.

As the size of the matrix is too large, the computational complexity of SVD is infeasible. Therefore, the decomposition step of SSA is performed as follows. Let us denote $\lambda_1, \lambda_2, ..., \lambda_M$ and $\mathbf{v}_1, \mathbf{v}_2, ..., \mathbf{v}_M$ as the eigenvalues and the eigenvectors of the covariance matrix $\mathbf{C}$=$\mathbf{X}\mathbf{X}^T$. Note that based on the magnitude, the eigenvalues were rearranged in the descending order and the corresponding eigenvectors also. Denote $\mathbf{u}_i = \mathbf{X}^T\mathbf{v}_i/\sqrt{\lambda_i}$ and substitute in (2.11). Then the i^{th} trajectory matrix $\mathbf{X}_i$ is represented as

$$\mathbf{X}_i = \mathbf{v}_i\mathbf{v}_i^T\mathbf{X} \tag{2.12}$$

The term $\mathbf{v}_i\mathbf{v}_i^T$ in (2.12) represents the subspace for i^{th} component present in $\mathbf{x}$ and $\mathbf{v}_i$ is i^{th} column eigenvector in $\mathbf{V}$.

In the grouping step of SSA, the resulted trajectory matrices $\mathbf{X}_1, \mathbf{X}_2, ..., \mathbf{X}_M$, split into c groups based on the magnitudes of eigenvalues. Let $I_1 = \{l_1, l_2, ..., l_q\}$ represents the indices of q eigenvalues of group one. Then the trajectory matrix of the I_1^{th} group is given by

$$\mathbf{X}_{I_1} = \mathbf{X}_{l_1} + \mathbf{X}_{l_2} +, ..., +\mathbf{X}_{l_q} \tag{2.13}$$

The trajectory matrix in (2.9) can be written as

$$\mathbf{X} = \sum_{k=1}^{c} \mathbf{X}_{I_k} \tag{2.14}$$

In the reconstruction step, the estimated trajectory matrices mapped into single channel signals. Let, $\hat{\mathbf{S}}$ be the estimated trajectory matrix of the desired signal and $\hat{s}_{ij}$ is its elements in i^{th} row and j^{th} column. Then, n^{th} sample of the estimated desired signal $\hat{s}(n)$ is given by

$$\hat{s}(n) = \begin{cases} \frac{1}{n}\sum_{i=1}^{n} \hat{s}_{i,n-i+1} & \text{for } 1 \geq n < M \\ \frac{1}{M}\sum_{i=1}^{M} \hat{s}_{i,n-i+1} & \text{for } M \geq n \leq K \\ \frac{1}{N-n+1}\sum_{i=n-K+1}^{N-K+1} \hat{s}_{i,n-k+1} & \text{for } K < n \leq N \end{cases} \tag{2.15}$$

2.3 Conclusion

In this chapter, the mathematical preliminaries of artifact removal technique for both multi and single channel EEG signals were discussed. In addition we also discussed the limitations of the existing technique.

3

A new Grouping Criteria for SSA to Remove Motion Artifact from Single Channel EEG

In this chapter, first, the issues associated to the grouping step in traditional SSA technique is addressed. Next, a new grouping criteria for SSA is introduced and evaluated its performance in removing the motion artifact from single channel EEG signal. The performance of the modified SSA technique is compared with the existing EEMD-CCA method in removing the motion artifact from single channel EEG signal and presented the effectiveness of the proposed algorithm in removing the motion artifact. Additionally, the computational complexity of the proposed algorithm is also presented.

3.1 Introduction

Recently, in health care applications, the measurement of biomedical signals in ambulatory situations has been increased in order to shift health care systems from hospital-centric to ambulatory based. Ambulatory EEG (AEEG) system facilitates recording of

brain electrical activity for a long period and is often preferred where the diagnosis is unclear. Since the ambulatory EEG test allows the subject to move around, the measured EEG signals often contaminated by motion artifacts along with the common artifacts, such as ocular and muscle artifacts [44]. ICA is often used to remove the artifacts from multichannel EEG signals [38–44]. In the literature, few works have been reported to remove the motion artifacts from the multichannel EEG signals [44, 103]. The canonical correlation analysis (CCA) [54] is another class of BSS technique and applied on the multichannel EEG data to remove muscle artifacts [55]. The difference between the ICA and CCA is that the former uses the higher order statistics (HOS) of the data to extract the source signals, whereas the later uses the second order statistics (SOS). As ICA uses the HOS of the data, the computational complexity of the ICA is more than CCA. In [103], CCA has been employed to observe the extent to which the motion artifact is reflected in the skin-electrode contact impedance.

In general, the most of the ambulatory EEG systems comprise either single or few EEG channels to reduce the cumbersome to the subject and maintain the minimum instrumentation complexity [104–106]. However, the techniques presented in [34, 44, 103, 107], can not be implemented for analysis of single channel EEG signals. The application of ICA on a single channel signal has been proposed in [56]. However, this technique is not suitable to remove the artifacts from a single channel EEG signal due to the following two constraints: first, the signal of interest should be a stationary and secondly, they should be disjoint in the frequency domain. In [66], the EEMD [57] and ICA techniques are jointly used to remove different artifacts from a single channel EEG and EMG signals. In ambulatory EEG systems, as the high computational signal processing algorithm consumes more power, use of such algorithms will reduce the battery lifetime [108]. So, a low computational as well as the single channel operated signal processing techniques are greatly demanded in such applications. Since CCA involves less computations as compared with the ICA, use of such algorithm also reduces the computational complexity of the artifact removal system. However, CCA technique is mostly suitable for analysis of multichannel EEG signals. In order to employ CCA on the single channel EEG signal, first, the single channel signal has to be mapped into multivariate data. Recently, in [98], a combined EEMD and CCA technique, namely EEMD-CCA, has been proposed to remove the motion artifact from a single channel EEG signal. In this technique, first, the single channel signal is mapped into a multivariate signal or data using EEMD. Later, CCA

extracts the source signals from the multivariate data and its delayed version. However, EEMD involves computationally intensive operations and hence increases the computational complexity of the overall EEMD-CCA technique. Moreover, the EEMD-CCA technique exhibits poor performance to remove the low frequency motion artifact.

In this work, we used SSA [67, 68] technique with new grouping criteria to remove the motion artifact from single channel EEG signal and we also compared its computational complexity with the existing EEMD-CCA technique. The modified SSA technique is tested on the single channel EEG signals, contaminated by motion artifact, and is compared with the existing EEMD-CCA technique in terms of computational complexity, signal to noise ratio (SNR) and the percentage reduction in artifact. The simulation results show that an improvement in the SNR as well as the percentage reduction in artifact is achieved with lower computational complexity than the EEMD-CCA

3.2 A New grouping criteria for SSA

However, as it discussed in Chapter 2, in traditional SSA, after decomposing the matrix $\mathbf{X}$ into M low rank trajectory matrices, they were split into q groups based on the magnitudes of the eigenvalues. For example, consider an eigenspectrum , of a covariance matrix $\mathbf{C}$, shown in Fig. 3.1. Where, the magnitude of eigenvalues λ_1 and λ_2 are highly distinguishable as compared with remaining eigenvalues $i.e$ from λ_3 to λ_{32}. Therefore, the trajectory matrices $\mathbf{X}_1$ and $\mathbf{X}_2$ categorized into one group and the remaining matrices from $\mathbf{X}_3$ to $\mathbf{X}_M$ are categorized into another group. Note that the number of groups $c = 2$. However, in traditional SSA, this step has to be performed manually. In [69, 70], minimum description length (MDL) criteria [109] is used for automatic grouping of trajectory matrices corresponding to the desired signal. However, such criteria can be applicable in the cases where the signal of interest is well defined [71]. For example, the EOG artifact in the frontal EEG signal (F_{p_1} and F_{p_2}) is well distinguishable and causes an abrupt change in the baseline. The use of such criteria for motion artifact removal may not work well, as motion artifact does not causes abrupt change. Thus, the use of such criteria will not work well due to the fact that the motion artifact signal is a slowly time varying signal. Therefore, we investigated an alternate criteria for grouping the decomposed matrices and is presented in the following section.

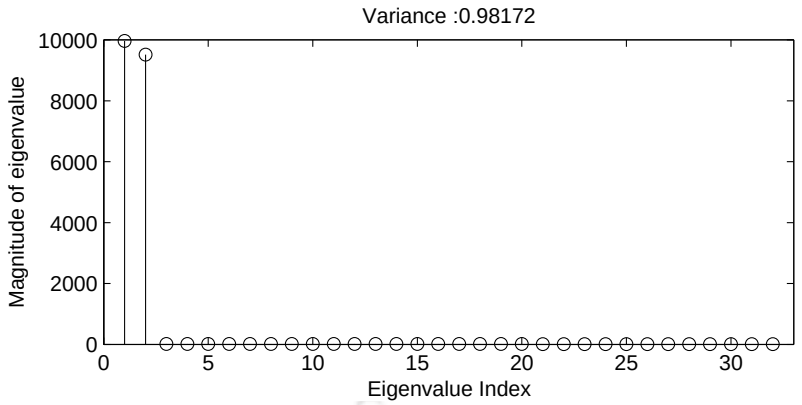

FIGURE 3.1: Eigenspectrum for $M = 32$

The signal mobility is a signal complexity measure and is often used in the analysis of biomedical signals, such as EEG and ECG [110]. The mobility of an EEG signal recorded from healthy person will be high as compared with the EEG signal measured from the patient suffering from epilepsy. Moreover, when it is contaminated by either motion artifacts, the mobility of the EEG signal is still smaller. This is because, as motion artifact deviates the base line of EEG, that results less number of zero crossing. Hence, the mobility of an EEG signal contaminated by motion artifact is very small. When the EEG signal is contaminated by muscle artifact, its local mobility is increased. As the mobility of the signal measures the local variations of signal, we refer this as local mobility m_v of a signal. Fig. 3.2 shows $10\,s$ EEG epochs in different conditions and their local mobility m_v. It is noticed that when EEG signal is contaminated by motion artifact its m_v is very small as compared with EEG signal in other conditions.

First, after computing the eigenvalues and eigenvectors of a covariance matrix $\mathbf{C}$, using either eigendecomposition or SVD, unlike in traditional SSA, where the magnitudes of eigenvalues are used to group the components, here, the local mobility of each eigenvector is computed to group them. Eigenvectors of a covariance matrix basically describes the variability of the data. Therefore, we except that the local mobility of eigenvector associate to the motion artifact is small as compared with the eigenvector associated to the EEG. Hence, the use of such signal complexity measure might be useful in the grouping the eigenvectors associated to the EEG and artifact signals. The local mobility m_v of k^{th} eigenvector vector $\mathbf{v}_k = [v_k(1), v_k(2), ..., v_k(M)]$, defined as in [110] is given by

$$m_v = \frac{f_1}{f_0} \tag{3.1}$$

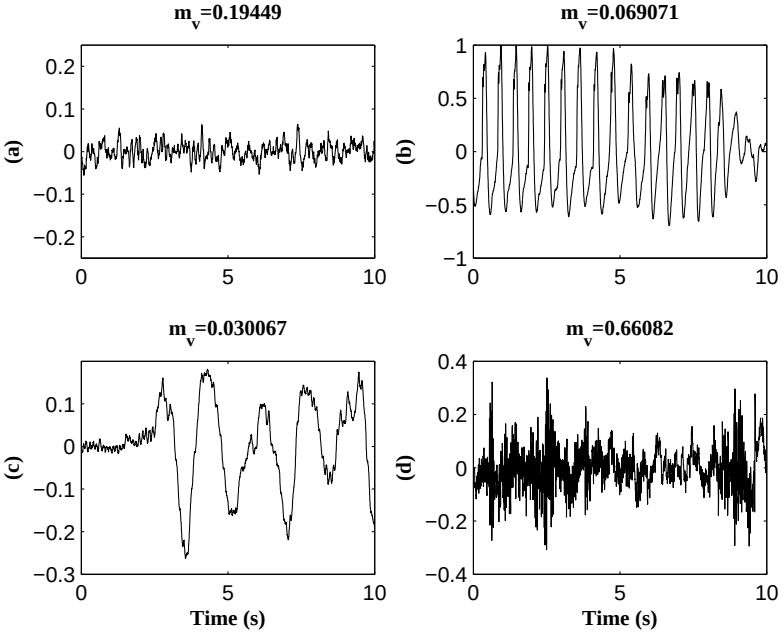

FIGURE 3.2: EEG signal (a) during normal state, (b) during epilepsy, (c) contaminated by motion artifact and (d) contaminated muscle artifact, respectively

where,

$$f_1 = \sqrt{\frac{\sum_{n=2}^{M-1} y^2(n)}{M-1}} \qquad and \qquad f_0 = \sqrt{\frac{\sum_{n=1}^{M} v_k^2(n)}{M}} \tag{3.2}$$

The difference signa $y(n) = v_k(n) - v_k(n-1)$, $n = 2, 3, ..., M-1$. It is clear that f_1, which represents the average of the difference signal and is increases with the local variations of $\mathbf{v}_k$. Whereas, it will be small when the local variations of $\mathbf{v}_k$ is small. In other words, the local mobility of the eigenvectors associated to artifact (low for motion and eye blink artifacts) is small and it is increased for eigenvectors associated to the EEG signal. We exploited this fact to separate the basis function (eigenvectors) associated to the artifact component and EEG component. However, to distinguish these basis function, pre-computed threshold is used. As most of the energy associated to motion artifact is below $4Hz$, we computed the local mobility of a sinusoidal signal of $4Hz$ and set as threshold to identify the eigenvectors corresponding the motion artifact. Using this pre-computed threshold, the eigenvectors associated to the desired signal were identified and the corresponding trajectory matrix computed. Finally, the estimated trajectory matrix is mapped into single channel EEG signals using (2.15), as discussed in Chapter 2.

3.3 Simulation Studies

In order to validate the performance of the modified SSA technique, we considered motion artifact contaminated single channel EEG signals recorded using a novel technique proposed in [5]. This technique involves the recording of two highly correlated EEG signals measured using two active electrodes chosen from an array of 256 electrode cap secured to the scalp of the subject under test. The two recordings are taken from electrode positions Fpz and Fp_1 over the scalp. To make proper contact with the scalp, an electrode gel is applied under the two electrodes. Using these two electrodes, labeled as channel 1 and channel 2, two EEG signals were recorded. As the spacing between them is $20mm$, recorded two EEG signals were highly correlated. While recording the EEG signals, the subject is advised not to perform any activity. Moreover, in order to minimize the other artifacts such as ocular and movement artifacts, subject is also instructed to keep their eyes closed and stationary head position throughout the experiment. In order to induce an electrode motion artifact in one of the measured EEG signals, for every 2-min interval, channel 2's electrode is mechanically disturbed by pulling on the connective lead. As the electrode cap is manufactured by a fabric material, the movement of one electrode (channel 2) can not alter the position of the adjacent electrode (channel 1), therefore the EEG signal recorded from first electrode or channel 1 is more immune to the induced motion artifact.

The EEG signals so obtained are maintained in Physio Bank Database [3]. This data comprises two highly correlated EEG signals: one is an artifact free EEG signal (channel 1), *i.e.* "ground truth" and the other is the motion artifact contaminated EEG signal (channel 2). As these EEG signals recorded at high sampling rate ($f_s = 2048Hz$), the computational load at the signal processing stage is increased, thus results in increased processing time [111]. To reduce the processing time, first the raw EEG signals were down-sampled to $256Hz$. However, as the EEG signals were recorded from the frontal lobe of each subject with eyes closed, most of the EEG components will fall in the frequency band $0.5Hz - 30Hz$. Hence, the raw EEG signals were filtered by an appropriate second order Butterworth band-pass filter with lower and upper cut-off frequencies $0.5Hz$ and $30Hz$ respectively.

The contaminated as well as the ground truth EEG signals, and it's zoomed version

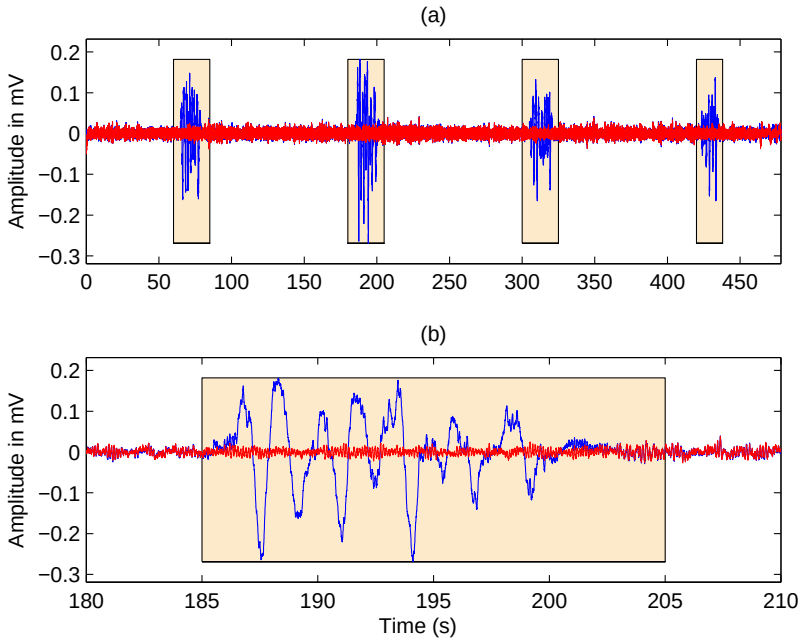

FIGURE 3.3: (a) Superimposition of contaminated EEG signal (blue) and the ground truth EEG signal (red), (b) zoomed portion of plot (a) in the time interval $180 - 210\,s$.

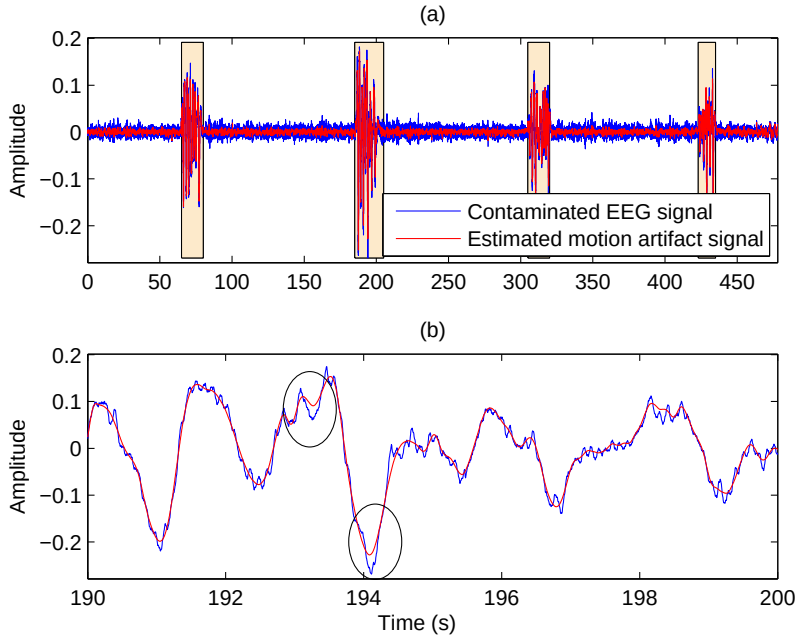

FIGURE 3.4: (a) Superimposition of contaminated EEG signal and the estimated motion artifact signal by EEMD-CCA, (b) the zoomed portion of the above plot in the time interval $190 - 200\,s$.

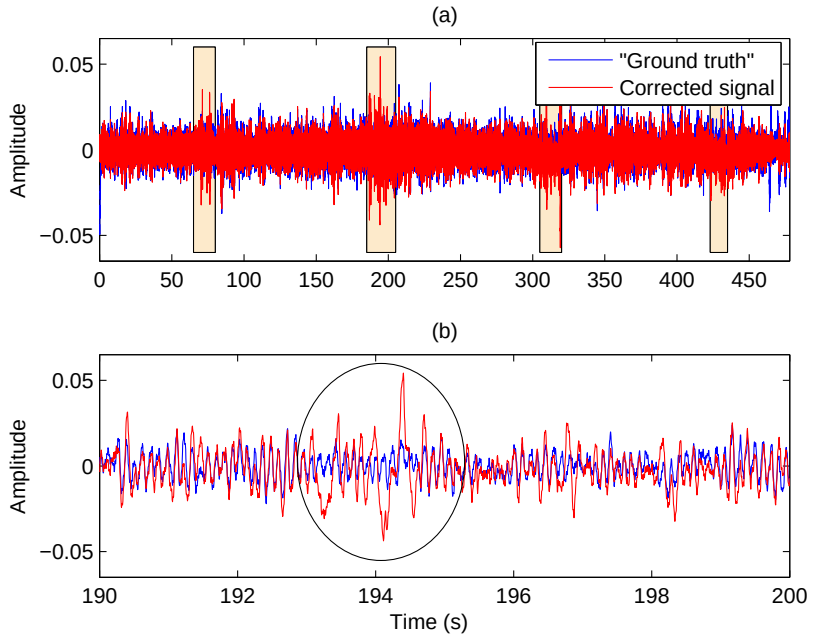

FIGURE 3.5: (a) Superposition of ground truth EEG signal, and the corrected EEG signal by EEMD-CCA technique, (b) the zoomed version of the above plot in the time interval $190 - 200\,s$.

between the time interval $180 - 210s$ are shown in Fig. 3.3(a) and Fig. 3.3(b) respectively. Before employing the EEMD-CCA technique on single channel EEG signal, its free parameters, such as the number of ensembles (ne) and the noise parameter (np) are set to 5 and 0.1 times the standard deviation (SD) of the signal respectively. Fig. 3.4(a) shows the super imposition of the contaminated EEG signal (blue) and the estimated motion artifact signal (red). In order to have a clear view of the estimated motion artifact signal obtained by EEMD-CCA technique, the magnified version of Fig. 3.4(a) between the time interval $190 - 200s$ is shown in Fig. 3.4(b). It is clear from Fig. 3.4(b) (encircled portion) that the EEMD-CCA technique failed to extract the motion artifact faithfully. Fig. 3.5(a) shows superimposition of the corrected EEG signal (resulted by subtracting the estimated motion artifact from the contaminated EEG signal) and the ground truth signal. The corresponding magnified version of Fig. 3.5(a) between time interval $190 - 200s$ is shown in Fig. 3.5(b). It is observed from Fig. 3.5(b) that the remnants of the motion artifact signal were present in the corrected EEG signal, marked in the circle. This is because of the fact that the correlation coefficient ρ between the sources hidden in the lower set of $IMFs$, for example, $IMF14$ to $IMF16$ as shown in Fig. 3.7, and its delayed version is almost same and hence the condition in (2.5) may not be hold.

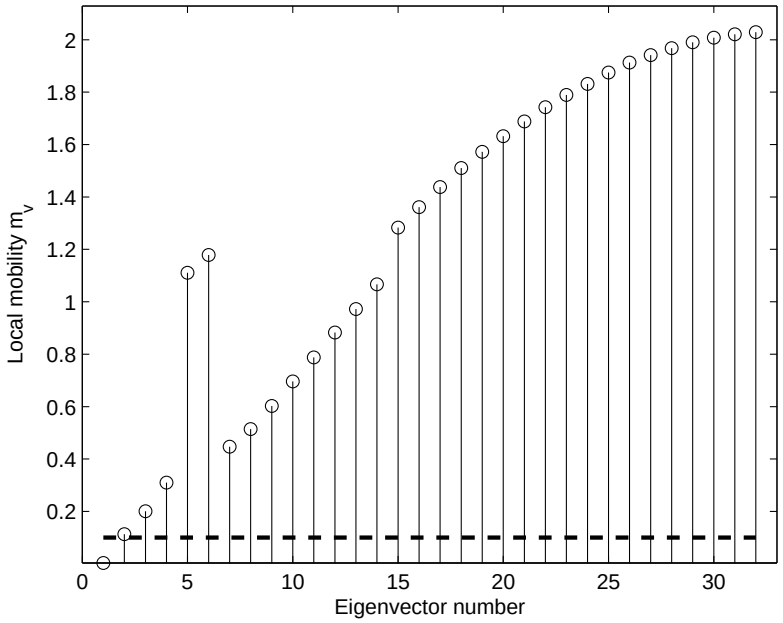

FIGURE 3.6: Local mobilities of M eigenvectors, dashed line indicates the threshold to identify the eigenvectors corresponds to the motion artifact signal.

This problem can be overcome by using the proposed modified SSA technique. After the application of embedding step, for window length $M = 32$ and SVD step of SSA on the contaminated EEG signal, the local mobility of each eigenvector is computed. Fig. 3.6, illustrates the local mobility of 32 eigenvectors, the dotted line indicates the threshold and is set to 0.1. It is clear from Fig. 3.6 that the eigenvector *i.e.* $\mathbf{q}_1$ is the basis vector to extract the motion artifact signal. The estimated trajectory matrix of the motion artifact signal $\hat{\mathbf{A}} = \mathbf{v}_1\mathbf{v}_1^T\mathbf{X}$ can be obtained by projecting the data matrix $\mathbf{X}$ onto the subspace span by the eigenvector $\mathbf{v}_1$. By performing the diagonal averaging step in (2.15)on the trajectory $\hat{\mathbf{A}}$, the motion artifact signal is derived as single channel signal and is subtracted from the contaminated EEG signal to obtain corrected EEG signal. The estimated motion artifact and the corrected EEG signal using the modified SSA technique were shown in Fig. 3.8 and Fig. 3.9 respectively. From Fig. 3.8(b), it is observed that the modified SSA technique efficiently extracts the motion artifact and hence, the corrected EEG is not having any remnants of the motion artifact, as shown in Fig. 3.9(b). We have also plotted the power spectral density (PSD) of contaminated and corrected EEG signals obtained by EEMD-CCA and the modified SSA techniques shown in Fig. 3.10. From Fig. 3.10, it is clear that the remnants of the motion artifact $(0.5 - 4Hz)$ still present in the corrected EEG signal, obtained by EEMD-CCA and are

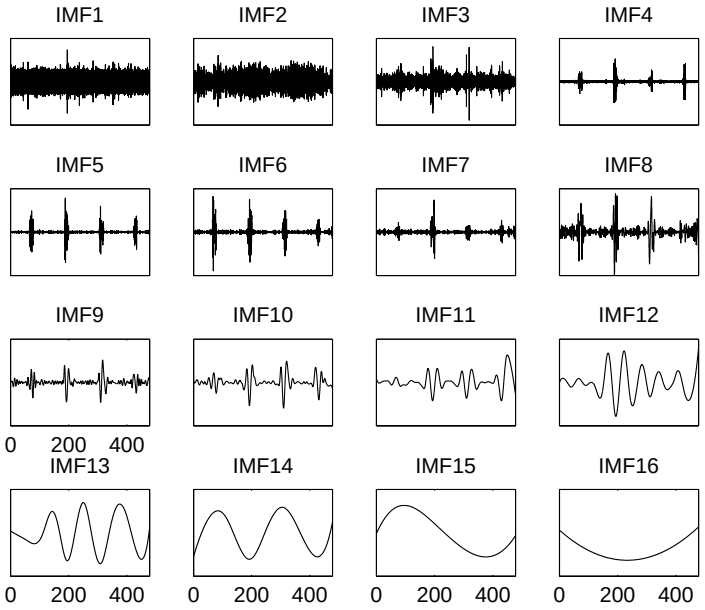

FIGURE 3.7: EEMD decomposition of motion artifact contaminated EEG signal.

not present in the corrected EEG signal obtained using the modified SSA techniques.

3.3.1 Performance measures

To quantify the ability of the proposed modified SSA technique in the removal of motion artifact from a single channel EEG signal, we consider two performance measures, namely, the difference in the signal to noise ratio ΔSNR and the percentage reduction in artifact η. The difference in SNR is given by

$$\Delta SNR = 10\,log_{10}\left(\frac{\sigma_a^2}{\sigma_{r_{after}}^2}\right) - 10\,log_{10}\left(\frac{\sigma_a^2}{\sigma_{r_{before}}^2}\right) \tag{3.3}$$

where σ_a^2 is the variance of the "ground truth signal" and $\sigma_{r_{before}}^2$ and $\sigma_{r_{after}}^2$ are the variance of the error signal before and after performing the artifact removal operation. Here, the error signal is the difference between the contaminated and ground truth EEG signals. The percentage reduction in artifact η is given by

$$\eta = \left(1 - \frac{C_{clean} - C_{after}}{C_{clean} - C_{before}}\right) \times 100 \tag{3.4}$$

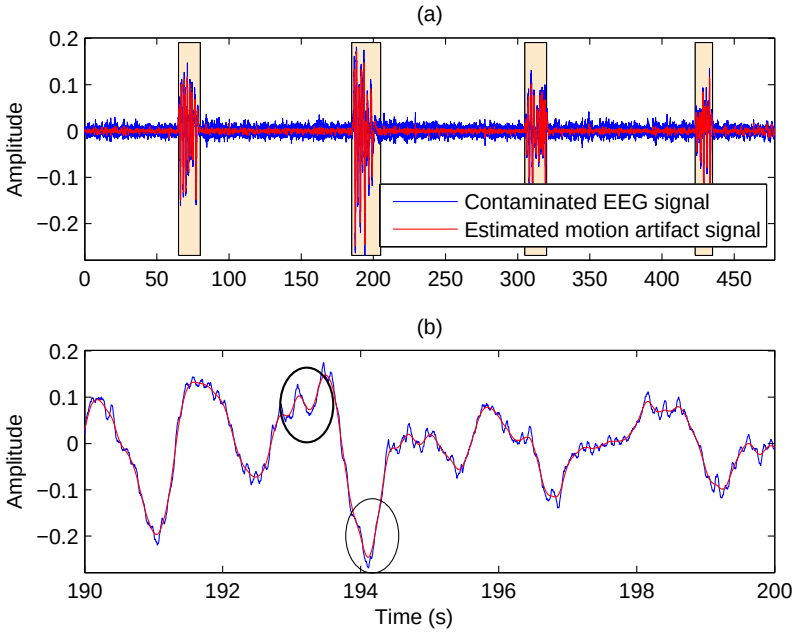

FIGURE 3.8: (a) Superimposition of contaminated EEG signal and the estimated motion artifact signal by the proposed modified SSA technique, (b) the zoomed portion of the above plot in the time interval $190 - 200s$.

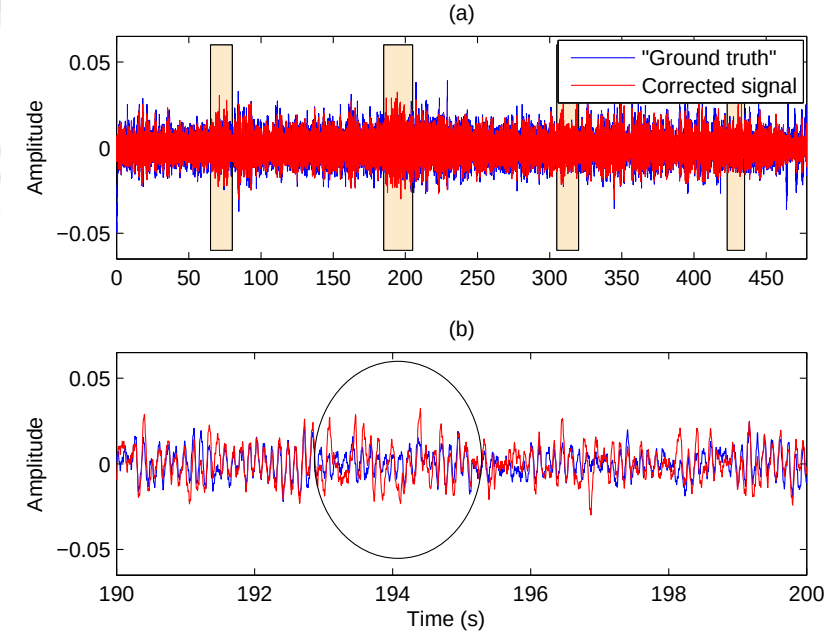

FIGURE 3.9: (a) Superposition of ground truth EEG signal and the corrected EEG signal by the proposed modified SSA technique, (b) the zoomed version of the above plot in the time interval $190 - 200s$.

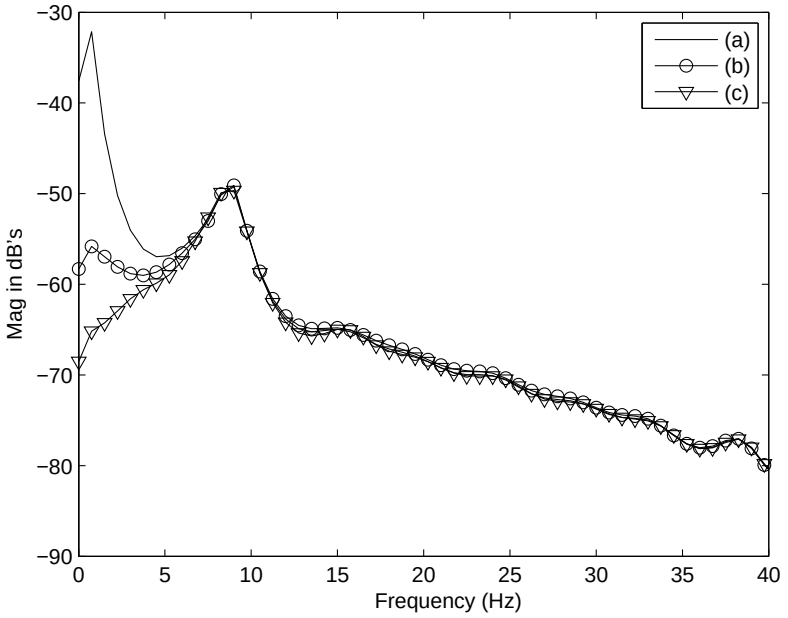

FIGURE 3.10: PSD of (a) contaminate EEG signal, (b) corrected EEG signal by EEMD-CCA and (c) corrected EEG signal by the proposed modified SSA respectively.

where C_{before} is the correlation between the ground truth signal and the motion artifact contaminated EEG signal, C_{after} is the correlation between the ground truth signal and corrected EEG signal and C_{clean} is the correlation between the contaminated and ground truth EEG signals over an artifact free time interval and on an average for all records it is found to be 0.9. It is worth noting that efficient artifact reduction is achieved if $C_{after} \approx C_{clean}$. However, this depends on how well the artifact removal technique estimates the motion artifact signal.

To quantify the results, 23 single channel EEG records are considered. After visual inspection of all records, it is found that no brain activity is registered in 12 and 15 records. Moreover, the poor correlation coefficient was found over the clean epochs, *i.e.* non shaded region as shown in Fig. 3.3. Hence, we tested the proposed modified SSA technique on the remaining 21 motion artifact contaminated single channel EEG records in which α component of the EEG signal is registered. Fig. 3.11 shows the comparison of proposed modified SSA and the EEMD-CCA technique in terms of ΔSNR, and η. It is clear from Fig. 3.11 that for all the records there is an improvement in ΔSNR, as well as in η, using the proposed modified SSA technique. On average, there will be $0.91507dB$ improvement in ΔSNR and 11.388% improvement in η.

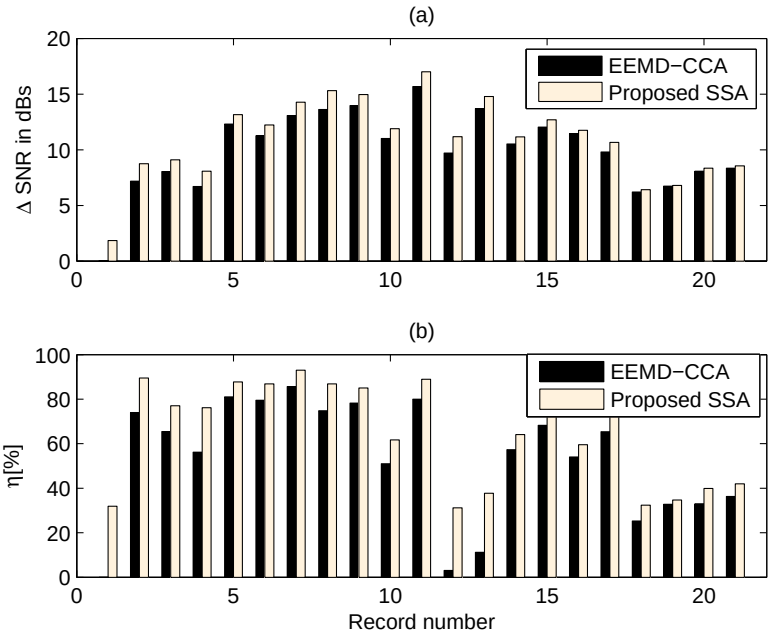

FIGURE 3.11: Performance comparison of EEMD-CCA and proposed modified SSA techniques in terms of (a) ΔSNR and (b) η.

TABLE 3.1: Computational Complexities of EEMD, CCA, EEMD-CCA and proposed modified SSA techniques.

Methods	Computational Complexity
EEMD	$N_e N_s(41 N_{imf} N)$
CCA	$5NJ^2 + 5NJ + 19J^3/3$
EEMD-CCA	$N_e N_s(41 N_{imf} N) + 5NJ^2 + 5NJ + 19J^3/3$
Proposed modified SSA	$M^2K + M^3 + M^2(1+K) + NM$

3.4 Computational complexity Analysis

In order to compute the computational complexities of EEMD, CCA, EEMD-CCA and the proposed modified SSA techniques, we considered N sampled signal vector. As the first step in the proposed modified SSA technique involves mapping of univariate signal into multivariate data, no computations are required. In the second step of the proposed modified SSA, the SVD of $\mathbf{D}$ is computed in two steps: first, finding the covariance matrix $\mathbf{C}$ and secondly computing the eigendecomposition of $\mathbf{C}$. The computation of the covariance matrix of $\mathbf{D}$ of size $M \times K$, involves $\mathcal{O}(M^2K)$ computations. In addition, $\mathcal{O}(M^3)$ computations are needed to find eigendecomposition of $\mathbf{C}$, as the covariance matrix $\mathbf{C}$ is a square matrix. The third step in the proposed modified SSA

is estimating the trajectory matrix of motion artifact signal using (2.12), which involves $\mathcal{O}(M^2(1+K))$ computations. For evaluation of the final step of proposed modified SSA, $\mathcal{O}(NM)$ computations are needed to map the estimated trajectory matrix into single channel signal. To compare the computational complexity of the proposed modified SSA technique with EEMD-CCA, we define the free parameters N_e, N_s, N_{imf} and J as the number of ensembles, the number of sifting operations, the number of IMFs and the number of observations. Then, the computational complexity of the EEMD as reported in [112] is $\mathcal{O}(41N_eN_sJN)$ computations. In practice, to make use of CCA on single channel signal, first it should be mapped into multivariate data. In EEMD-CCA, this will be performed by EEMD. As the output of EEMD is given as input to the CCA, the number of observations $J = N_{imf}$. So, the computational complexity of CCA as it is claimed in [113] is $\mathcal{O}(5NJ^2 + 5NJ + 19J^3/3)$ computations. Finally, the overall computational complexity of EEMD-CCA is equal to the sum of individual complexities of both EEMD and CCA. Table 3.1. provides the overall computational complexities of EEMD, CCA, EEMD-CCA and proposed modified SSA techniques. For $N = 2560$, $M = 32$, $N_e = 5$, $N_s = 5$ and $J = N_{imf} = 11$, proposed modified SSA technique reduces the computational complexity by factor of $five$ times compared with the EEMD. Although CCA reduces the computational complexity $three$ time compared with the proposed modified SSA technique, CCA alone can not be used for single channel signal analysis. For single channel EEG signal analysis, CCA has to be used in combination with EEMD which can increase the overall complexity. From Table . 3.1 it is clear that for the parameters mentioned above, the proposed modified SSA technique reduces the computational complexity by a factor of approximately six times compared with EEMD-CCA.

3.5 Conclusion

In this chapter, grouping step issue in traditional SSA technique is discussed and a new grouping criteria proposed. To evaluate the performance of modified SSA technique, it is used to remove the motion artifacts from single channel EEG signals. The proposed SSA technique gains approximately $1dB$ improvement in the difference signal to noise ratio and 11.388% improvement in percentage reduction in motion artifact. In addition to that the computational complexity of the modified SSA technique is analyzed and

showed *six* times faster than the EEMD-CCA technique, which enables the low power implementation of ambulatory EEG health care systems.

4

Removal of EOG Artifact from Single Channel EEG Signal using SSA-ANC Technique

With the recent advancement in technology, the use of portable brain computer interface (BCI) systems has been increased, in which the features of single or few EEG channels signals were used to control the output device. Several studies claimed that the performance of BCI system will be degraded due to presence of EOG artifacts. In this chapter, an adaptive noise canceler (ANC) is used to remove EOG artifact from single channel EEG signal. However, to process the EEG signals, ANC need a reference signal (EOG signal) and is recorded from eye site using a separate electrode. In general, the electrode over the eye is very discomfort to the subject under test. To avoid this SSA technique which extract the reference signal for ANC from the contaminated EEG is presented in this chapter. Further, the estimated reference EOG signal using SSA is applied to ANC to remove the EOG component. Simulation results presented its performance over the existing technique.

4.1 Introduction

Conventional augmentative communication is not possible for the people who are suffering from motor disability, for example a person with totally paralyzed or locked-in. For such people, the brain computer interface (BCI) provides a new communication channel [114–122]. Basically, in BCI systems the features of EEG signals were used to control the output device. In general, while recording EEG signals, the physiological artifacts originated from the non-cerebral regions (eye and facial muscles) often contaminates the EEG signals. The presence of such artifacts will modify the neurological phenomenon in the measured EEG signal that needs to drive the BCI system [123, 124]. In this chapter, we mainly focussed on the removal of EOG artifact. In [30, 31], it is claimed that the presence of EOG artifacts degrades the performance of BCI system. One possible solution to reduce these artifacts in the measured EEG signals is instructing the subject to make no eye blink or movement. But, such instruction may impose the secondary task on the subject who is under test. Hence, the removal of eye blink artifacts plays an important role in the EEG signal processing.

In the early stages, the regression-based techniques both in time and frequency domain often used to remove the EOG artifacts [125, 126]. In these techniques, the average transfer coefficients between the EOG and each EEG channels were estimated using calibrated EEG data measured in various conditions. However, as the EEG and EOG signals are non-stationary signals, the average transfer coefficients are inadequate to remove EOG artifact from the real-time EEG signals. Hence, there is a need of adaptive filters [127] to track such non-stationary signal variations is highly desirable. Independent component analysis (ICA) is blind source separation (BSS) technique extensively used to remove EOG artifacts from multichannel EEG data [38–44]. But, ICA can be applied on single channel EEG signals, as it demands the number of channels should be more or equal to the sources to be decomposed.

Adaptive noise cancelers (ANCs) [77] are widely used to remove artifacts from the biomedical signals [78–81]. However, all these techniques assumes that the reference signal for ANC is available. In [128], ANC has been used along with the ICA to identify the independent components representing the EOG artifact. The reference signals for ANC is obtained by employing the ICA on the EEG signals recorded at electrodes closet

to the eye (F_{p_1} or F_{p_2}). However, this technique is applicable for analysis of multichannel EEG signals and hence cannot applicable for portable BCI devices.

Recently, the use of subspace based technique, such as singular spectrum analysis (SSA) [67, 68], has been used to remove high amplitude EOG artifact from single channel EEG signals [69, 129]. In this technique, the feature vectors of the embedded matrix, obtained by arranging delayed version of original signal, are clustered by k-means [130] algorithm. The eigenvalues and the eigenvectors of the covariance matrix of each cluster are computed using singular value decomposition (SVD). In order to estimate EOG artifact, the minimum description length (MDL) [109] criteria is used, which gives the information regarding the dimension of signal subspace or the number of eigenvectors needed to estimate the EOG signal. However, for reliable estimation of the dimension of the signal subspace using MDL criteria is not possible when the magnitude difference between the eigenvalues, representing EOG and EEG signals is small [129]. Particularly, in frontal EEG signals EOG artifact appears as high magnitude signal, therefore, the local SSA exhibits good performance in removing EOG artifact. In applications, such as BCI motor imagery task, to capture the useful information associated to the power differences in EEG α $(8-12Hz)$ and β $(18-26Hz)$ rhythms [131], EEG signals often measured from the electrode positions C_3 and C_4 [132]. As these electrodes are far from the eye site, which is a source of generating EOG artifact, the contribution (magnitude) of EOG component in the measured EEG signal is small compared with the EEG signal recorded from the frontal electrodes. As the contribution of EOG component is small, there will be no much difference in the magnitudes of eigenvalues associated to the EOG and EEG components. Hence, minimum description length criteria fail to estimate the appropriate dimension of the signal subspace corresponding to the EOG, therefore, the corrected EEG signal still having the remnants of the EOG artifact.

Recently in [71], adaptive line enhancer (ALE) based on the SSA has been proposed to separate electrocardiogram (ECG) signal from the electromyogram (EMG) signals by exploiting the periodicity of ECG signal. Unlike ANC, where two separate inputs are needed to filter out the artifact, here, by exploiting the periodicity of the artifact (ECG) present in the contaminated signal (EMG) and its delayed version, the ALE removes the ECG artifact signal. In general, this delay is set based on the periodicity of the artifact present in the contaminated signal. However, as EOG signals is non-periodic signal, such technique exhibits poor performance in removing the EOG artifact from the EEG signal.

More recently, a combined use of discrete wavelet transform (DWT) and ANC, namely DWT-ANC, has been proposed in [85] to remove EOG artifact from EEG signals. In this technique, firstly, the DWT is used to construct the reference signal, *i.e.* EOG, from the contaminated EEG signal and applied to reference input of the ANC. Finally, the ANC removes the EOG artifact from the contaminated EEG signal by changing the adaptive filter coefficients based on the adaptive algorithm. However, the performance of this technique mainly depends on how good is the reference signal (EOG) estimated by DWT, which in turn depends on the selection of wavelet function and the number of decomposition levels. However, the selection of wavelet function and decomposition levels depends on the morphology of the EOG artifact and its frequency spectrum.

In order to overcome these limitations, in this chapter, we combined SSA with ANC, shortly called SSA-ANC, to remove EOG artifact from the single channel EEG signal. SSA is a subspace based decomposed technique represents the given signal into trend, oscillating and noise components. However, it is extensively used in the analysis of climatic and geophysics time series [67, 68]. Like in DWT-ANC technique, the reference signal needed for ANC is estimated from the contaminated EEG signal using SSA. To estimate the reference EOG signal for ANC, local mobility of the eigenvectors is accounted. As the EOG signal is reconstructed based on heuristic approach, (*i.e.*, threshold defined by the user), EOG artifact is partially reconstructed. Hence, direct subtraction of this component from the contaminated signal may retain some of the EOG components in the corrected EEG signal. To remove the remnants of the EOG artifact, we combined with ANC. Simulation results show that proposed SSA-ANC technique exhibits better performance than the DWT-ANC.

4.2 SSA-ANC Methodology to Remove EOG Artifact from Single Channel EEG signal

Consider SSA-ANC based EOG artifact removal system as shown in Fig. 4.1, that receives the contaminated EEG signal $x(n) = s(n) + pr_1(n)$, with $s(n)$ representing EEG signal and $r_1(n)$ representing the EOG artifact. The parameters p is a propagation constant which decides the contribution of EOG signal in $x(n)$ and is assumed as one in Fig. 4.1. As the SSA technique can be operated on block of data, first, the incoming

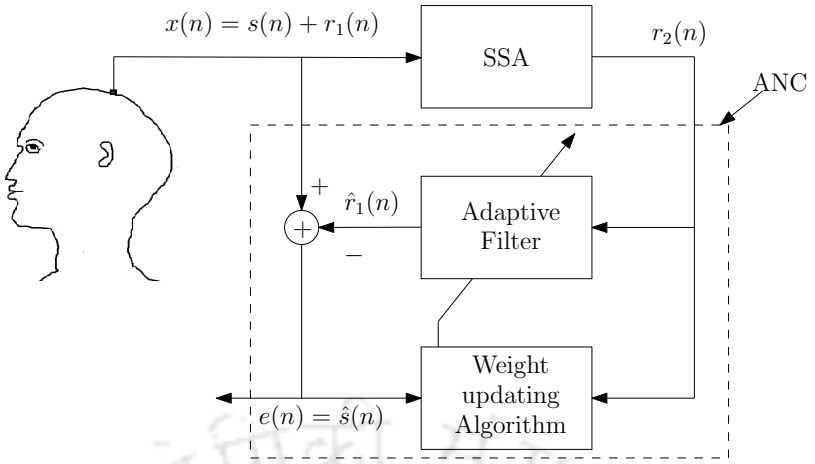

FIGURE 4.1: Block diagram of SSA-ANC technique.

data sequence $x(n)$ is stored into a buffer of length N, results a signal vector $\mathbf{x} = [x(1), x(2), ..., x(N)]$. After that, SSA is applied on the signal vector $\mathbf{x}$ to extract reference signal for the ANC.

4.2.1 Extraction of EOG reference signal for ANC

The critical step in SSA is identifying the subspace of the interested signal. In [69, 129], MDL criteria has been proposed to automatically identify the subspace of the EOG signal. However, such criteria impose constraint that the energy of the signal of interest should be high and it should be well defined signal. For example, in the EEG signal recorded at frontal electrodes F_{p_1} or F_{p_2} the magnitude of EOG artifact is high and well defined or clearly observable, hence such criteria might work well. But, for some specialized applications such as motor imagery task in BCI, the EEG signals often recorded from the C_3 and C_4 electrode positions, where the contribution of EOG artifact in EEG signal is small as compare with the EEG signal recorded from the frontal electrode positions. This is because of the fact that the placement of the EEG electrode is far from the site of the eye. So, in such conditions, the use of MDL criteria gives false estimation of the EOG signal subspace dimension. Therefore, unlike in local SSA, where the signal subspace is identified based on the magnitudes of the eigenvalues, we use a novel grouping criteria based on the local mobility of the eigenvectors, as discussed in Chapter 3, to identify the approximate EOG signal subspace. Here, in order to identify the subspace of EOG signal, first, local mobility of each eigenvector is computed. Later, by setting the threshold, which is selected based on priory information, such as max frequency

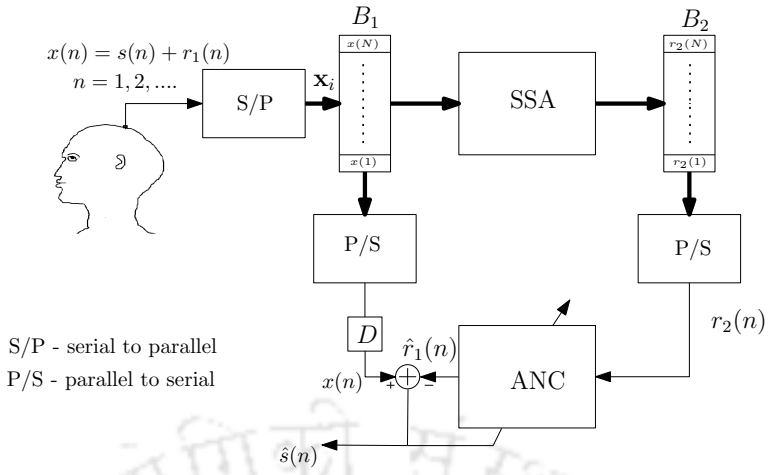

FIGURE 4.2: Proposed SSA-ANC technique for online removal of eye blink artifact.

of EOG signal, the arguments of the corresponding eigenvectors are identified. Once after identifying the eigenvectors representing the EOG signal, corresponding trajectory matrices are estimated by computing equation (2.12). After adding all the trajectory matrices, representing the EOG signal, the resultant trajectory matrix is mapped into single channel EOG signal vector $\mathbf{r}_2 = [r_2(1), r_2(2), ..., r_2(N)]$.

After estimating the reference EOG signal using SSA, the contaminated EEG $\mathbf{x}$ and the extracted EOG signal vectors $\mathbf{r}_2$ are fed to primary and reference inputs of the ANC respectively. Adaptive filter process these two signals sample by sample by updating the filter coefficients using RLS algorithm. The estimated reference EOG signal $\hat{r}_1(n)$ at the output of the filter is subtracted from the contaminated EEG signal $x(n)$ at every time instant n, results a corrected EEG signal $\hat{s}(n)$. This process will be repeated for each block of data separately.

4.2.2 Real Time Implementation of Proposed SSA-ANC Technique

It is assumed that EEG data is fed to the proposed SSA-ANC technique showed in 4.1 block by block. However, to make use of the proposed technique for online removal of EOG artifact, its modified version is presented in Fig. 4.2. Let us consider continuous EEG signal $x(n)$, $n = 1, 2, ...$, recorded from scalp. First, the serial input samples are mapped into parallel data using serial to parallel (S/P) converter and loaded into buffer B_1 as a signal vector $\mathbf{x}_i$, where i is the block index. Next, the buffered data in B_1 is fed to SSA block to estimate the reference EOG signal for ANC (steps to extract the EOG signal is outlined in Section 4.2.1). Since ANC process the signal sample by sample, so,

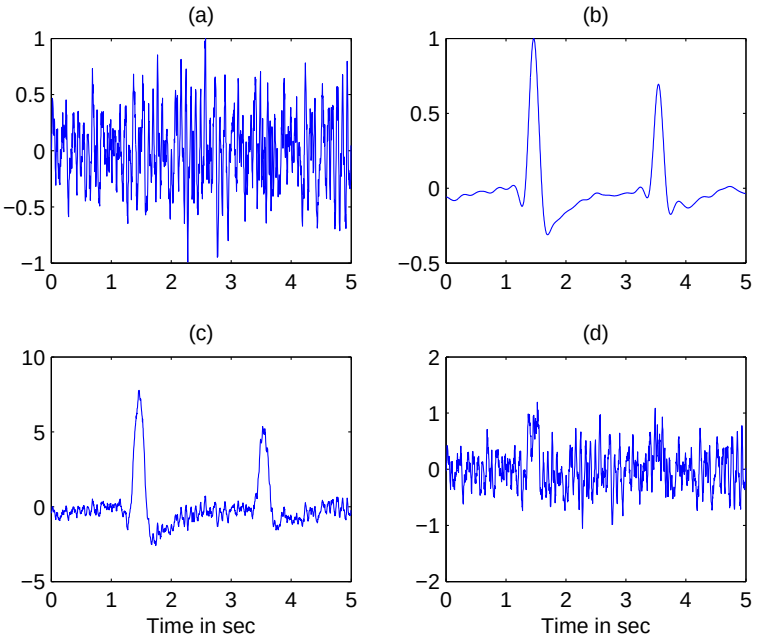

FIGURE 4.3: (a) True EEG signal $s(n)$, (b) EOG signal $r_1(n)$, (c) and (d) contaminated EEG signal $y(n)$ for $SNR = 0.2$ and 2, respectively.

first the estimated EOG signal is buffered into B_2 and fed to the reference input of ANC through parallel to serial (P/S) convertor. ANC modifies the filter coefficient based on the adaptive algorithm and estimates $\hat{r}_1(n)$. To obtain the corrected EEG signals, the output of ANC $i.e.\hat{r}_1(n)$ has to be subtracted from $y(n)$. However, the arrival time of these two samples at the summer should be same. For that the data in B_1 is mapped into serial data and passed through a delay D. To synchronize the arrival of these two samples at the summer, we set the delay time to $T_{SSA} + T_{AF}$. where, T_{SSA} the computational time of SSA and T_{AF} is the computation time of adaptive filter to process one sample. With the advancement in the technology sum of the computational time of SSA and adaptive filter is less than the sampling interval T_s. Therefore, the proposed technique is feasible for online removal of EOG artifact from single channel EEG signal.

4.3 Simulation Studies

To validate the performance of proposed SSA-ANC, simulations were performed on synthetic and real life contaminated EEG signal. In both cases, the following mixing model was used. We used relative root mean square error(RRMSE) on synthetic EEG signals and mean absolute error (MAE) between the contaminated and corrected EEG signals

in the frequency domain.

$$x(n) = s(n) + pr_1(n) \tag{4.1}$$

where, $s(n)$, $r_1(n)$ and $x(n)$ are the true EEG, artifact (EOG) and contaminated EEG signals, respectively. The term p is a propagation constant depends on the distance between the EEG electrode placement from the eye and hence decides the amount of EOG artifact buried in the EEG signal. The signal to nose ratio (SNR) of $y(n)$ is given by

$$SNR = \frac{\frac{1}{N}\sum_{n=1}^{N} s^2(n)}{\frac{1}{N}\sum_{n=1}^{N} pr_1^2(n)} \tag{4.2}$$

where, N represent the number of samples in the signal vector $\mathbf{y}$. Fig. 4.3, shows the true EEG signal $s(n)$ and EOG signal $r_1(n)$ as well as synthetically generated contaminated EEG signal $x(n)$ for two different SNR values 0.2 and 2. The synthetic contaminated EEG signal is generated as follows: we have considered a 5 sec of artifact free EEG epoch segmented from *slp*32 polysomnographic record [3, 133]. A five second EOG epoch is segmented from a lengthy EOG signal recorded from one of the author's left eye. Later, we removed high frequency components from that epoch by passing it through a low pass filter of cutoff frequency $5Hz$ and is added to the true EEG segment as per the model given in (4.1). To quantify the performance of both techniques, relative root mean square error (RRMSE) is used as performance measure and is defined as

$$RRMSE = \frac{RMS(\mathbf{s} - \hat{\mathbf{s}})}{RMS(\mathbf{s})} \tag{4.3}$$

where, $RMS(\mathbf{s})$ and $RMS(\hat{\mathbf{s}})$ represent the root mean square of true and corrected EEG signals, respectively.

In order to achieve better performance, in all the simulations the free parameters, *i.e.* wavelet function and number decomposition levels, for DWT-ANC, are set to Daubechies4 and seven decomposition levels. The reference signal (EOG) for ANC, is estimated by applying the soft threshold on the low level detailed coefficients (*i.e.* 3 or 5). In the case of proposed SSA-ANC technique, the window length L is chosen based on the criteria $M > f_s/f$ specified in [69]. Here, as we are interested in removing the EOG signal, and whose frequency is $< 4Hz$, f is set to $3.7Hz$. Thus, window length M is set to 68. Moreover, in order to identify eigenvectors corresponding to the EOG signal, we compute

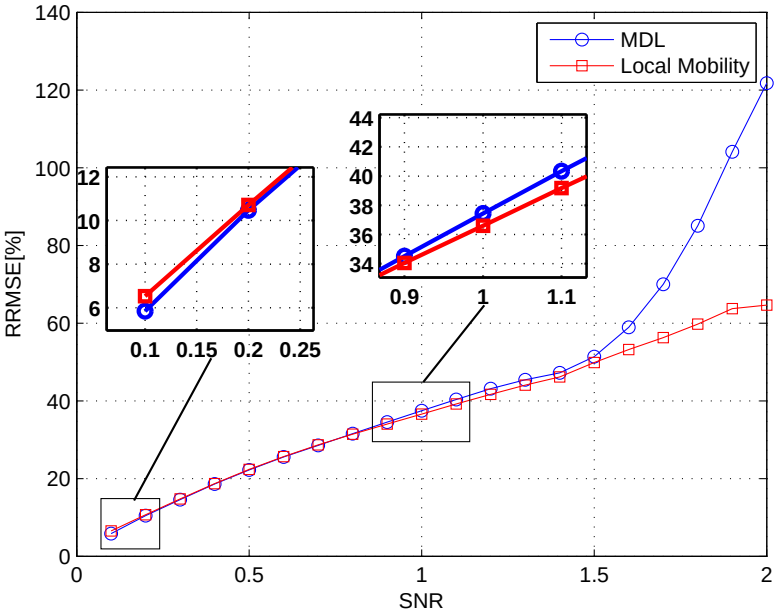

FIGURE 4.4: RRMSE in estimating the EOG artifact using MDL and local mobility criterions.

the local mobility m_f of a sinusoidal signal of frequency $3.7Hz$, given $m_f \approx 0.09$, thus threshold is set to 0.1. The reason for selecting sinusoidal signal for setting the threshold is that, as the eigenvectors are oscillating in nature. As the estimated reference signal and artifact in the EEG signal have high similarity, adaptive filter length P is set to one, which intern reduces the computational complexity and increases the convergence rate. The simulation results shows that even if adaptive filter order increases the performance improvement is marginal.

4.3.1 Comparative Study of MDL and New Grouping Criteria in the Removal of EOG Artifact

To evaluate the comparative study of both MDL and local mobility criterions, we consider the mixing model given in (4.1). Using the MDL and the local mobility criterions as a grouping techniques, SSA is applied on the single channel contaminated EEG signal and estimate the EOG artifact. The relative root mean square error (RRMSE) obtained in estimating the EOG artifact present in the measured EEG signal using MDL and local mobility criterions is shown in Fig. 4.4. It is observed from Fig. 4.4 that for the lower SNRs (0.1), where the EOG artifact is high in magnitude, the MDL criteria is better than the proposed local mobility criteria (shown as subplot in Fig. 4.4). This is due to

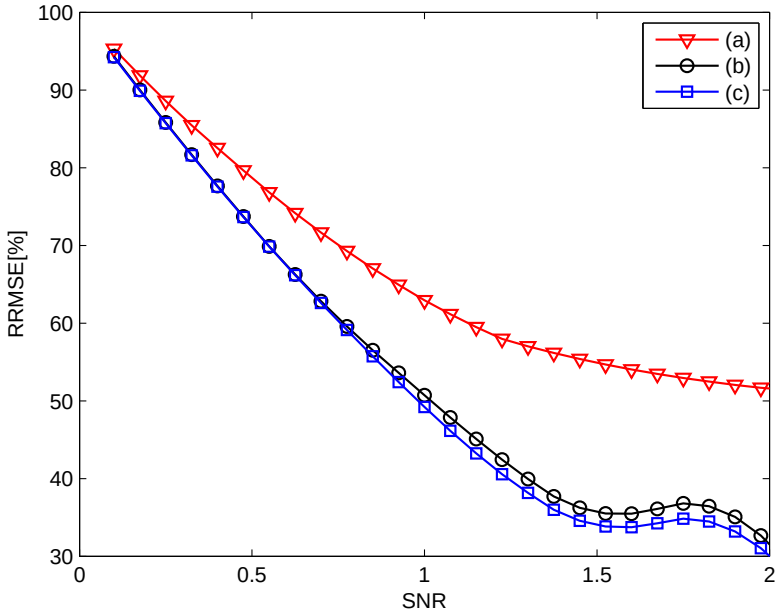

centering

FIGURE 4.5: RRMSE curves for corrected EEG signals using (a) DWT-ANC, (b) Proposed SSA without ANC and (c) Proposed SSA-ANC techniques, respectively.

the fact that the magnitude of the eigenvalues associated to the EOG artifact are well clustered from the eigenvalues associated to the EEG signal. Hence, the MDL criteria is able to find the EOG artifact subspace efficiently.

However, for higher SNRs (≥ 1), for example the EEG signals recorded at central electrodes *i.e.* C_3 and C_4, the contribution of EOG artifact is small in magnitude and so the magnitudes of the eigenvalues associated to the EOG and EEG signals are not well clustered. Hence, the MDL criteria fails to find the subspace of the EOG artifact for higher SNRs. In general as the EOG signal is a slowly time varying signal, the numerator quantity in (3.1) is small. Thus, the local mobility of the eigenvectors associated to the EOG artifact is small as compared with the local mobility of the eigenvectors associated with the EEG signal. Hence, the proposed local mobility criteria shows better performance than the MDL criteria for higher SNRs.

4.3.2 Simulation using Synthetic EEG signals

With the above parameter settings, DWT-ANC, proposed SSA without ANC and proposed SSA with ANC techniques are applied on synthetically contaminated EEG signal

for different $SNRs$. The RRMSE curves for the corrected EEG signals using the DWT-ANC, proposed SSA without ANC and proposed SSA-ANC techniques as a function of SNR are shown in Fig. 4.6. It is clear from the Fig. 4.6 that in terms of RRMSE the proposed SSA-ANC gives superior performance than the DWT-ANC and proposed SSA without ANC for different SNRs. It is clear from the Fig. 4.6 that for higher SNRs (≥ 1) it is found that introduction of ANC enables a reduction in RRMSE by 1.5% compared to SSA alone and 22% compared to the DWT-ANC. As the proposed SSA-ANC exhibits superior performance than SSA alone, in the subsequent simulations, the performance comparison of proposed SSA-ANC is made with DWT-ANC. Fig. 4.6 shows the estimated reference signals by DWT and SSA decomposition techniques from the contaminated EEG signal for $SNR = 1$. From Fig. 4.6 it is observed that the reference signal estimated by DWT has EEG components also, whereas SSA effectively estimate the reference signal without altering the EEG components. This can be observed in the reference signals as smooth base line in the artifact free time zones as compare with the reference signal estimated by DWT. The corrected EEG signals by DWT-ANC and proposed SSA-ANC techniques are shown in Fig. 4.7. It is clear from encircled portion of Fig. 4.7 (b) that the corrected EEG signal by DWT-ANC technique is deviates from the EEG signal. This is because of the mother wavelet function. But, the proposed SSA-ANC technique extract the EEG signal efficiently.

4.3.3 Simulation Results using Real Life EEG Signals

To assess the efficacy of proposed SSA-ANC technique on the real life contaminated EEG signals, we consider EEG data recorded for BCI motor imagery study [83, 134]. As this data is recorded for movement imagery task, there will be a α $(8 - 12Hz)$ component present in the measured EEG signal. To evaluate the proposed SSA-ANC technique on this data, 8 sec of EEG epoch contaminated by EOG artifact is considered. Fig. 4.8. shows the estimated EOG reference signal and corrected EEG signal by DWT-ANC.

It is noticed from Fig. 4.8(b)-(c) that the reference and corrected EEG signals using DWT-ANC are poorly reconstructed, shown in circle. The reason is that the morphologies of the wavelet function and eye blink at that instant are not matched. From these results it is noted that the performance of the DWT-ANC is depends on the selection of mother wavelet function. In the proposed SSA-ANC technique, after performing first

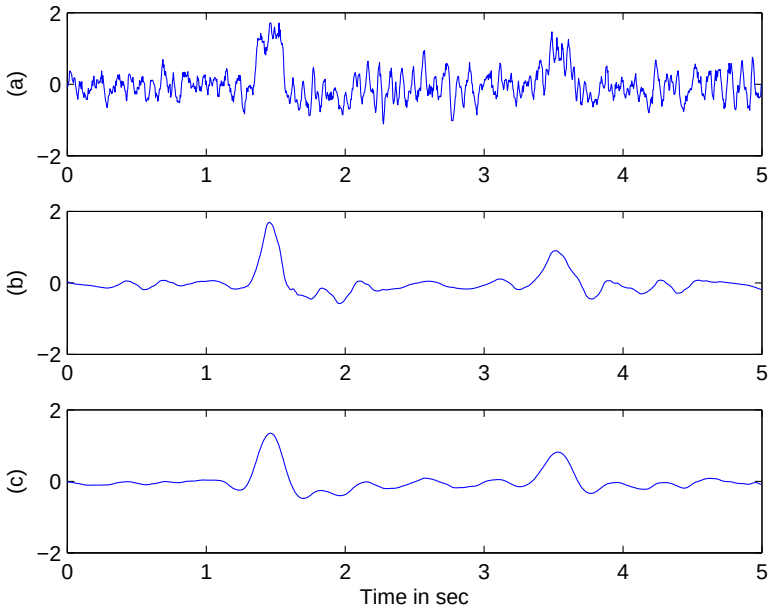

FIGURE 4.6: (a) synthetic contaminated EEG signal $y(n)$ for $SNR = 1$, (b) extracted reference signals for ANC using DWT and (c) extracted reference signal for ANC using SSA.

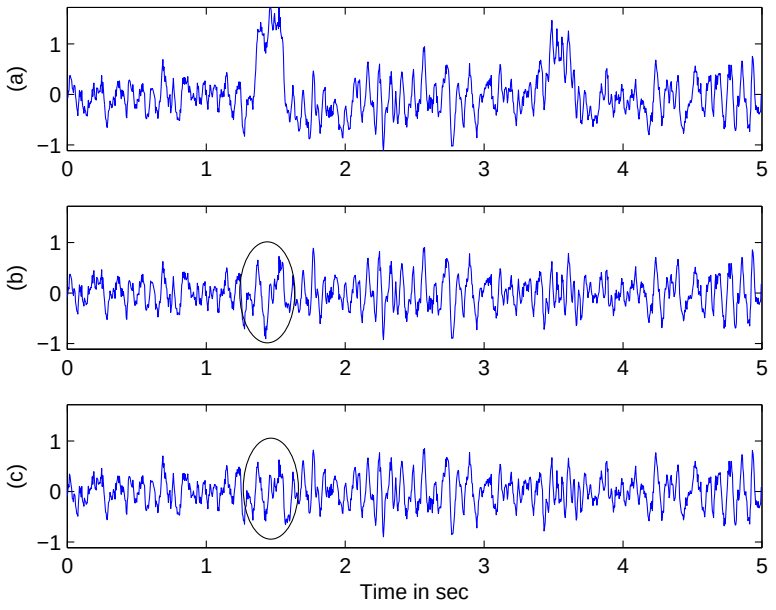

FIGURE 4.7: (a) Synthetically contaminated EEG signal $y(n)$ for $SNR = 1$, (b) corrected EEG signal by the DWT-ANC and (c) corrected EEG signal by the proposed SSA-ANC.

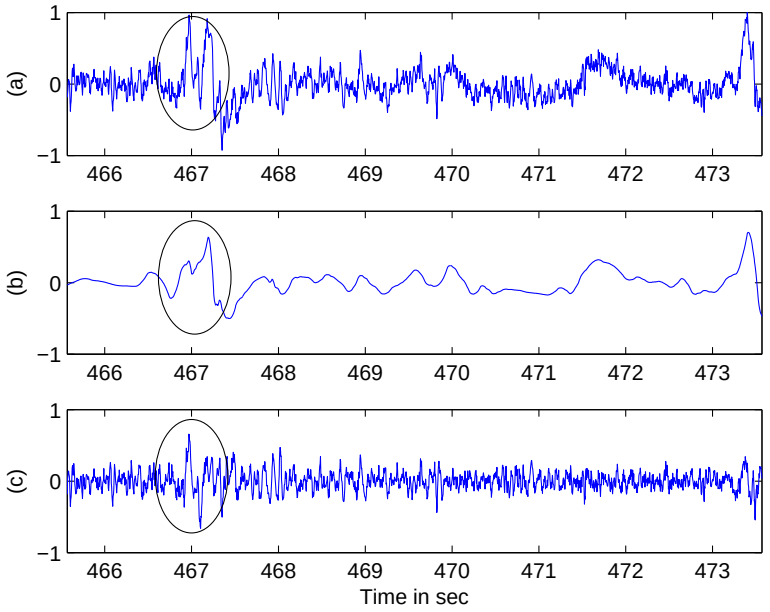

FIGURE 4.8: (a) contaminated EEG signal, (b) estimated reference signal for ANC using DWT and (c) corrected EEG signal by DWT-ANC.

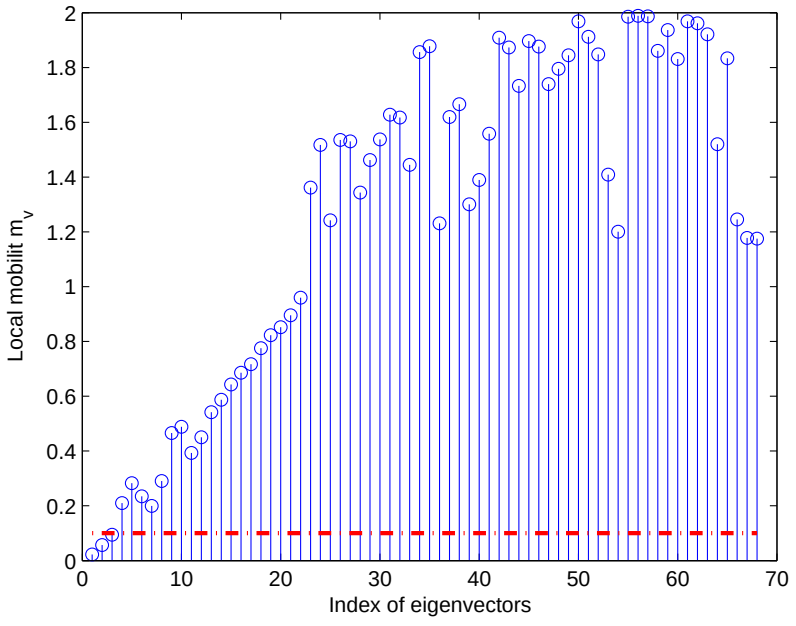

FIGURE 4.9: Local Mobilities of eigenvectors for window length $L = 68$.

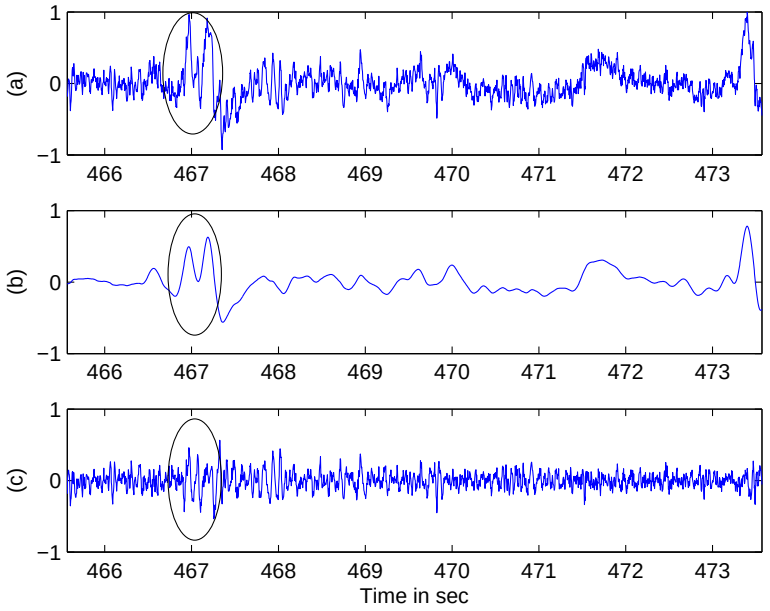

FIGURE 4.10: (a) contaminated EEG signal, (b) estimated reference signal for ANC using SSA and (c) corrected EEG signal by proposed SSA-ANC.

two steps of SSA, local mobility of each eigenvector is computed. Fig. 4.9 shows the local mobility of each eigenvector and dotted line indicates the threshold 0.1. From Fig. 4.9 it is found that eigenvectors $\mathbf{v}_1, \mathbf{v}_2$ and $\mathbf{v}_3$ are the basis vectors to construct the EOG signal (reference) for ANC. The reconstructed reference and corrected EEG signals using proposed SSA-ANC technique are shown in Fig. 4.10. Comparing the reference signals obtained by DWT-ANC (Fig. 4.8(b)) and proposed SSA-ANC (Fig. 4.10(b)), SSA outperforms in reconstructing the EOG signal than the DWT. In conventional methods, the extracted EOG signal is simply subtracted from the contaminated EEG to obtained artifact free EEG signal. However, this technique fails to track the signal changes due to the eye blink. Hence use of ANC enhance in the process of estimating EOG artifact. Fig 4.11(a) shows the reconstructed EOG signals at output of SSA and adaptive filter blocks. The improvement in the estimated EOG signal can be clearly observed in Fig. 4.11(b). From the above simulations it is concluded that, unlike DWT-ANC, where the performance is depends on the morphology of the EOG artifact, the proposed SSA-ANC performance does not depend on the morphology of the EOG signal, hence is a suitable candidate for the removal of EOG artifact from the EEG signal. The efficiency of the proposed SSA-ANC technique in removing the EOG artifact can be observed from the power spectral density (PSD) of the contaminated and corrected EEG signals, shown in Fig. 4.12. It is clear from Fig. 4.12 that the proposed SSA-ANC technique efficiently

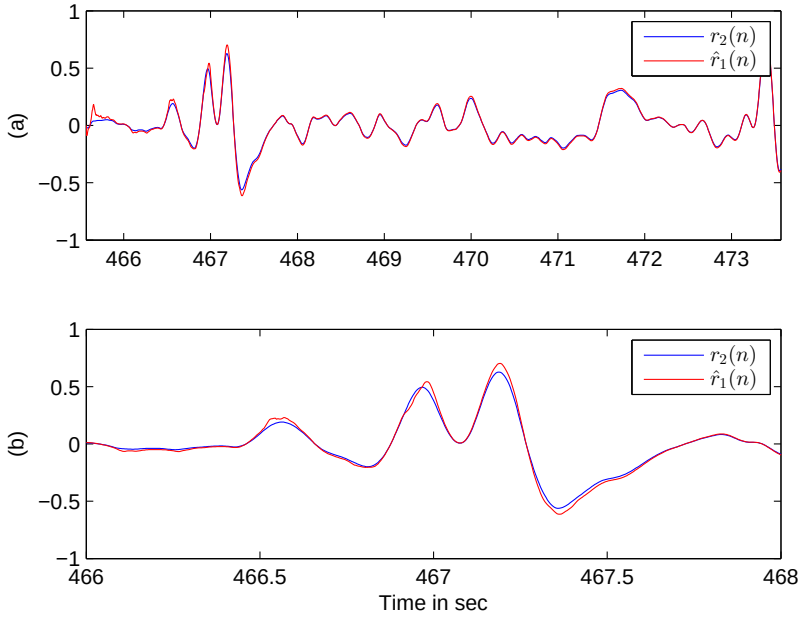

FIGURE 4.11: (a) estimated EOG reference signal by SSA $\mathbf{r}_2(n)$ and adaptive filter output $\hat{r}_1(n)$, (b) zoomed version of above plot between time interval 466 to 468sec.

attenuate the EOG signal and is justified as small power in frequency band $0.5-4Hz$ than the PSD of the corrected EEG signal by DWT-ANC. In order to show that the proposed SSA-ANC technique is preserves the EEG α component, we define a parameter called, mean absolute error (MAE) and is given by

$$MAE = \frac{\sum_{k=j}^{l} \mid \mathbf{p}_e(k) - \mathbf{p}_y(k) \mid}{l-j} \tag{4.4}$$

where, $\mathbf{p}_e$ and $\mathbf{p}_y$ are the PSD of the corrected and contaminated EEG signals respectively and j and l are the specific frequency bands. First, we applied DWT-ANC and proposed SSA-ANC techniques on the five EEG epochs which are fully contaminated by EOG artifacts and compute the PSDs of contaminated and corrected EEG signals. Later MAE for the EEG α band $10-12Hz$ is computed. Table. 4.1 shows the MAE for both techniques and is clear that on average MAE for proposed SSA-ANC results $0.1671dB$ error, which is smaller than the DWT-ANC. Hence we can conclude that proposed SSA-ANC technique is not altering the EEG α component.

The proposed SSA-ANC technique is also applied on the CHB-MIT scalp EEG database [3, 8] to remove EOG artifact in online perspective as shown in 4.2. Fig 4.13 and 4.14 shows the estimated EOG signals at the output of SSA and ANC blocks. After careful

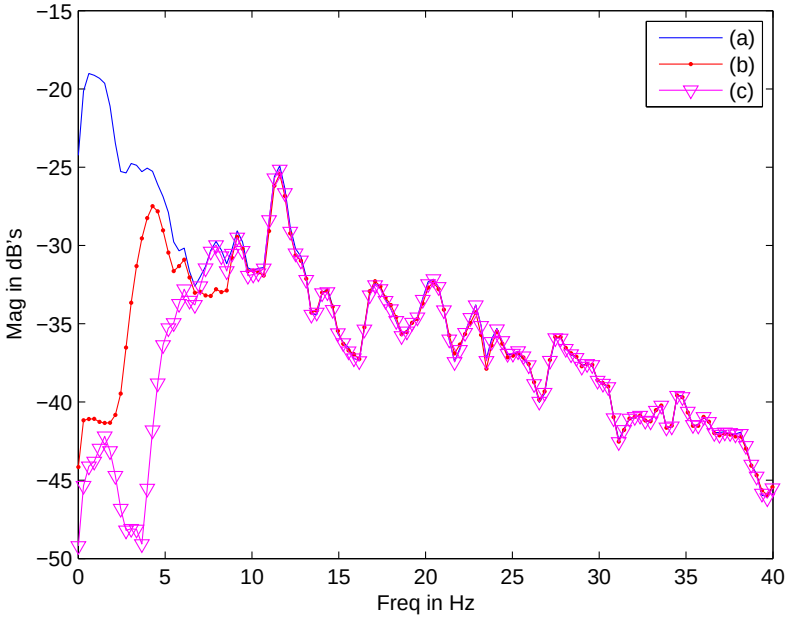

FIGURE 4.12: PSD of (a) contaminated EEG signal, (b) corrected EEG signal by DWT-ANC and (c) corrected EEG signal by SSA-ANC.

TABLE 4.1: Mean Absolute Error (MAE) of Two Techniques.

Segment	DWT-ANC (dB)	Proposed SSA-ANC (dB)
1	0.4382	0.1949
2	0.7456	0.2072
3	0.2440	0.2152
4	0.1057	0.0980
5	0.5501	0.1206
Average	0.4167	0.1671

observation of Figs. 4.13 and 4.14 it is noticed that SSA partially estimated the EOG artifact and is fully reconstructed by the adaptive filter. Once again the combination of SSA-ANC technique enhances ability of the EOG artifact removal.

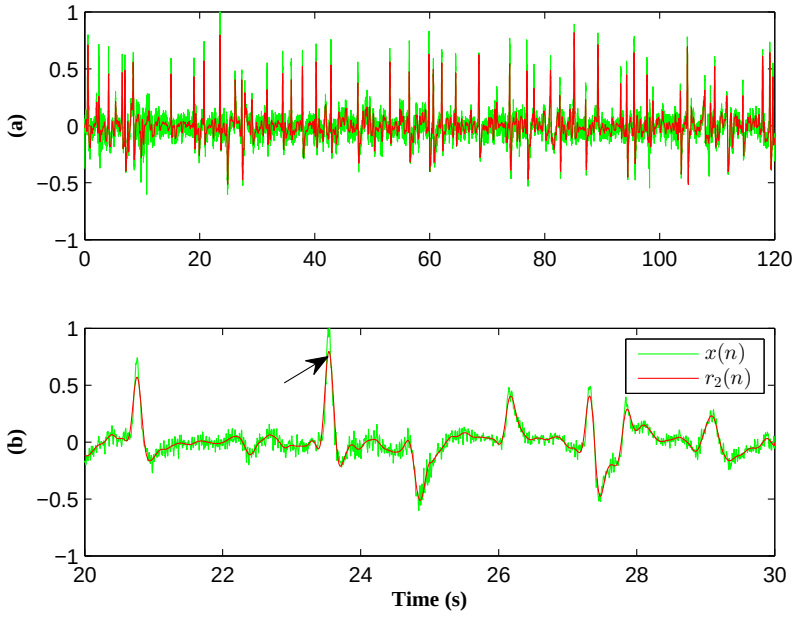

FIGURE 4.13: (a) Contaminated EEG signal (green) $x(n)$ and the estimated EOG $r_2(n)$ by SSA technique, and (b) zoomed version of (a) between $20-30\,s$ time period.

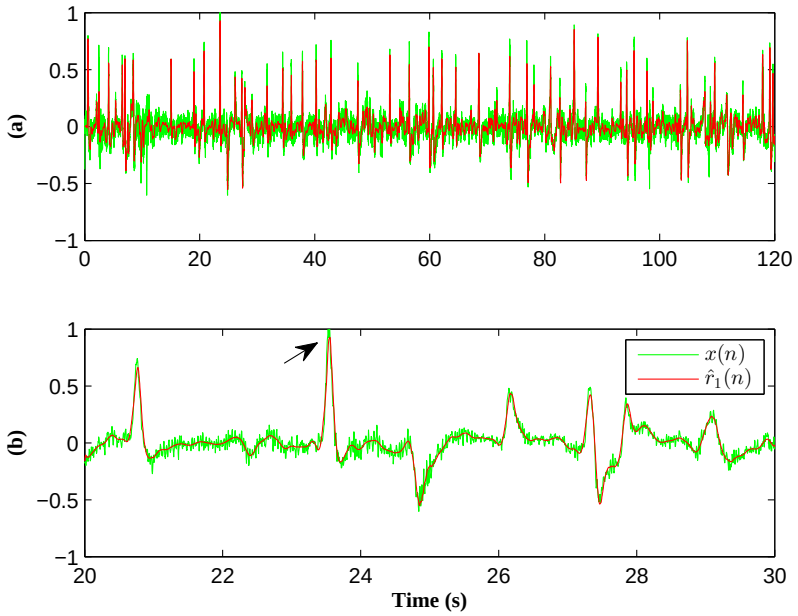

FIGURE 4.14: (a) Contaminated EEG signal (green) $x(n)$ and estimated EOG $\hat{r}_1(n)$ at ANC, and (b) zoomed version of (a) between $20-30\,s$ time period.

4.4 Conclusion

In this chapter, combined SSA and ANC technique is presented to remove the EOG artifacts from the single channel EEG signals. In this technique, the reference signal (EOG) for ANC is extracted using SSA, thus avoids the use of separate electrodes to record EOG signal. More importantly, unlike DWT-ANC, where the performance is depends on the morphology of the EOG artifact, the proposed SSA-ANC performance is independent of the morphology of the EOG signal, hence better performance is achieved by proposed SSA-ANC. The simulation results also demonstrate the efficiency of the proposed SSA-ANC over DWT-ANC in terms of RRMSE and MAE. As the proposed SSA-ANC technique is able to operate on single channel EEG signals, this can be applicable for portable applications.

5

Application of Independent Component Analysis to Single Channel EEG signal

While recording EEG signals, they were often mix with several components originated from non-cerebral regions. ICA technique extensively used to separate the EEG and non cerebral components. The main limitation of ICA is that cannot be applied on the single channel signals, as it demands the number of measured signals should be greater than or equal to the number of sources to be extracted. In this chapter, we proposed a new scheme to adapt ICA technique to single channel EEG signals. In which, first, SSA is employed on single channel signal to map into multivariate data. Next, ICA is applied to separate the EEG and non-cerebral components from the so obtained multivariate data. The performance of the SSA-ICA technique is evaluated on real EEG signals and compared with the existing techniques such as EEMD-ICA and w-ICA.

5.1 Introduction

Blind source separation (BSS) and blind signal extraction (BSE) techniques often used to estimate the statistically independent sources from the mixed data, recorded using multi sensors [34, 135, 136]. Independent component analysis (ICA) is a class of BSS technique and widely used to separate hidden source signals from mixed EEG data [38–44].

Recently, the use of portable/wearable EEG devices has been increased due to their low-power consumption and facilitate the recording of EEG signals in home environment and implemented in applications [137–140]. However, as these systems contain single or few EEG channels, direct application of ICA is not possible. As EEG and other source components spectrally overlapped, developing a signal processing technique that can separate the sources from a single channel EEG signal is a challenging task. In [56], Devis. et. al has proposed single channel ICA (SCICA) technique and employed on univariate signal by imposing the following two conditions on the source signals of interest: (i) the source signals to be extract should be disjoint in their spectral domain, (ii) they should be stationary signals. However, these conditions may not hold for EEG signals, which results in poor source separation.

To make use of ICA on the single channel signals, firstly, the signal should be mapped into multivariate data. Later, ICA can be applied on it to separate source signals. In fact, such mapping could be done using decomposition techniques, such as wavelet transform and ensemble empirical mode decomposition. The combined use of wavelet transform and ICA (w-ICA) techniques has been first proposed in [141]. Later, in [65], it has been used for analyzing biomedical signals. In this technique, first, the measured single channel biomedical signal is decomposed into several components. Next, ICA is employed on the decomposed components and finds the de-mixing matrix to extract the sources. However, the performance of w-ICA technique is depends on the selection of mother wavelet function, which intern needs the prior knowledge of the sources to be extracted.

Recently, in [66], EEMD and ICA techniques are combined (EEMD-ICA) to separate the sources from single channel EEG and EMG signals. Like w-ICA technique, first, the single channel signal is decomposed into intrinsic mode functions (IMFs) using EEMD. After that ICA is applied on the set of IMF components to extract the hidden sources.

Unlike w-ICA, where prior knowledge of the sources to be extracted is required to select the mother wavelet function, EEMD-ICA do not need any prior knowledge of sources to be extracted, as the EEMD technique is data-driven algorithm. However, the performance of EEMD-ICA is depends on the noise parameter (np) and the number of ensembles. The noise parameter *np* is defined as the ratio of noise standard deviation (SD) to SD of the signal [57].

SSA is another decomposition technique widely used in analyzing climatic time series [67, 68]. Basically, it decompose the real-valued time series signal into sum of interpretable components such as trend, oscillating and noise components. The use of SSA technique for analyzing EEG signals is firstly presented in [142], where it is used to detect seizures in infants. The separation of EOG artifact from EEG signals, the lung sound from heart sound signals and the ECG artifact from EMG signals from single channel EEG signals were discussed in [69–72] respectively. Grouping (signal subspace identification) is one of the critical step in SSA technique, where the basis vectors (eigenvectors) associated to the desired and undesired signals has to be identified. In [69, 70, 72], the magnitude of the eigenvalues is considered to group the basis vectors. However, such grouping criteria may be useful when the signal to noise ratio (SNR) of the measured signal is high. To overcome the limitation of ICA for single channel EEG signals, SSA jointly combined to it. Like w-ICA and EEMD-ICA techniques, here, SSA is employed to decompose the single channel EEG signal into set uncorrelated components, forms a multivariate data matrix $\mathbf{X}$. To estimate the sources which are statistically independent, ICA is employed on $\mathbf{X}$. The proposed SSA-ICA technique is applied on single channel synthetic as well as real life EEG signals and compared with w-ICA and EEMD-ICA techniques. The simulation results exhibits superior performance as compared with w-ICA and EEMD-ICA techniques.

5.1.1 Proposed SSA-ICA Technique

The direct adaptation of ICA on single channel signal is not possible, as the number of measured signals should greater than or equal to the number of sources to be extracted. To make use of ICA on single channel EEG signal, first it should be mapped into multivariate data, thereafter, ICA can be applied. Fig. 5.1 shows the source separation using sequential singular spectrum analysis. The basic idea here is that extracting the

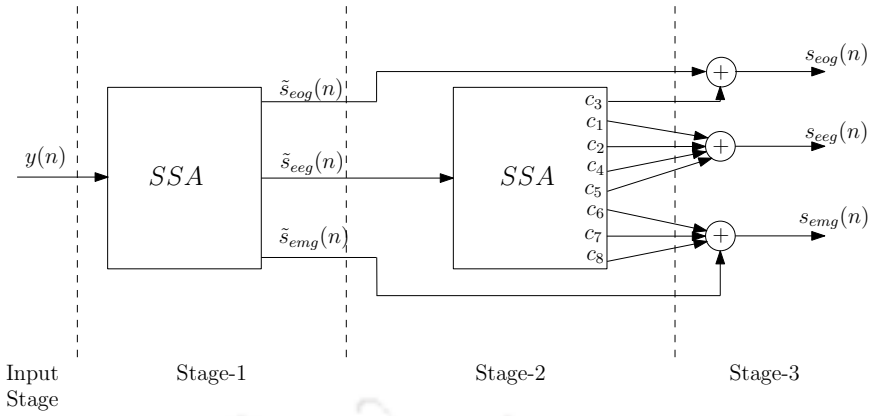

FIGURE 5.1: Block diagram of source separation using sequential singular spectrum analysis.

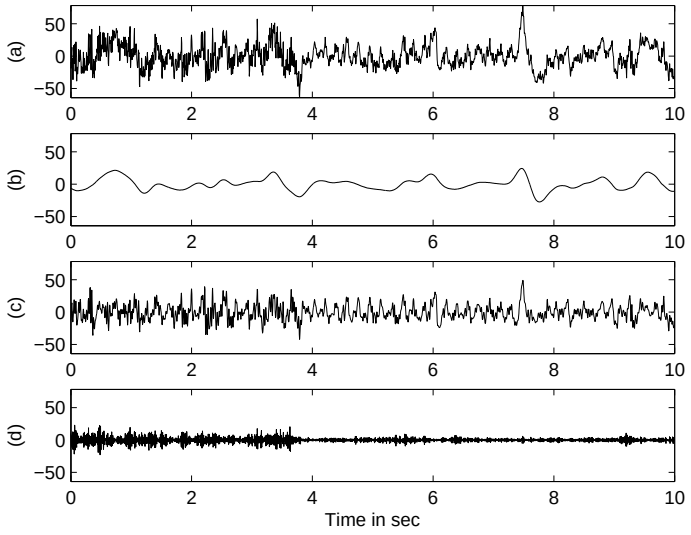

FIGURE 5.2: Decomposed components at Stage−1 (a) EOG, (b) EEG and (c) muscle components.

source components from the signal, if any remnants of the extracted components still present in the residual signals, then basic SSA is applied again on the residual signal with different window length M. However, the source components obtained are not statistically uncorrelated. Fig. 5.2, 5.3 and 5.4 shows the decomposed components at stage1, 2 and 3 respectively. It is clear from Fig. 5.4 that the remnant of EOG component still can be seen in the extracted EEG component (spike at $7.5\,s$). Moreover, the grouping step involved in this technique is based on the magnitude of eigenvalues; such grouping limits the automatic decomposition procedure. Hence, we proposed fully automatic decomposition procedure, where SSA is recursively applied on the single channel EEG signal with fixed window length, as shown in Fig. 5.5. The multivariate data matrix so

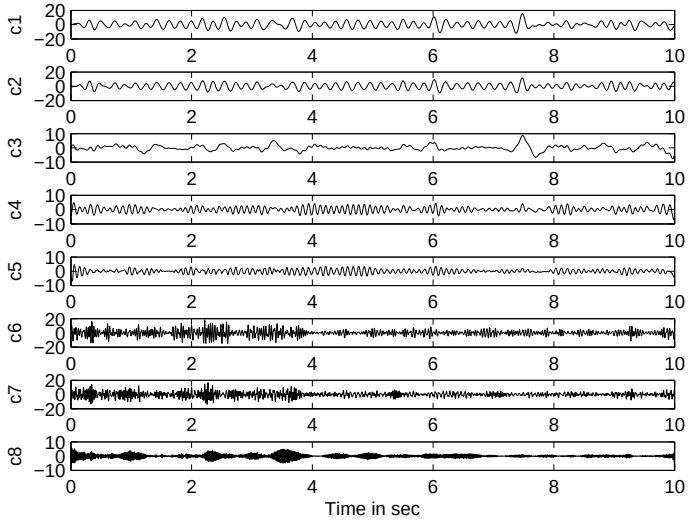

FIGURE 5.3: Decomposed components at Stage−2.

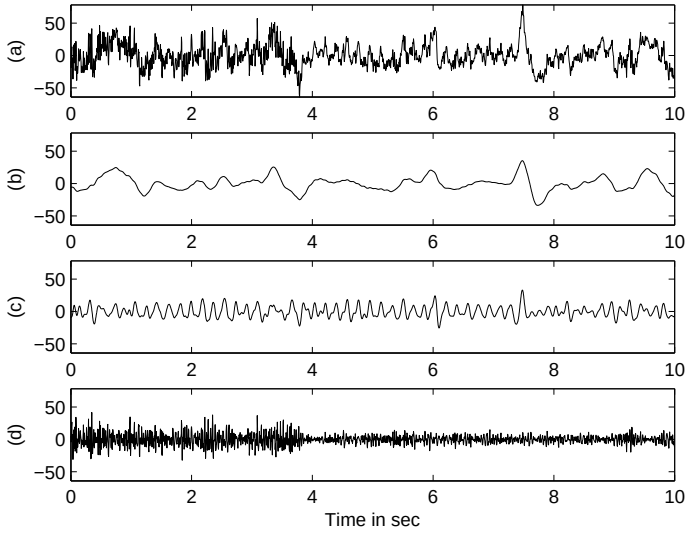

FIGURE 5.4: Separated source components using sequential singular spectrum analysis (Stage−3) (a) EOG, (b) EEG and (c) muscle components.

obtained is applied to ICA to extract the statistically independent source signals. Fig. 5.5 illustrates the proposed SSA-ICA technique for 3 level decomposition.

Consider $s_d(n)$ and $a(n)$ as desired and undesired statistically independent source signals originated from two sources s_0 and s_1, respectively. Then, the mixed single channel EEG signal is given by

$$y(n) = s_d(n) + pa(n) \tag{5.1}$$

where, p is a propagation constant, which decides the contribution of a particular source

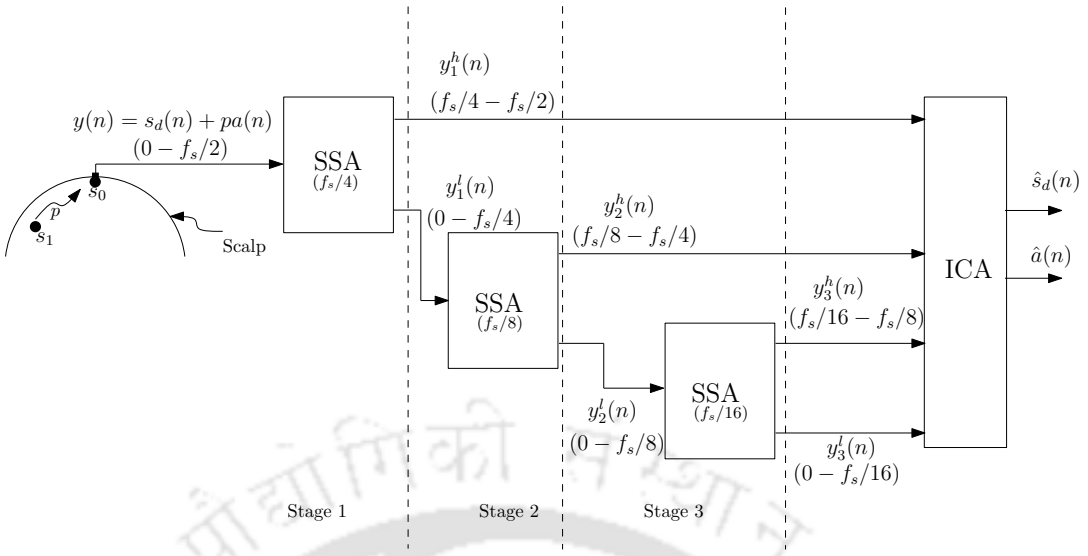

FIGURE 5.5: Block diagram of the proposed SSA-ICA technique using three level decomposition.

signal in $y(n)$. However, the propagation constant p depends mainly on the density of the tissue present along the path between the source s_0 and s_1. In ordered to separate the sources from the mixed signal $y(n)$, in this work, first, SSA is employed on $y(n)$ and decomposed into higher and lower frequency components, say $y_1^h(n)$ and $y_1^l(n)$, respectively. Here, the bandwidths of $y_1^h(n)$ and $y_1^l(n)$ are $f_s/4 - f_s/2$ and $0 - f_s/4$, respectively. The way of decomposition of the signal $y(n)$ into two components, *i.e.* higher and lower frequency components, will be discussed below. However, in order to decompose the given signal into higher and lower frequency components, threshold T_h is set to $f_s/4$ at the first decomposition stage, where f_s is the sampling frequency of $y(n)$. Again, the SSA is applied on the low frequency component $y_1^l(n)$ and decomposed into two components $y_2^h(n)$ and $y_2^l(n)$. Now, at this second decomposition stage, the threshold for SSA is set $f_s/8$. This process will be continued for P number of decomposition levels, that results a multivariate data matrix $\mathbf{X}$ of size $(P+1) \times N$. In general, for i^{th} decomposition level, the threshold T_h is given by $f_s/2^{i+1}$, where, $i = 1, 2, ..., P-1$. As SSA decompose the signal $y(n)$ based on the SOS, the decomposed components so obtained are uncorrelated. Hence, to extract the statistically independent source signals, FastICA algorithm [89, 96] is applied on the data matrix $\mathbf{X}$ and it will provides the mixing and the de-mixing matrices $\mathbf{A}$ and $\mathbf{B}$ respectively along with the IC matrix $\mathbf{S}$ as outputs. After this, IC of interest is mapped into original signal form by multiplying it with the corresponding column vector of the mixing matrix $\mathbf{A}$, ($i.e.\mathbf{B}^{-1}$). That results a set of newly derived SSA decomposed components for that IC. Finally, by summing over

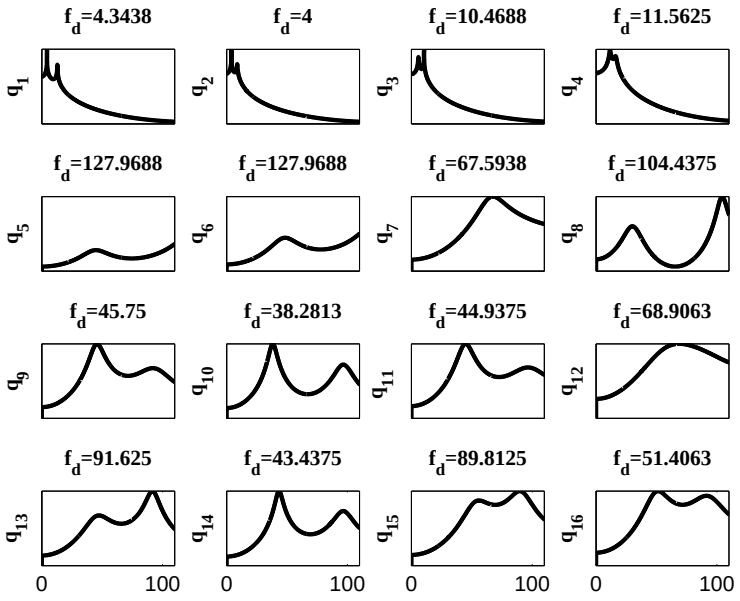

FIGURE 5.6: PSDs of sixteen eigenvectors and corresponding dominant frequency f_d.

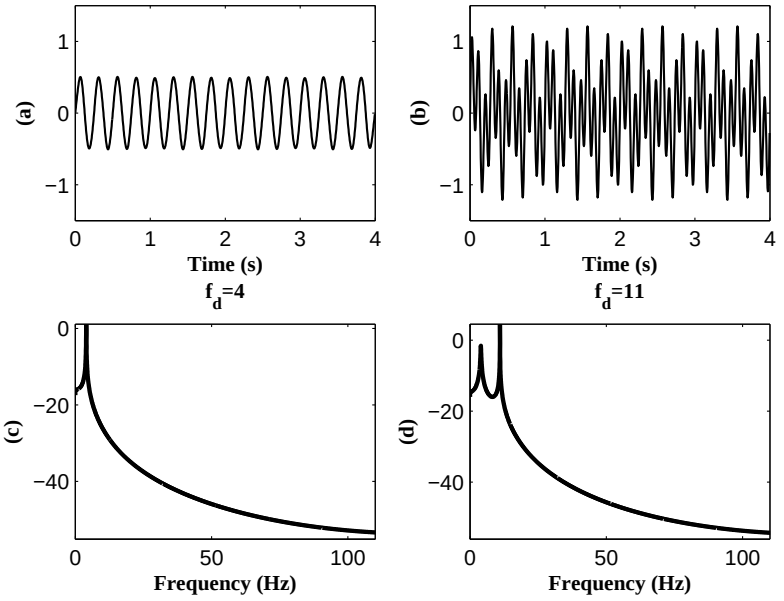

FIGURE 5.7: The two decomposed signals using SSA (a) $4\,Hz$ and (b) $11\,Hz$. The PSD of (c) $4\,Hz$ and (d) $11\,Hz$ for signal $SNR = 0\,dB$.

all the newly derived SSA components, the desired source signal is resulted as a single channel signal.

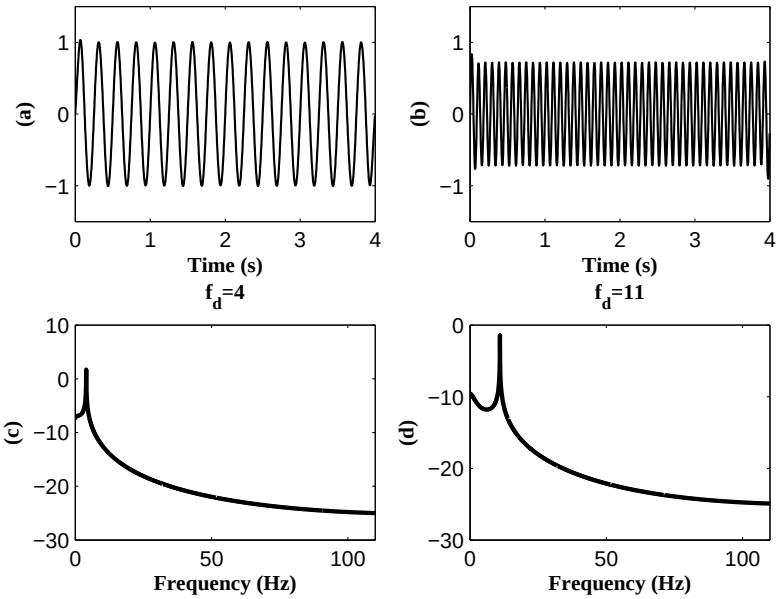

FIGURE 5.8: (a) The extracted $4\,Hz$ and (b) $11\,Hz$ sources after application of ICA. The PSDs of estimated (c) $4\,Hz$ and (d) $11\,Hz$ sources.

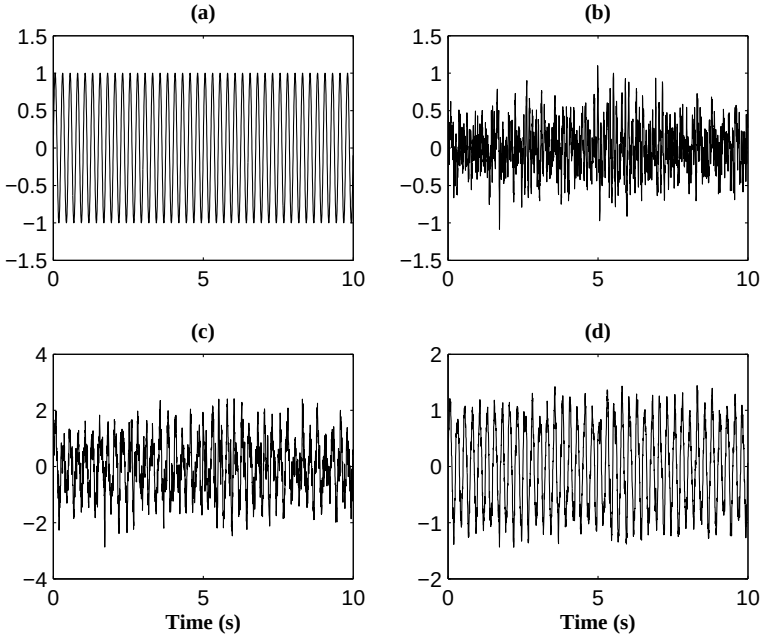

FIGURE 5.9: (a) Sinusoidal signal oscillatory type source signal $s_d(n)$, (b) unwanted signal $a(n)$, (c) and (d) mixed signal $y(n)$ for $SNR = -5dB$ and $5dB$, respectively.

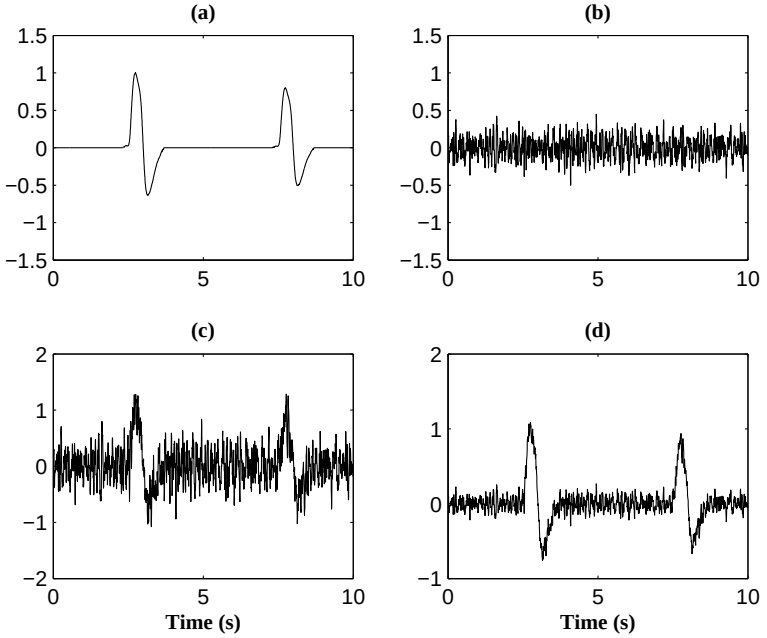

FIGURE 5.10: (a) Spike type signal $s_d(n)$, (b) unwanted signal $a(n)$, (c) and (d) mixed signal $y(n)$ for $SNR = -5\,dB$ and $dB5$, respectively.

5.1.2 Decomposition of Single Channel Signal into Two Components using SSA

In the proposed technique, SSA is recursively applied to map single channel signal into multivariate data. At every decomposition stage the input signal applied to SSA block is decomposed into higher and lower frequency components. However, to decompose the given input signal into two components, the basis vectors (eigenvectors) associated to the higher and lower frequency signals has to be identified. In another words, splitting the eigenvectors of the covariance matrix $\mathbf{C}$ into two groups. The identification of subspace is a critical step in traditional SSA and several grouping criterions have been reported in [69, 70, 72]. In all these criterions, the magnitude of the eigenvalues of the covariance matrix $\mathbf{C}$ is exploited to split the basis vectors by assuming that the signal to noise ratio (SNR) of the measured signal is high. In general, this assumption may not hold in certain cases, where the contribution of all the source are almost similar in the mixed signal $y(n)$. For example, the contribution of EOG artifact in EEG signal, measured from the central electrode position C_3 or C_4, is more or equal. Then, such criteria may results in inefficient grouping of eigenvectors.

As the eigenvectors describes the variability of the data, hence, we exploit this information in the grouping step of SSA. After computing EVD of $\mathbf{C}$, the power spectral density (PSD) of each eigenvector is estimated using *burg* method. Later, the dominant frequency is identified from computed PSD. In general the selection of model order depends on the number of peaks in the power spectrum [143]. As we are looking for the dominant frequency of the eigenvector, the model order for burg method is set to 4 [144]. Based on the obtained dominant frequency information of each eigenvector and threshold T_h, the arguments of eigenvectors associated to the desired signal are identified and the corresponding trajectory matrix is computed using (2.10). The resultant trajectory matrix is mapped into single channel signal and is subtracted from the mixed signal vector $\mathbf{y}$ to obtain the residue signal of $\mathbf{y}$. However, since the eigenvectors are derived by exploiting the covariance of the data, they exhibits multi frequency band responses. As we group the eigenvectors based on the dominant frequency of it, therefore, the decomposed components obtained by SSA are uncorrelated. It can be noted that at each decomposition stage, SSA is used as low-pass filter (LPF). Although LPFs can be used to separate the low frequency components, SSA is mostly preferred for this purpose due to several reasons. Firstly, the EEG components spectrally overlap with the non-cerebral source signals, such as eye blink and muscle artifacts, therefore, low-pass filters are inefficient to separate the artifacts. Secondly, the use of LPFs leads to signal distortion due nonlinear phase-frequency response [55]. In all the subspace based techniques either SVD/EVD is very common and its finite impulse response (FIR) representation is discussed in [145]. The use of SSA in linear time invariant (LTI) system perspective which corresponds to the FIR filter has been studied in [146]. However, the filter coefficients are eigenvectors of the covariance matrix. Interestingly, the output of this filter is in phase with the input signal.

Here, we present the simulation results for better understanding of new grouping criteria. First, we added two sinusoidal signals of frequency $4\,Hz$ and $11\,Hz$ as per (5.1) to obtain a mixed signal $y(n)$. In this example, we assume $4\,Hz$ and $11\,Hz$ signals as low and high frequency components in $y(n)$. The SSA technique, with $M = 32$ and threshold $T_h = 4\,Hz$, is applied on the mixed signal $y(n)$. The PSDs of sixteen eigenvectors and their dominant frequencies were shown in Fig. 5.6. It is evident from Fig. 5.6 that the obtained eigenvectors comprise the multi frequency band response. As the threshold T_h is set to $4\,Hz$, the eigenvector $\mathbf{q}_2$ is found to be the basis vector to reconstruct the

$4\,Hz$ signal and other eigenvectors are associated to mixer of $11\,Hz$ and $4\,Hz$ signal. After extracting the $4\,Hz$ component, it can be directly subtracted from $\mathbf{y}$, to obtain $11\,Hz$ signal. In this way the given mixed signal is decomposed into two components. The decomposed $4\,Hz$ and $11\,Hz$ signals and their corresponding PSDs are shown in Fig. 5.7. However, upon careful observation of Fig. 5.7(b) and (d), it is clear that the remnants of $4\,Hz$ component still present in the $11\,Hz$ signal. This is due to the fact that the SSA uses the covariance of the data to derive the eigenvectors. When ICA is applied on the two decomposed components, then efficient source separation is achieved, obvious from Fig. 5.8.

5.2 Simulation Studies

In order to validate the proposed SSA-ICA technique, we carried out simulations on synthetic as well as on real EEG signals. To evaluate the performances of all the techniques, we consider the mixing model represented in (5.1). Here, p is a propagation constant that will decide the SNR of the measured signal. The SNR of measured signal $y(n)$ is given by

$$SNR = \frac{RMS(\mathbf{s}_d)}{RMS(p\mathbf{a})} \tag{5.2}$$

where, $RMS(\mathbf{s}_d)$ is the root mean square of the desired source signal. To assess the performance of the proposed SSA-ICA technique with the existing w-ICA and EEMD-ICA techniques, we considered the relative root mean square error (RRMSE) as parametric measure. The RRMSE of the desired source signal $\mathbf{s}_d$ is given by

$$RRMSE = \frac{RMS(\mathbf{s}_d - \hat{\mathbf{s}}_d)}{RMS(\mathbf{s}_d)} \times 100[\%] \tag{5.3}$$

where, $RMS(\hat{\mathbf{s}}_d)$ is the root mean square of the estimated desired source signal.

5.2.1 Application of proposed SSA-ICA technique on Synthetic Signals

Construction of Oscillatory Type Source Signal

In our first simulation study, we consider an oscillatory type source signal separation from a mixed single channel EEG signal $y(n)$. Here, the oscillatory type source signal

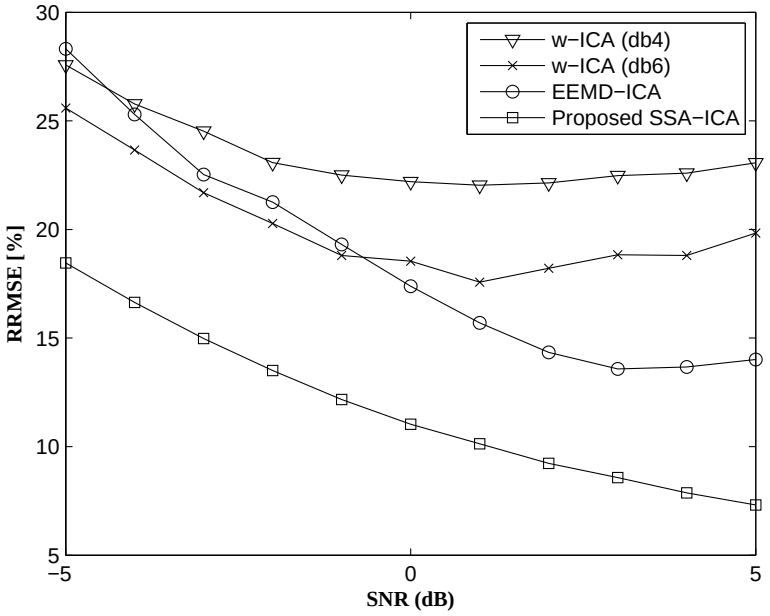

FIGURE 5.11: Comparison of RRMSE curves obtained in estimating the oscillatory type source signal using the existing and the proposed SSA-ICA techniques.

$s_d(n)$ is a representative of a low frequency rhythmic component in ictal EEG signal during seizure or a sleep spindle rhythmic component in sleep EEG signal. To construct synthetic mixed EEG signal $y(n)$, first, a ten second EEG epoch, say $a(n)$, is segmented from a lengthy EEG signal, measured from one of the authors scalp and added to the $4\,Hz$ oscillatory type source signal based on the mixing model given in (5.1). Fig. 5.9 shows a ten second epoch of oscillatory type and unknown source signals, $s_d(n)$ and $a(n)$ respectively and the mixed signal $y(n)$ for $SNRs = -5dB$ and $5dB$.

Construction of Spike-Type Source Signal

In general, eye blink artifact often appears in the measured EEG signals as a spike type source signal. Hence, we consider the spike type signal separation from a single channel mixed signal as our second simulation study. To construct such spike type source signal, first, one second eye blink epoch was segmented from a length EEG signal. Later, it was positioned at $2.5\,s$ and $7.5\,s$ with different magnitudes in a zero magnitude ten second signal. After that, Matlab *smooth* command is used to remove the high frequency component. Finally, the mixed signal $y(n)$ is constructed by adding the unknown source signal $a(n)$ to spike type source signal based on the mixing model given in (5.1). Fig.

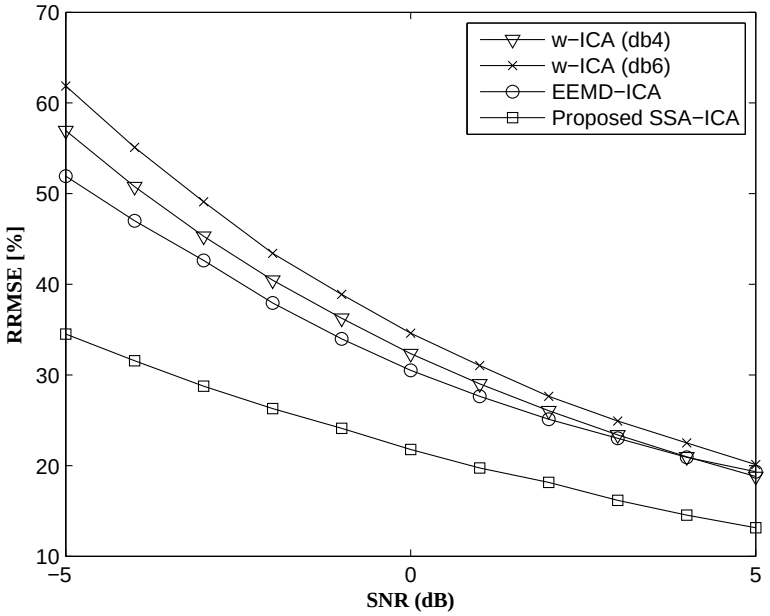

FIGURE 5.12: Comparison of RRMSE curves obtained in estimating the spike type source signal using the existing and the proposed SSA-ICA techniques

5.10 shows a ten second epoch of spike type and unknown source signals, $s_d(n)$ and $a(n)$ respectively and the mixed signal $y(n)$ for $SNR = -5$ and 5.

For efficient separation of sources from the single channel mixed signal, the parameters of all the algorithms were selected carefully. In w-ICA, the wavelet functions *db*6 and *db*4 are chosen, respectively, to extract the oscillatory and the spike type sources. In case of EEMD-ICA, the noise parameter (np) and the number of ensembles (ne) are set to 0.2 and 50, respectively. The window length for SSA is set between 32 to 50. The more details regarding the selection of the window length range is discussed in the subsequent section. The number of decomposition levels for w-ICA and proposed SSA-ICA is set between 4 to 5.

On comparing the RRMSE curves shown in Fig. 5.11 and 5.12, it is clear that the proposed SSA-ICA technique exhibits superior performance than existing w-ICA and EEMD-ICA techniques, both in estimating the oscillatory as well as the spike type source signals. In case of w-ICA, the performance is significantly depends on the predefined basis functions (mother wavelet). From Figs. 5.11 and 5.12, it is clear that w-ICA using *db*6 gives superior performance in estimating the oscillatory type source signal and w-ICA using *db*4 outperforming performance in estimating the spike type source signal extraction, respectively. Moreover, the selection of mother wavelet function demands

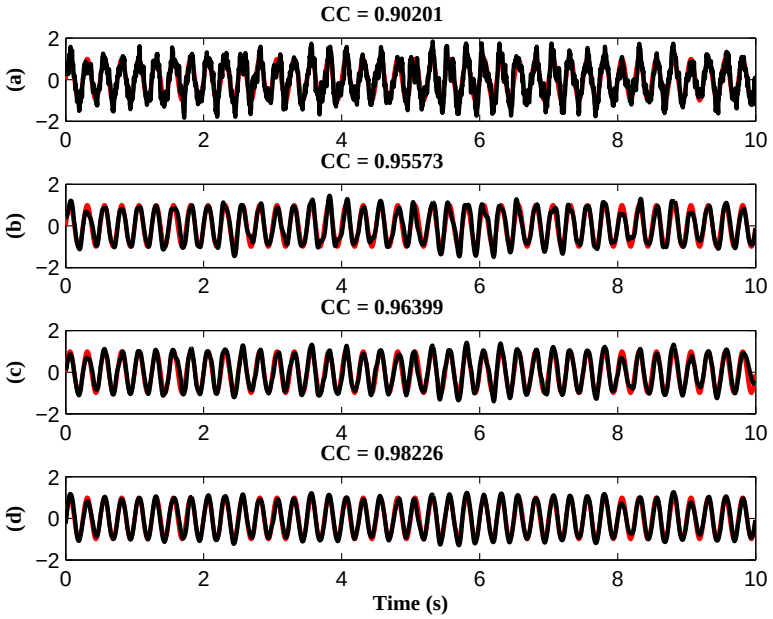

FIGURE 5.13: Superimposition of $s_d(n)$ (red) with (a) mixed signal $y(n)$ (black), as well as the estimated $\hat{s}_d(n)$ (black) by (b) w-ICA (db6), (c) EEMD-CCA and proposed SSA-ICA techniques for $SNR = 0dB$ respectively.

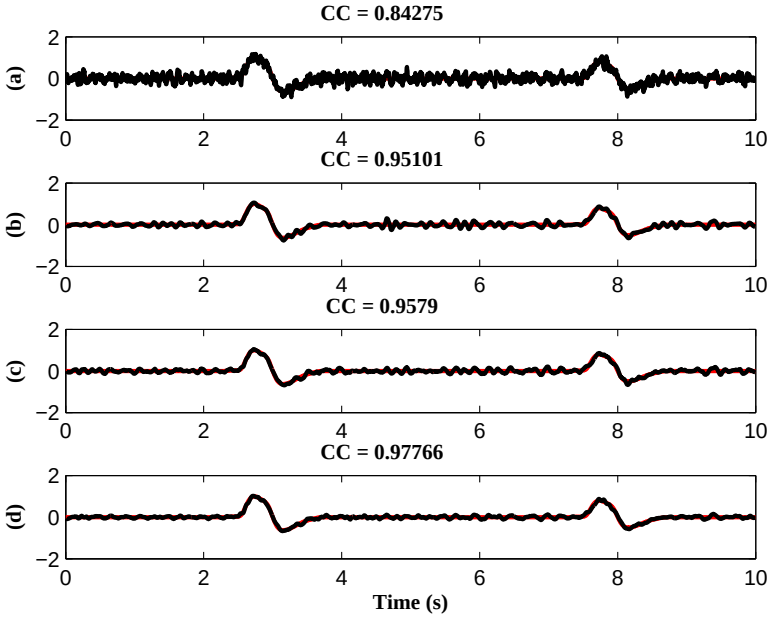

FIGURE 5.14: (a) Superimposition of $s_d(n)$ (red) with (a) mixed signal $y(n)$ (black), as well as the estimated $\hat{s}_d(n)$ (black) by (b) w-ICA (db4), (c) EEMD-CCA and proposed SSA-ICA techniques for $SNR = 0dB$ respectively.

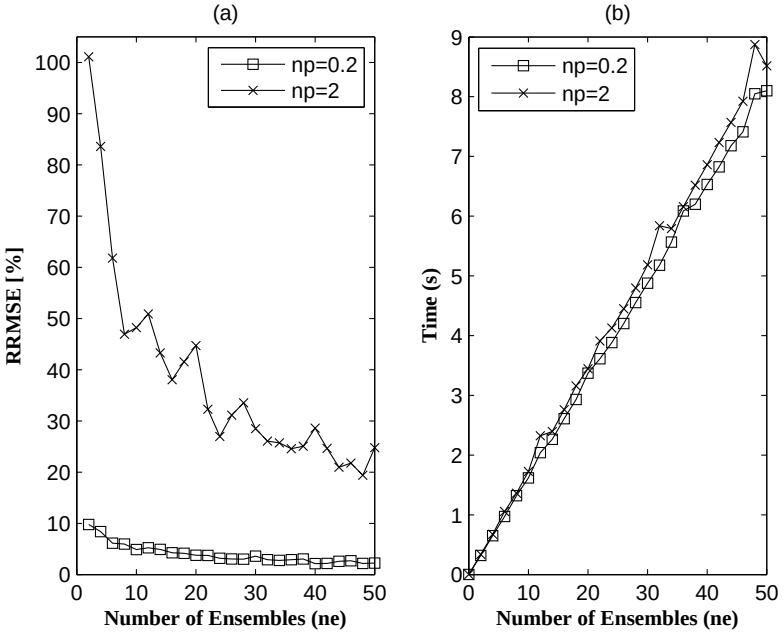

FIGURE 5.15: (a) RRMSE resulted by EEMD decomposition process as a function of ne and np, (b) computation time of EEMD for a 10 s signal for different ne.

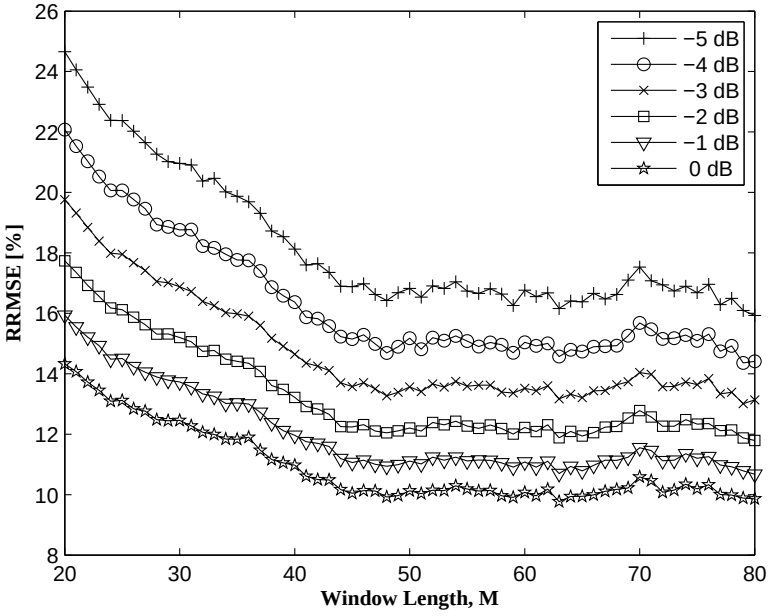

FIGURE 5.16: Averaged RRMSE curves of proposed SSA-ICA technique as function of window length M and SNR.

the knowledge of source signal morphology. Therefore, the performance of w-ICA is inconsistent. Even though even though the EEMD is a data-driven technique, the overall EEMD-ICA performance is significantly effected by the parameters such as np and ne [66]. However, adjusting these parameters is not easy, as these parameters depends on the signal noise level as well as on the frequency information. Particularly, at lower $SNRs$, of the order $-5dB$, the performance of EEMD-ICA is almost similar to w-ICA ($db4$), which is evident from Fig. 5.11. In the case of spike type source signal extraction, EEMD-ICA shows superior performance than w-ICA. However, it will be insignificant when the $SNR > 0dB$, which is obvious from Fig. 5.12.

Fig. 5.13 and 5.14 shows respectively the estimated oscillatory and spike type source signals using all the three techniques. It is clear from the correlation coefficient (CC) between $s_d(n)$ and $\hat{s}_d(n)$ that the proposed SSA-ICA technique preserves the shape of the desired source signal. In the decomposition process of SSA, the basis vectors were derived by accounting the local structure between the samples, which means the covariance between the samples. However, the decomposed components are statistically uncorrelated, as SSA accounts the covariance information of the data. Therefore, the post processing of ICA further enhances the separation of the oscillating component. When we look into the decomposition process of EEMD, an independent, identically distributed white noise is added to the target signal for ne trails. After that, averaged IMF set is derived using EMD and considered them as an optimal decomposed components. However, poor selection of np and ne values may not cancel the added white noise components. Therefore, post processing of ICA on these IMF set may modify the final result of EEMD-ICA technique. In [57] it is clear that that np value should be small when the signal to be extracted has high-frequency content and should be large when signal to be extracted has low-frequency content. We evaluated the performance of EEMD for $np = 0.2$ and 2. The RRMSE between the signal to be decomposed $\mathbf{y}$ and the sum of averaged IMFs ($i.e.\ \sum_{j=1}^{q} \mathbf{b}_j$) derived by the EEMD operation is shown in Fig. 5.15(a). It is evident from Fig. 5.15(a) that the RRMSE of EEMD process for $np = 2$ is higher than the $np = 0.2$ and is decreased when the number of ensembles are increased. However, when the number of ensembles are increased, then the computation time consumed by the EEMD is also increased which is evident from Fig. 5.15(b). Using Intel $i5$ CPU, with an operating frequency $3.2GHz$ and $8GB$ RAM, the computation time consumed by the EEMD to decompose $10\,s$ signal epoch with $ne = 50$ is approximately $9\,s$. For

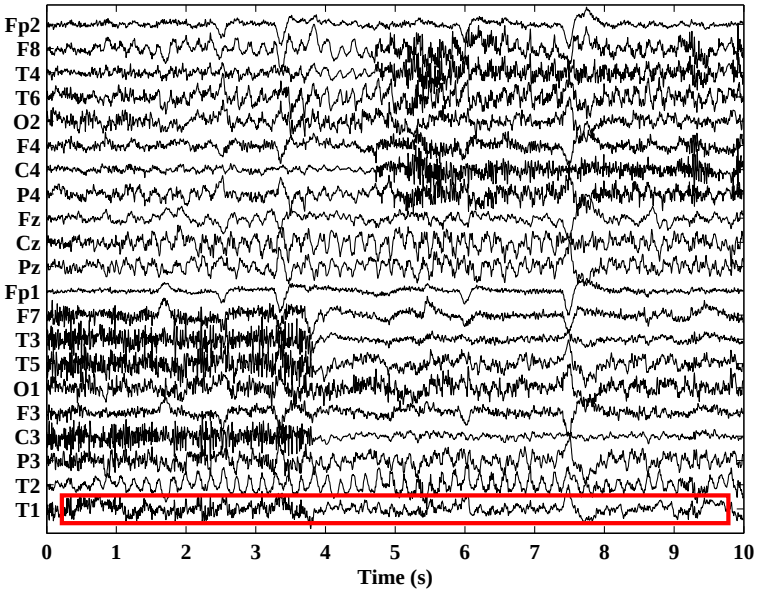

FIGURE 5.17: Ten second multichannel EEG epoch recordings.

$np = 0.2$, RRMSE is very small and the computational time is almost similar to EEMD for $np = 2$.

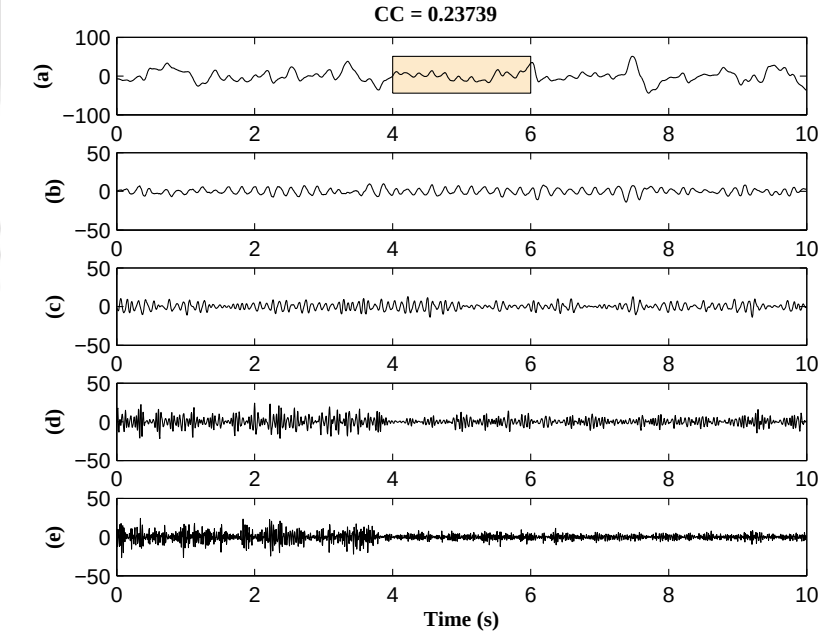

FIGURE 5.18: The estimated sources from single channel EEG signal (a) eye blink, (b) $5.456Hz$, (c) $10.96Hz$, (d) high band beta (e) muscle artifact components using w-ICA ($db6$) technique.

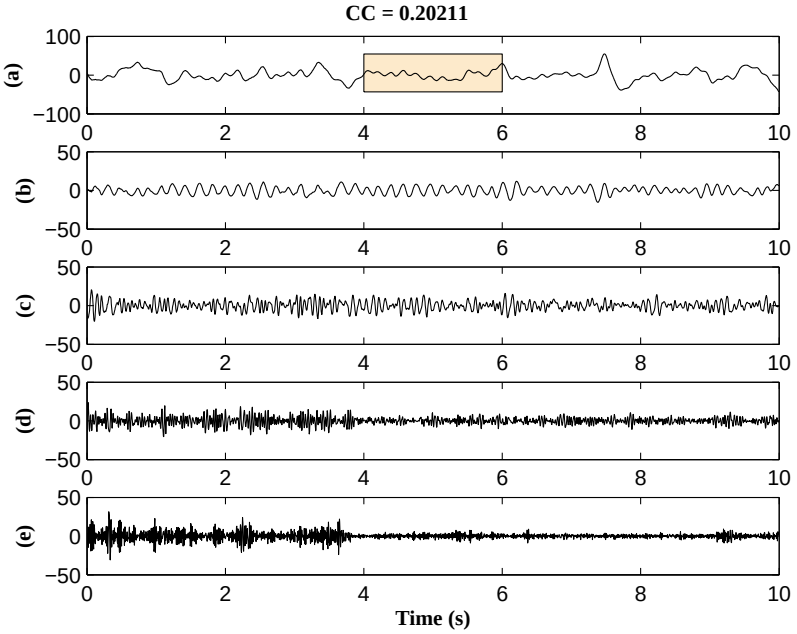

FIGURE 5.19: The estimated sources from single channel EEG signal (a) eye blink, (b) 5.456Hz, (c) 10.96Hz, (d) high band beta (e) muscle artifact components using EEMD-ICA technique.

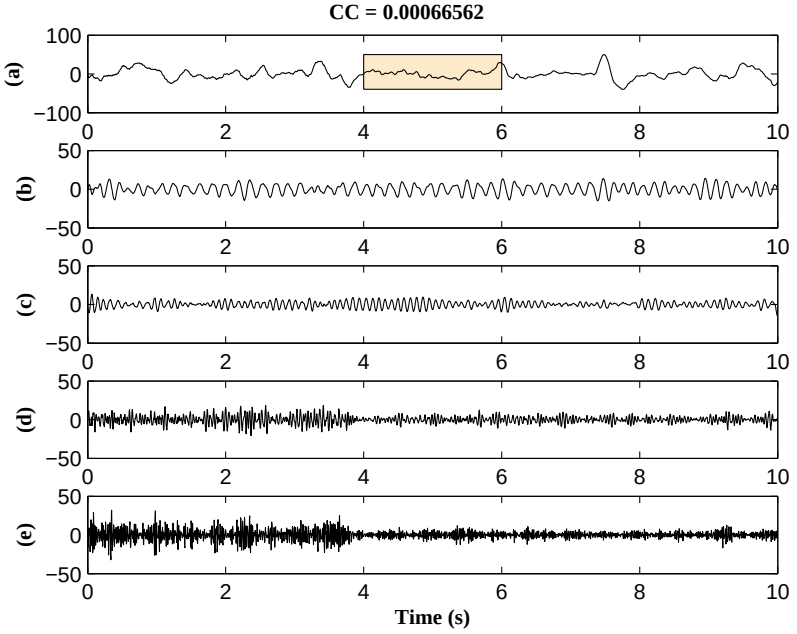

FIGURE 5.20: The estimated sources from single channel EEG signal (a) eye blink, (b) 5.456Hz, (c) 10.96Hz, (d) high band beta (e) muscle artifact components using proposed SSA-ICA technique.

Effect of M on the Proposed SSA-ICA Technique Performance

In the case of proposed SSA-ICA technique, the selection of parameter M does not depends on signal morphology and statistics. In order to validate this fact, we carried out simulations to study the performance of proposed SSA-ICA technique for different window lengths. Fig. 5.16 shows the average RRMSE as function of M and SNR. It is obvious from Fig. 5.16 that the performance of the proposed SSA-ICA technique is almost constant for M greater than 50. Therefore, the window length M is set below 50. When M is set to smaller values of the order of 20, then all the components were squeezed into one or two decomposed component, as a result post processing based on ICA fail to extract the source signal. After performing several simulations, we have chosen M between 30 to 50. From the above simulations, it is clear that unlike w-ICA and the EEMD-ICA, the selection of parameter M of proposed SSA-ICA technique is neither depends on the morphology nor the signal noise level.

5.2.2 Application of Proposed SSA-ICA Technique on Real Life EEG Signals

Here, we showed some simulation results obtained by employing the proposed SSA-ICA and the existing techniques (w-ICA and EEMD-ICA) on three real life EEG signals measured in different scenarios.

Source Separation from Single Channel Ictal EEG Signal

We evaluated the performance of proposed SSA-ICA technique using $10\,s$ ictal EEG signals recorded from a patient suffering with *mesial temporal lobe epilepsy* (MTLE) and maintained at the BioSource database [6]. These signals were recorded with a sampling frequency $f_s = 250\,Hz$ as shown in Fig.5.17. In this data, along with two rhythmic components of $5.456\,Hz$ and $10.96\,Hz$, the non-cerebral source signals associated to eye blink and muscle activity are also registered. The proposed SSA-ICA and the existing techniques are applied on the EEG signal measured from $T1$ electrode position (indicated in rectangular box). The reason is that this electrode position is opposite to the seizure location T_2, *i.e.* SNR is very low. The second reason is to be consistent with the results showed in [66]. Moreover, it will be the great challenge to process these signals, as the

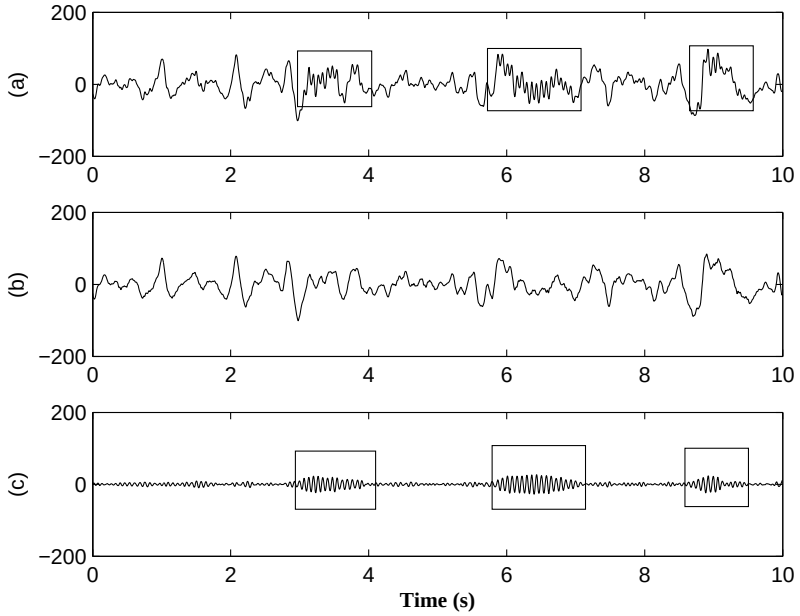

FIGURE 5.21: (a) The mixed single channel sleep EEG signal, (b) extracted low frequency EEG component and (c) sleep spindle component using proposed SSA-ICA technique.

spectrums of eye blink and seizure activity components were spectrally overlapped in the frequency domain.

We applied proposed SSA-ICA and other existing techniques on single channel EEG signal obtained from $T1$ channel and extracted the source components. The estimated source signals from single channel EEG using w-ICA, EEMD-ICA and the proposed SSA-ICA techniques were shown in Figs. 5.17, 5.18 and 5.19 respectively. The number of ICs to be extracted is set to 6 for w-ICA and proposed SSA-ICA and 7 for EEMD-ICA. We have also obtained some of the components such as the eye blink, the rhythmic components $5.456\,Hz$ as well as $10.96\,Hz$, the high frequency β band and the muscle artifact signals. As it was mentioned earlier, the eye blink and seizure components are spectrally overlapped. Therefore, to examine that whether the eye blink and $5.456Hz$ rhythmic components are mutually independent or not, the CC is computed as separability measure, this is necessary condition but not sufficient. The correlation coefficient close to zero indicates that the two components are efficiently separable and close to unity represents the components are poorly separable. It is clear from Figs. 5.17 to 5.18 and the CC values that both w-ICA and EEMD-ICA techniques are able to partially separate the eye blink and $5.456\,Hz$ components. Whereas, the proposed SSA-ICA technique is capable of separating the eye blink and ictal activity components and is evident from

CC values also. It is clear from Fig. 5.19, that rhythmic components of $5.456\,Hz$ and $10.96\,Hz$ were efficiently isolated from the mixed single channel EEG signal.

Sleep Spindle Separation from Single Channel EEG Signal

Sleep spindles appears in the EEG signal as sinus-like bursts with progressive increase and decease in amplitude. The minimum duration of these burst is $0.5\,s$ and the frequencies between $12-16\,Hz$. The reason for presence of sleep spindle in the EEG signals are due to brain pathology, medication and aging [147]. Separation of sleep spindle from single channel EEG remains as open problem. The application of ICA for sleep spindle detection was studied in [148]. However, separation of sleep spindle from single channel EEG is yet to be addressed. Therefore, in second simulation study, we applied proposed SSA-ICA technique on single channel EEG signal to extract the sleep spindle component. We use the sleep spindle EEG data, recorded at the Sleep Laboratory of the André Vésale hospital (Belgium) [149], to evaluate the proposed SSA-ICA technique and applied on the single channel EEG signal recorded from $C_z - A_1$ electrode position and the EEG signals recorded at sampling frequency $f_s = 200\,Hz$. The window length M and the number of decomposition levels for proposed SSA-ICA technique are set to 40 and 4 respectively. Fig. 5.21 shows the extracted low frequency and sleep spindle EEG components. The sleep spindle activity in the EEG signal (indicated in boxes) is efficiently isolated the low frequency EEG components. Since sleep spindle components between $12-16\,Hz$, the separation of sleep spindle component can be extracted using steps discussed in section 5.1.2. First, the eigenvectors associated to this band are identified and the sleep spindle activity is extracted and subtracted from the sleep EEG signal shown in Fig. 5.21(a), thus results EEG low frequency components. However, the extracted two EEG signals are uncorrelated, as SSA accounts the covariance of the data. Post processing of ICA on these decomposed components results efficient separation of sleep spindle and low frequency EEG components. In order to validate its effectiveness of the proposed technique in separating the EEG components, we adapted the scheme discussed in Fig. 5.5.

5.3 Conclusion

In this chapter, the SSA and ICA techniques were combined to separate/decompose the hidden sources from a single channel EEG signal. Simulation results shows that the proposed technique is capable of efficiently separating the sources as compared with the existing techniques (w-ICA, EEMD-ICA). The performance of the proposed SSA-ICA technique is evaluated on two real life single channel EEG signals. In addition, upon performing simulations for different M values it is noticed that the window length for the proposed SSA-ICA technique is independent of signal morphology and noise level and the performance is also constant for $M > 50$. However, the parameters of w-ICA and EEMD-ICA has to select based on the signal morphology and the signal noise level. As proposed SSA-ICA technique is capable of separating the sources from single channel EEG signals, this might be useful in applications where single channel EEG signal is available.

6

Muscle Artifact Removal Technique for Efficient Seizure Detection

The muscle artifact is an interference signal often superimposed on the EEG signal due to the activation of head muscles and obscure the valuable information present in the signal. Several studies reported that the presence of muscle artifacts degrade the performance of seizure detection algorithm. The BSS technique such as CCA is used to remove muscle artifacts from the multichannel EEG signals. In this chapter, an efficient muscle artifact removal technique for single channel EEG signal using modified SSA technique is presented and the performance of proposed technique was compared with single channel based decomposition techniques such as DWT and EEMD. Also, we applied this technique individually to each channel to compared its performance with BSS-CCA technique. In addition, its performance is evaluated in seizure detection algorithm as preprocessing technique.

6.1 Introduction

Epilepsy is a neurological disorder which causes seizure and nearly 1% of worlds population is suffering with this serious disorder [150]. Epileptic seizure is a period where a group of neuronal cells synchronously activated and reflected as high amplitude rhythmic component in the measured EEG signal [151, 152]. To diagnosis the epilepsy disorder the expert physician do the visual inspection of lengthy EEG records. However, it is very time consuming, as the length of EEG records usually lasting for 24 to 72 h. Therefore, automatic seizure detection system is often used to reduce the volume of the data to be observed by the physician. As a result they can see the detected seizure parts in the lengthy EEG record. In general, the EEG signals contaminated by muscle artifacts, due to the activation of head muscles during seizure period. However, the presence of these artifacts hampers the visual inspection of seizure activity registered EEG signals as well as degrades the performance of seizure detection systems [33, 153]. Therefore, removal of muscle artifact play an important role in the field of EEG signal processing.

In the early stages of EEG signal processing, low-pass filters often used to remove the muscle artifacts from EEG signals. However, as the frequency spectrums of both EEG and muscle artifacts overlap are in nature, use of such filters may alter the information in the EEG signals [154]. ICA is often used to remove the muscle artifacts from the mixed multichannel EEG data [43, 155]. However, the remnants of muscle artifact still present in the corrected EEG signals. In [55], CCA technique has been proposed to remove the muscle artifacts from multichannel EEG data. Even though ICA and CCA are BSS techniques, the principle of estimating the sources from multichannel EEG data is different. In ICA, it is assumed that the sources to be extracted are statistically independent, whereas in CCA, they were maximally autocorrelated and mutually uncorrelated [55]. Moreover, to extract the sources from multichannel EEG data, ICA uses higher order statistics (HOS) of data, whereas CCA uses the second order statistics (SOS) of the data. Therefore, the computational complexity of CCA is low as compared with ICA. More importantly, as muscle artifacts inherits the white gaussian noise property, then the corresponding HOS of muscle artifact is zero [154], hence, the performance of CCA is similar with that of ICA [55].

Recently, in [93], a combined EEMD and multi set CCA, so called EEMD-MCCA, has

been proposed to remove the muscle artifacts from the single channel EEG signal. However, this technique is computationally inefficient, due to the fact that EEMD has to be performed to make use of MCCA on single channel EEG signals. More importantly, performance of the techniques in [66, 93] depends on the free parameters of the EEMD, noise parameter (np) and number of ensemble (ne), as it is discussed in Chapter 5.2.1.

Singular spectrum analysis is a subspace based decomposed technique often used in the analysis of climate time series data. However, the performance of SSA mainly depends on the grouping step. In traditional SSA, this step is performed based on the magnitude of the eigenvalues. As the eigenvectors represent the direction of the spread of the data, therefore, use of such information in grouping step might be desirable. Initially, we have used the grouping criteria discussed in Chapter 3 and applied to remove the muscle artifact. However, it noticed that too much smoothing of EEG components takes place. As a result, the loss of EEG components having smaller magnitudes would be great. Moreover, we have to pre-compute the threshold to identify the eigenvectors for faithful reconstruction of EEG components. Therefore, in this Chapter, a new grouping criteria discussed in Chapter 5.1.2 is used. Where the EEG basis vectors were chosen based on the dominant frequency of the PSD of the eigenvector. Unlike in our previous work discussed in Chapter 3, it is very easy to set the threshold. Initially, we compared its performance with it state-of-art decomposition techniques (DWT and EEMD), as SSA is a subspace based decomposition technique. To evaluate the performance of proposed SSA technique over DWT and EEMD, simulation studies are carried on synthetic as well as on real life EEG signals. Simulation studies shows that the proposed technique outperforms compared to the state of art techniques.

6.2 Simulation Studies

To compare the performance of proposed SSA technique with that of DWT and EEMD techniques, we conducted the simulation studies on synthetic as well as on real life EEG signals. In general, ictal EEG signals inherits the rhythmic activity, hence, synthetic rhythmic activity of EEG signal is modeled by adding of two sinusoidal signals of frequencies 5.5 and $11Hz$, with different magnitudes. Here, this rhythmic signal is a representative of ictal activity. We construct the muscle artifact contaminated EEG signal by adding white noise using to the rhythmic signal using the mixing model given

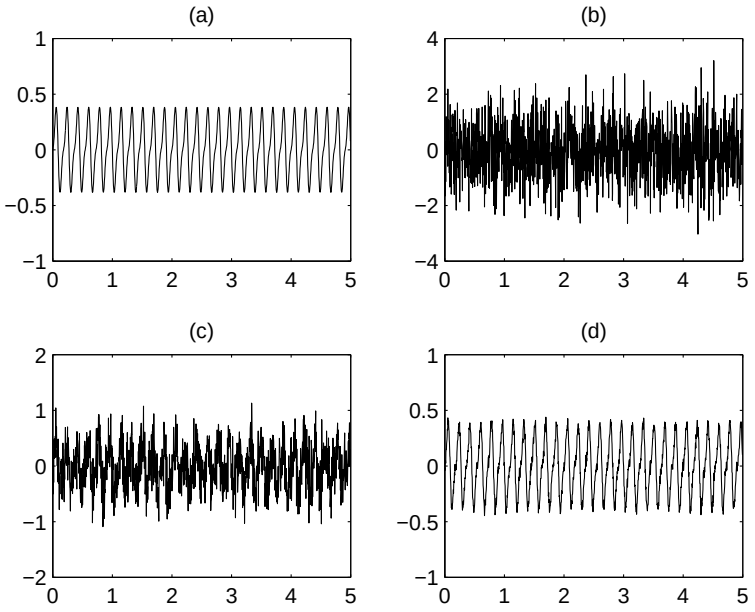

FIGURE 6.1: (a) synthetic EEG signal $s(n)$, (b) muscle artifact $r(n)$, (c) contaminated EEG signal $u(n)$ for $SNR = 0.2$ and $u(n)$ for $SNR = 2$, respectively.

in (2.8). Here, we assume that the white noise is representative of muscle artifact, as the muscle artifact inherits the white gaussian noise properties [94]. The contribution of the muscle artifact in the measured EEG signal depends on p *i.e.* a small change in p can alter the signal to noise ratio (SNR) of the measured EEG signal. The SNR of a signal in terms of root means square (RMS) is given by

$$SNR = \frac{RMS(\mathbf{s})}{RMS(p\mathbf{r})} \tag{6.1}$$

where, $RMS(\mathbf{s})$ is the root mean square value of the EEG signal vector. The true EEG, the muscle artifact and the contaminated EEG signals for different SNRs were shown in Fig. 6.1. It is obvious from Fig. 6.1 that for lower SNRs the muscle artifact impedes the visual inspection of EEG rhythmic activity. To compare the performance of proposed SSA decomposition technique with DWT and EEMD techniques, we use the relative root mean square error (RRMSE) as performance measure and is given by

$$RRMSE = \frac{RMS(\mathbf{s} - \hat{\mathbf{s}})}{RMS(\mathbf{r})} \times 100\% \tag{6.2}$$

where, $\hat{\mathbf{s}}$ is corrected EEG signal after application of the artifact removal technique.

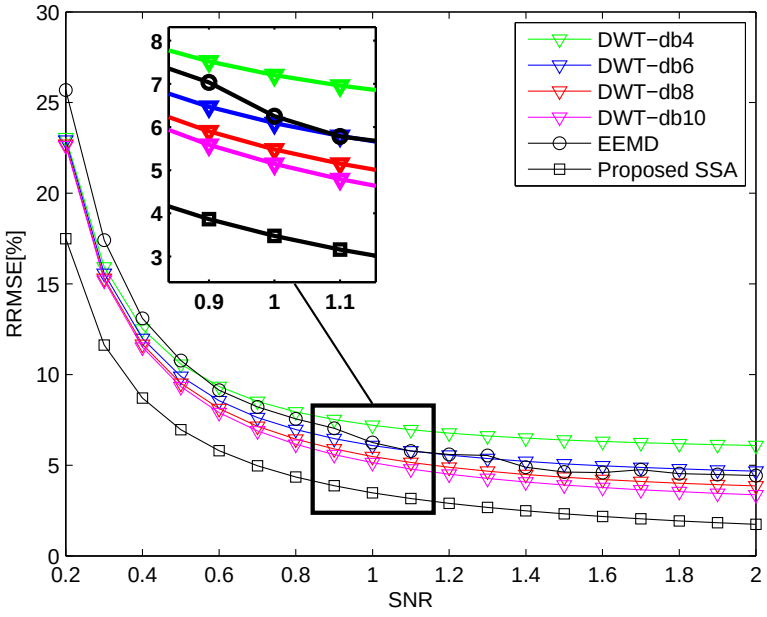

FIGURE 6.2: Performance of DWT with different mother wavelet, EEMD and proposed SSA techniques in terms of RRMSE.

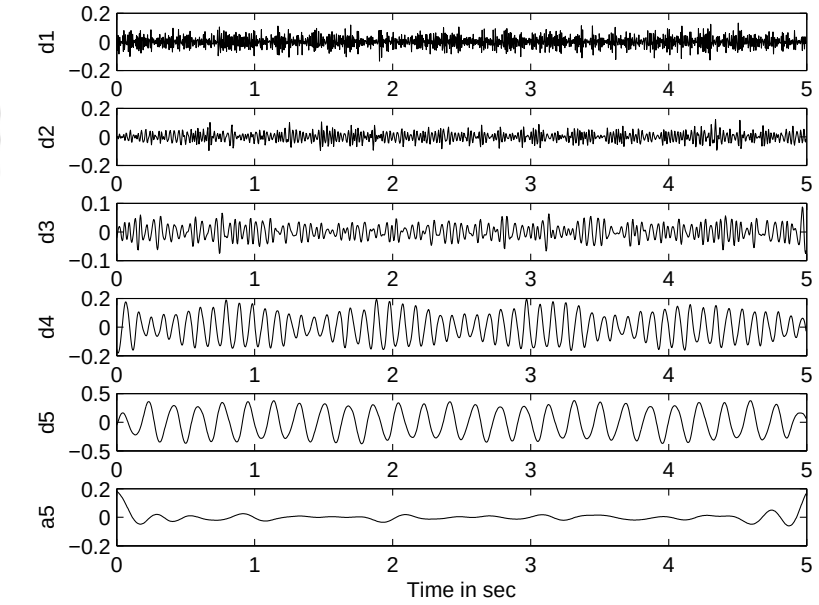

FIGURE 6.3: P+1 sub-band signals decomposed from a contaminated EEG signal of $SNR = 1$ using DWT.

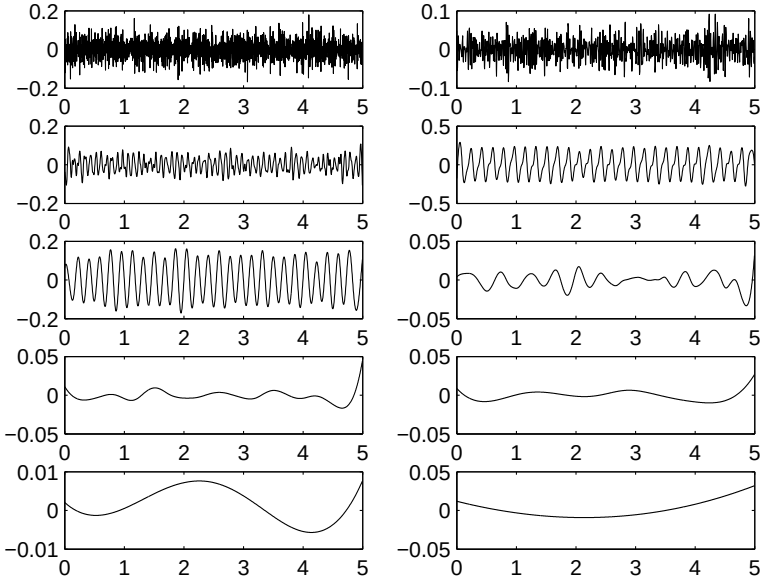

FIGURE 6.4: IMFs set derived from the contaminated EEG signal of $SNR = 1$ using EEMD decomposition technique.

6.2.1 Muscle Artifact Removal from Synthetic EEG Signals

Before applying the artifact removal technique on synthetic EEG signals, we set the free parameters of proposed SSA and other two decomposition techniques as follows. For DWT decomposition technique, Daubechie 10 ($db10$) mother wavelet and 5 decomposition levels were used. The free parameters of EEMD technique, *i.e.* np and ne were set to 2 and 100, respectively. Finally, the window length M of the proposed SSA technique is selected based on the criteria *i.e.* $M > f_s/f$ [69]. We considered $f_s = 250Hz$ and $f = 5.5Hz$ and $M = 64$. As most of the energy in the ictal EEG signal is concentrated in between $0.5Hz - 16Hz$ band, T_h for EEMD and the proposed SSA techniques is set to $16Hz$.

RRMSE curves of the three decomposition techniques as a function of SNR is shown in Fig. 6.2. Here, we evaluate the performance of DWT decomposition technique using $db4$, $db6$, $db8$ and $db10$ wavelet functions. It is obvious from Fig. 6.2 that DWT decomposition technique using $db10$ mother wavelet function showed better performance than DWT with other wavelet functions. However, it is observed from RRMSE curves that the performance of DWT mainly depends on the mother wavelet function. It is clear from Fig. 6.2 that EEMD exhibits poor performance as compared with than DWT ($db10$) and

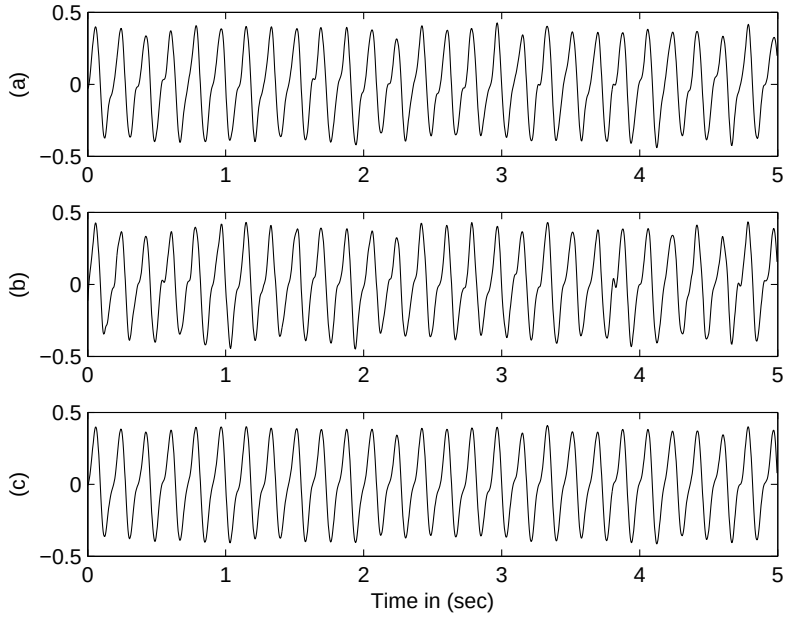

FIGURE 6.5: Reconstructed EEG signal for $SNR = 1$ using (a) DWT, (b) EEMD and (c) proposed SSA techniques respectively.

better performance compared to the DWT ($db4$ and $db6$) for SNRs greater than one. The reason is that noise components, added in the decomposition process were not canceled properly in the process of average of IMFs. To suppress these noise components, either ne should be increased or np should be decreased. In [66], it is stated that np value should be large when the signal to be extracted is low frequency component and should be small when the signal to be extracted is high frequency component. However, the computational complexity of EEMD algorithm is increased when ne is increased. Since SSA accounts the local covariance of the data the estimated basis vectors (eigenvectors) are robust. Therefore, the proposed SSA technique outperforms both DWT and EEMD techniques. Moreover, unlike DWT, the selection of the parameter M in SSA is straight forward and is independent of the signal morphology. To compare the performance of proposed SSA and other two decomposition techniques in a subjective way, synthetically contaminated EEG signal of $SNR = 1$ is used as a input signal. The decomposed sub-band signals of contaminated EEG signal using DWT are shown in Fig. 6.3. As the most of energy of ictal EEG signal is concentrated between $0.5 - 16Hz$ band, sub-band signals obtained by detailed coefficients at decomposition levels 4 and 5 and approximation coefficient at level 5 are used for the reconstruction of artifact free EEG signal. The sub-band signals and the corrected EEG signal using DWT are shown in Fig. 6.3 and Fig. 6.5(a) respectively. The IMF components of the contaminated EEG using EEMD

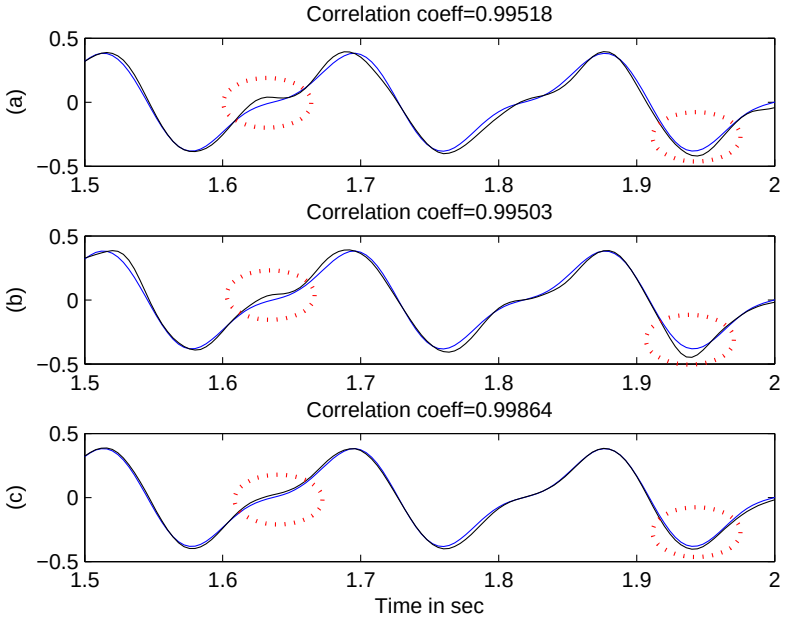

FIGURE 6.6: Zoomed version Fig. 6.5 between the time interval $1.5 - 2\,s$: (a) DWT, (b) EEMD and proposed SSA decomposition techniques, respectively.

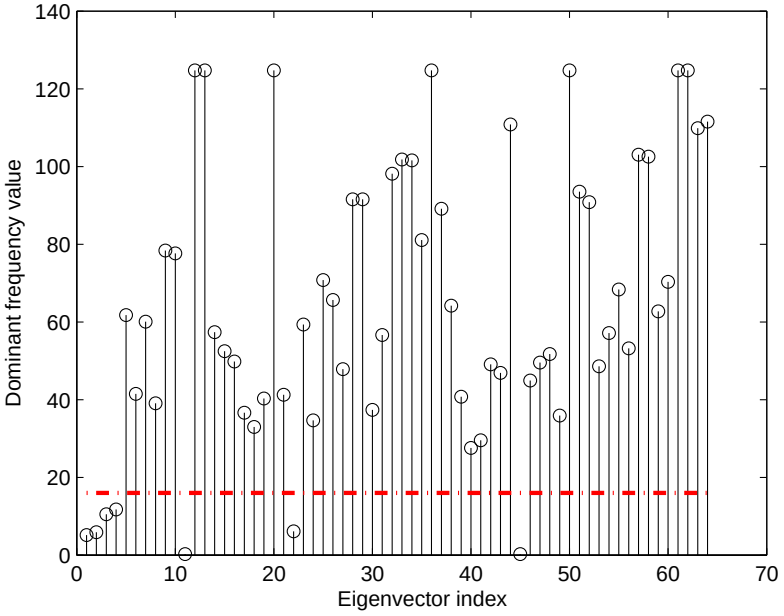

FIGURE 6.7: The dominant frequencies (f_d) of estimated eigenvectors of $\mathbf{u}$ for $SNR = 1$.

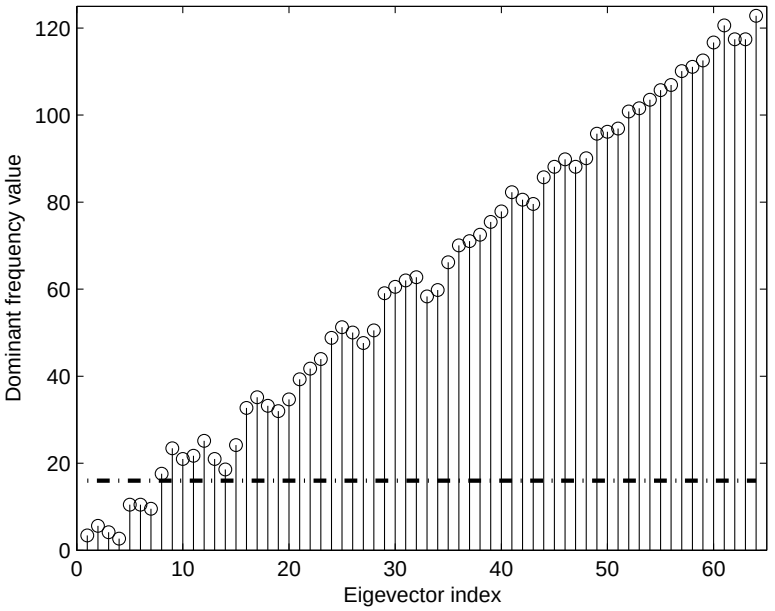

FIGURE 6.8: Dominant frequencies of M eigenvectors.

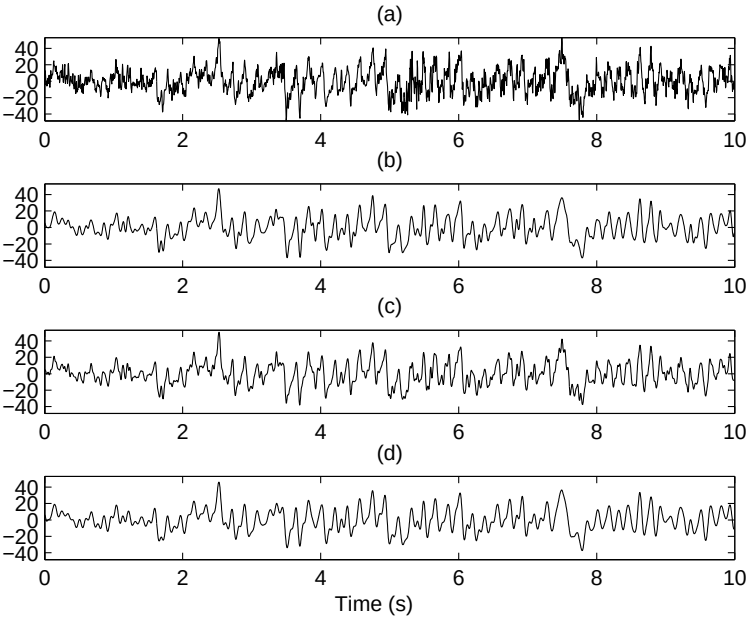

FIGURE 6.9: (a) Contaminated EEG signal, The corrected EEG signal using (b) DWT, (c) EEMD and (d) proposed SSA technique.

are shown in Fig. 6.4. In order to reconstruct the artifact free EEG signal, first, PSD of each IMF is computed. Later, the dominant frequency f_d of each IMF is identified. The artifact free EEG signal is reconstructed by adding IMF components whose dominant frequency is less or equal to specified threshold T_h, *i.e.* $16Hz$. The corrected EEG signal obtained by EEMD is shown in Fig. 6.5(b). In the proposed technique after deriving

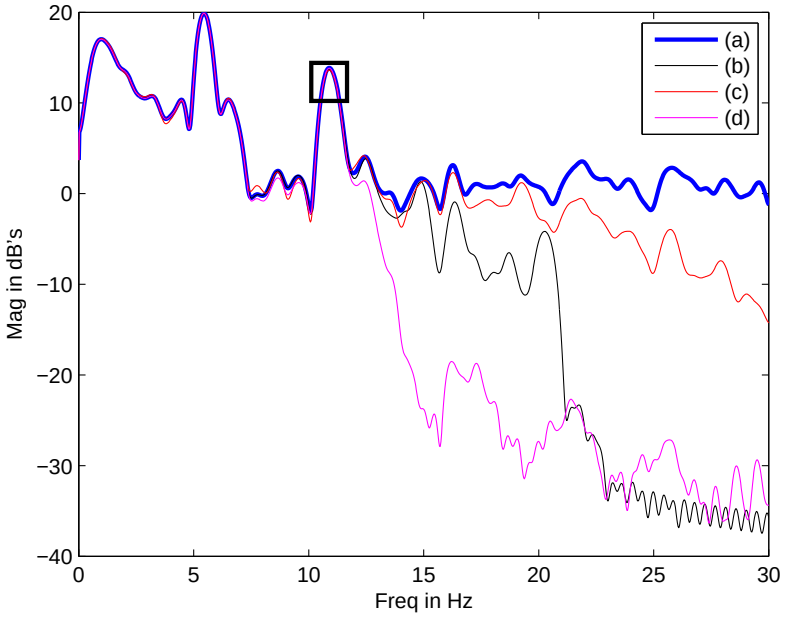

FIGURE 6.10: PSD of (a) contaminated EEG signal, corrected EEG signals using (b) DWT, (c) EEMD, and (d) proposed SSA decomposition techniques, respectively.

the eigenvectors of the covariance matrix, the dominant frequency of each eigenvector is computed, shown in Fig. 6.7. The dotted line in red color shows the threshold T_h, which is set to $16Hz$. In order to obtain the corrected EEG signal using proposed SSA decomposition technique, first, trajectory matrix associated to artifact free EEG signals is obtained by projecting trajectory matrix $\mathbf{U}$ onto the subspace spanned by the eigenvectors whose dominant frequencies are less than 16 ($\mathbf{v}_1$ to $\mathbf{v}_4$, $\mathbf{v}_{11}, \mathbf{v}_{22}$ and $\mathbf{v}_{45}$). Finally, the trajectory matrix associated to the artifact EEG signal is mapped into single channel EEG signal using (2.15). The corrected EEG signal estimated by the proposed SSA technique is shown in Fig. 6.5(c). To show the similarity between the true EEG and the corrected EEG signals, a zoomed version of Fig. 6.5(a-c) is showed with ground truth EEG signal (blue color) in Fig. 6.6. The correlation coefficient between the ground true and corrected EEG signals is computed. From the computed correlation coefficients, it shows that corrected EEG obtained by the proposed SSA technique is more similar with the true EEG signal.

6.2.2 Muscle Artifact Removal from Real Life EEG signals

To assess the performance of DWT, EEMD and proposed SSA techniques on real life ictal EEG signals, an EEG epoch of length 10 s is considered. This data is made available

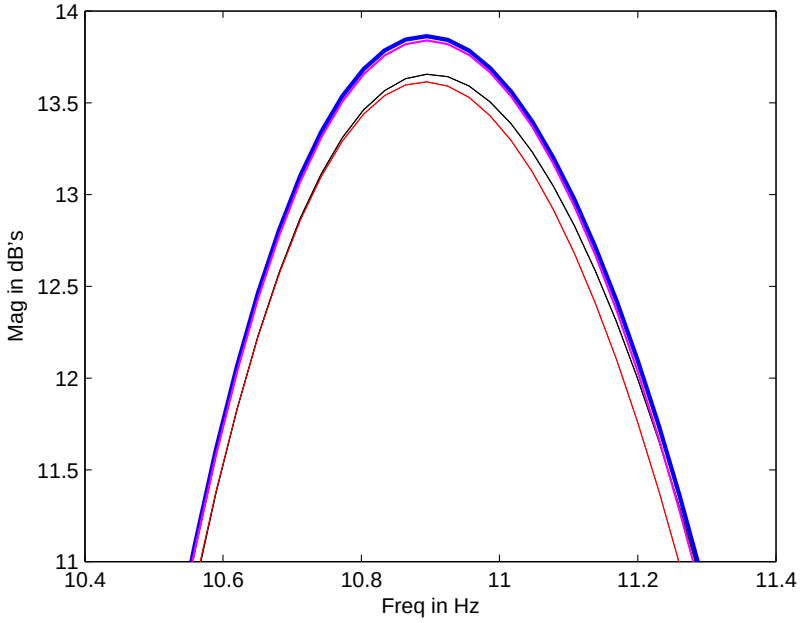

FIGURE 6.11: Zoomed version of Fig. 6.10 between the frequency band $10.4Hz - 11.4Hz$.

from the Biosource Database [6]. These EEG signals were recorded from a patient who is suffering with mesial temporal lobe epilepsy (MTLE) with the sampling frequency $f_s = 250Hz$. Fig. 2.4 shows $10\,s$ artifact contaminated multichannel EEG data. As the muscle artifacts are more predominant on the temporal regions, first, we applied the proposed technique on the EEG signal recorded from T_6 electrode location. Fig. 6.8. shows the dominant frequencies of M eigenvectors, where the dotted line indicates the threshold T_h equal to $16Hz$. We identified the eigenvectors whose dominant frequency is less than or equal to the threshold T_h, ($\mathbf{v}_1$ to $\mathbf{v}_7$), and added to obtain single eigenvector. Using the resulted eigenvector, the trajectory matrix associated to the artifact free EEG signal is estimated using (2.12). The estimated trajectory matrix is mapped into single channel EEG signal using (2.15). The artifact free EEG signal using DWT, EEMD and the proposed SSA decomposition techniques were shown in Fig. 6.9. It is obvious from Fig. 6.10 that the proposed SSA technique removes muscle artifact efficiently, the power reduction after $16Hz$ could be seen. The zoomed portion of Fig. 6.10 in the frequency band from $10.4Hz - 11.4Hz$ is shown in Fig. 6.11. From Fig. 6.11 it is observed that in the removal process of muscle artifacts, DWT and EEMD techniques partially extracted $11.5Hz$ component, as compared with the proposed SSA technique.

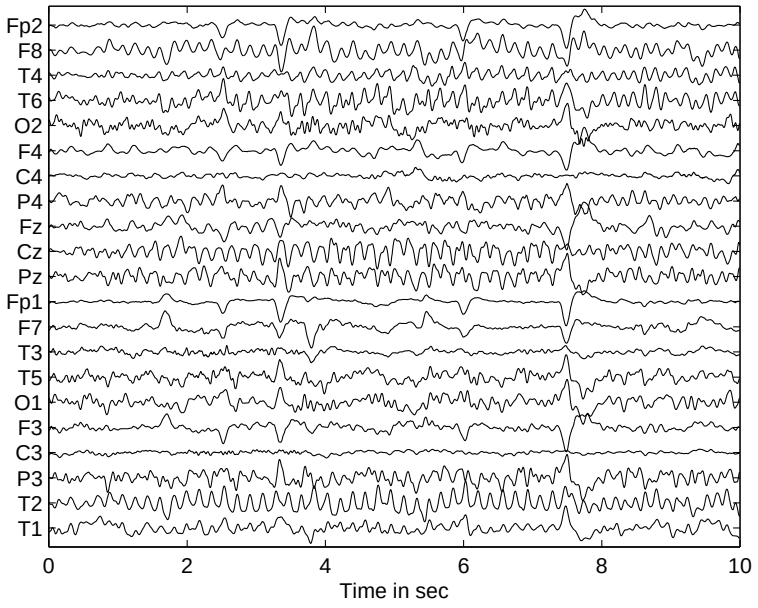

FIGURE 6.12: EEG reconstruction after the removal of muscle artifact using proposed SSA technique.

In general, when recording EEG signals, they contaminated by several artifacts, therefore, we do not know the ground truth EEG signal to evaluate RRMSE. Hence, to validate performance of three decomposition techniques on real-life ictal EEG signals in an objective way, we compute mean absolute error (MAE) in the specified band and is given by

$$MAE = \sum_{k=l}^{m} |P_u(k) - P_{\hat{u}}(k)|/(m-l) \tag{6.3}$$

where $P_u(k)$ and $P_{\hat{s}}(k)$ are PSDs of the contaminated and corrected EEG signals, respectively. The variables l and m defines specific frequency band. Table. 6.1 shows MAE in the frequency band $10.4Hz - 11.4Hz$. From Table. 6.1, MAE for the proposed SSA technique is $-20.116dB$, which as low as compared with MAE of DWT and EEMD techniques. Finally, the proposed SSA technique is applied to each EEG channel signal, shown in Fig. 2.4. From Fig. 6.12 it obvious that proposed SSA technique removed muscle artifact efficiently and no remanent of muscle artifact is present. It is noticed that the proposed technique exhibited the superior performance than the results obtained by the CCA technique as depicted in 2.7.

In addition, we also evaluated the performance of seizure detection algorithm by employing the proposed technique as preprocessing step. Support vector machine (SVM)

TABLE 6.1: Mean Absolute error for DWT, EEMD and SSA techniques

Methods	Mean Absolute Error (MAE) in (dBs)
DWT	−12.266
EEMD	−9.3496
SSA	−20.116

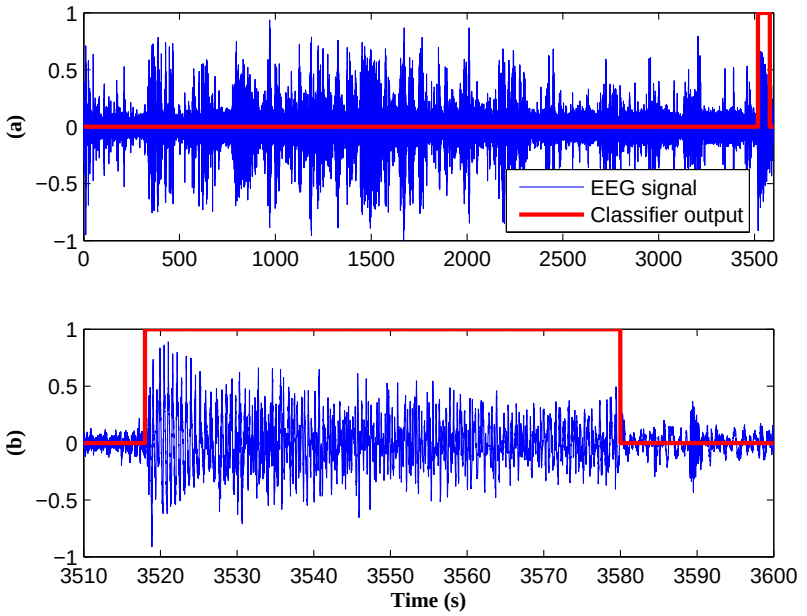

FIGURE 6.13: (a) seizure detection (red line) after removal of muscle artifact using proposed technique (b) Zoomed version of above plot between the time interval 3510 − 3600 s.

[156] classifier finds hyperplane between the positive and negative classes using predefined training data and labels. It has been used in many seizure detection classification problems. We use the LIBSVM toolbox to train the data [157]. As the muscle artifact is dominant in the temporal region, the performance of classifier is evaluated on the EEG signals recorded from the temporal region. Initially, the proposed technique is used to remove the muscle artifact from the EEG signals recorded from the temporal region. Next, we extracted eight features from every one second EEG epoch: four spectral energies features between the bands $0.5-4Hz$, $4-8Hz$, $8-12Hz$ and $12-30Hz$ and four time based features like kurtosis, skewness, fractal dimension and fluctuation index [27, 158]. The extracted feature vectors were applied to SVM classifier to find the hyperplane between the feature associated to the seizure and non-seizure feature vectors. In a similar manner, we built another classifier without removing the muscle artifacts.

We choose EEG signals of patient 24 from the CHB-MIT scalp EEG database [3, 8]. Fig. 6.13 shows the EEG signal and detector output, in which seizure is occurred at $3518 - 3580\,s$.

In order to validate the classifier performance, we evaluated five performance measures : true positive rate (TPR), true negative rate (TNR), false negative rate (FNR), and true negative rate (TNR).

$$\begin{aligned} TPR &= \frac{TP}{TP+FN} \\ FPR &= \frac{FP}{FP+TN} \\ TNR &= \frac{TN}{FP+TN} \\ FNR &= 1-TPR \end{aligned} \tag{6.4}$$

where, the true positive (TP) implies that the number of seizure epochs detected by both detector and the physician, false negative (FN) implies number of seizure epoches incorrectly detected by the detector but correctly detected by the physician, true negative (TN) implies the number non-seizure epochs detected by both detector and physician and false positive (FN) implies the number non-seizure epoches detected as seizures by the detector but correctly determined by the physician [159]. We tested the model on eight EEG record each lasting for one hour and Table. 6.2 shows the performance measures of seizure detector before and after removing the muscle artifact from the EEG data. From Table. 6.2 it is clear that on average, there will be 1.85% (TPR) improvement in sensitivity and 1.89% (TNR) improvement in specificity . More importantly, when the artifact removal technique is employed, the false positive rate is decreased.

TABLE 6.2: Seizure detection performance before and after muscle artifacts removal.

Record No	Before				After			
	TPR(%)	FPR(%)	FNR(%)	TNR(%)	TPR(%)	FPR(%)	FNR(%)	TNR (%)
1	85.71	0.13	0.05	99.86	78.57	0	0.08	100
2	92.30	1.61	0.02	98.38	84.61	0.41	0.05	99.58
3	100	3.42	0	96.57	100	0.30	0	99.69
4	76.92	4.65	0.08	95.34	92.30	1.17	0.02	98.82
5	76.92	4.71	0.08	95.28	61.53	1.17	0.14	98.82
6	61.53	3.62	0.14	96.37	61.53	3.62	0.14	96.37
7	90.62	0.05	0.16	99.94	96.87	0	0.05	100
8	96.87	0.14	0.05	99.85	96.87	0.02	0.05	99.97
Average	**85.07**	**2.29**	**0.07**	**97.69**	**86.92**	**0.40**	**0.05**	**99.58**

6.3 Conclusion

In this chapter, subspace based decomposition technique to remove muscle artifact from single channel EEG signals is presented. In this technique, the dominant frequency of eigenvectors is used to group the eigenvectors associated to the EEG and muscle artifact. Simulations on synthetic and real life EEG signals was carried to assess the performance of proposed technique over DWT and EEMD. From the simulation results it is also obvious that the performance of DWT technique mainly depends on the selection of mother wavelet function and whereas the EEMD decomposition technique mainly depends on the parameters np and ne. It is also noticed from PSDs that the proposed SSA technique removed muscle artifact without altering EEG components and is evident from from MAE. Moreover, it can be concluded that proposed SSA based muscle artifact removal could be used in seizure detection algorithms as preprocessing step.

7

Conclusion and Future scope

7.1 Summary of the thesis contributions

In this thesis, we explored several artifact removal technique for single channel EEG signals using SSA.

In **Chapter 3**, the issues in the traditional SSA technique is discussed and proposed a new grouping criteria to identify the desired signal (EEG) subspace. To validate this technique, first we applied to remove motion artifact from single channel EEG signals. The proposed modified SSA technique exhibited the superior performance than the existing EEMD-CCA technique. In addition to that the computational complexity of the modified SSA technique is also evaluated.

ANCs are applied to several biomedical signals to remove artifacts in online. In **Chapter 4**, ANC is used to remove EOG artifact from the single channel EEG signals. However, it need primary and reference signals; the primary signal is contaminated EEG signal and the reference signal is prototype of EOG artifact present in the contaminated EEG signal. Moreover, detailed structure of SSA-ANC technique for the online removal of EOG artifact is also discussed. Simulation results also demonstrated the benefit of combining both techniques.

Chapter 5 discussed about the steps to process single channel EEG signals using ICA technique and showed its performance by conducting experiments on the real-life single channel EEG signals. In addition to that the effect of window length in the overall performance of SSA-ICA technique discussed.

Finally, muscle artifact removal technique for single channel EEG signals is proposed and is validated by implementing it in seizure detection algorithm as preprocessing technique is discussed in **Chapter 6**. The performance measures of seizure detection algorithm also evaluated.

7.2 Future scope of the work

- Statistical based grouping criteria can be proposed for efficient and automatic identification of signal subspace.
- In SSA, as SVD accounts SOS of the data, the decomposed components are weakly separable. Implementing higher order SVD or tensor based decomposition techniques in place of SVD can enhance the decomposition step.
- For real-time applications, efficient architecture for the proposed techniques can be derived.

Bibliography

[1] J. Malmivuo and R. Plonsey, *Bioelectromagnetism: principles and applications of bioelectric and biomagnetic fields*. Oxford University Press, USA, 1995.

[2] R. Cooper, J. W. Osselton, and J. C. Shaw, EEG *technology*. Butterworth-Heinemann, 2014.

[3] A. L. Goldberger, L. A. Amaral, L. Glass, J. M. Hausdorff, P. C. Ivanov, R. G. Mark, J. E. Mietus, G. B. Moody, C.-K. Peng, and H. E. Stanley, "Physiobank, physiotoolkit, and physionet," *Circulation*, vol. 101, no. 23, pp. e215–e220, 2000.

[4] P. Campisi, D. La Rocca, and G. Scarano, "*EEG* for automatic person recognition," *Computer*, vol. 45, no. 7, pp. 87–89, 2012.

[5] K. T. Sweeney, H. Ayaz, T. E. Ward, M. Izzetoglu, S. F. McLoone, and B. Onaral, "A methodology for validating artifact removal techniques for physiological signals," *IEEE transactions on information technology in biomedicine*, vol. 16, no. 5, pp. 918–926, 2012.

[6] "Biosourcedatabase," . [Online]. Available: http://www.esat.kuleuven.be/stadius/members/biomed/data007.htm

[7] H. Berger, "Uber das Elektrenkephalogramm des Menschen," *Arch. Psychiatr. Nervenkr.*, vol. 87, p. 527, 1929.

[8] A. H. Shoeb, "Application of machine learning to epileptic seizure onset detection and treatment," Ph.D. dissertation, Massachusetts Institute of Technology, 2009.

[9] A. E. C Gray, P König and W. Singer, "Oscillatoryresponses in cat visualcortex exhibit intercolumnar synchronization which reects global stimulus properties," *Nature*, vol. 338, pp. 335–337, 1989.

[10] C. Gray and W. Singer, "Stimulus-specific neuronal oscillations in orientation columns of cat visual cortex," *Proceedings of the National Academy of Sciences of the United States of America*, vol. 86(5), pp. 1698–1702, 1989.

[11] D. J. McFarland, L. M. McCane, S. V. David, and J. R. Wolpaw, "Spatial filter selection for *EEG*-based communication," *Electroencephalography and Clinical Neurophysiology*, vol. 103, no. 3, pp. 386 – 394, 1997.

[12] S. S. Spencer, P. D. Williamson, S. L. Bridgers, R. H. Mattson, D. V. Cicchetti, and D. D. Spencer, "Reliability and accuracy of localization by scalp ictal *EEG*," *Neurology*, vol. 35, no. 11, pp. 1567–1567, 1985.

[13] N. Birbaumer, "Breaking the silence: brain–computer interfaces (*BCI*) for communication and motor control," *Psychophysiology*, vol. 43, no. 6, pp. 517–532, 2006.

[14] M. Jeannerod, "Neural simulation of action: a unifying mechanism for motor cognition," *Neuroimage*, vol. 14, no. 1, pp. S103–S109, 2001.

[15] S. Lemm, C. Schafer, and G. Curio, "*BCI* competition 2003-data set iii: probabilistic modeling of sensorimotor/spl mu/rhythms for classification of imaginary hand movements," *IEEE Transactions on Biomedical Engineering*, vol. 51, no. 6, pp. 1077–1080, 2004.

[16] L. F. Nicolas-Alonso and J. Gomez-Gil, "Brain computer interfaces, a review," *Sensors*, vol. 12, no. 2, pp. 1211–1279, 2012.

[17] D. Smith, B. Defalla, and D. Chadwick, "The misdiagnosis of epilepsy and the management of refractory epilepsy in a specialist clinic," *Qjm*, vol. 92, no. 1, pp. 15–23, 1999.

[18] E. Waterhouse, "New horizons in ambulatory electroencephalography," *IEEE Engineering in Medicine and Biology Magazine*, vol. 22, no. 3, pp. 74–80, 2003.

[19] B. Greene, G. Boylan, W. Marnane, G. Lightbody, and S. Connolly, "Automated single channel seizure detection in the neonate," in *Engineering in Medicine and Biology Society, 2008. EMBS 2008. 30th Annual International Conference of the IEEE*. IEEE, 2008, pp. 915–918.

[20] G. Zhu, Y. Li, and P. P. Wen, "Analysis and classification of sleep stages based on difference visibility graphs from a single-channel eeg signal," *IEEE journal of biomedical and health informatics*, vol. 18, no. 6, pp. 1813–1821, 2014.

[21] C. Berthomier, X. Drouot, M. Herman-Stoïca, P. Berthomier, J. Prado, D. Bokar-Thire, O. Benoit, J. Mattout, and M. d Ortho, "Automatic analysis of single-channel sleep *EEG*: validation in healthy individuals," *SLEEP-NEW YORK THEN WESTCHESTER-*, vol. 30, no. 11, p. 1587, 2007.

[22] B. Graimann, J. E. Huggins, A. Schlogl, S. P. Levine, and G. Pfurtscheller, "Detection of movement-related patterns in ongoing single-channel electrocorticogram," *IEEE Transactions on neural systems and rehabilitation engineering*, vol. 11, no. 3, pp. 276–281, 2003.

[23] B. Mahmoudi and A. Erfanian, "Single-channel *EEG*-based prosthetic hand grasp control for amputee subjects," in *Engineering in Medicine and Biology, 2002. 24th Annual Conference and the Annual Fall Meeting of the Biomedical Engineering Society EMBS/BMES Conference, 2002. Proceedings of the Second Joint*, vol. 3. IEEE, 2002, pp. 2406–2407.

[24] S. Ge, R. Wang, and D. Yu, "Classification of four-class motor imagery employing single-channel electroencephalography," *PloS one*, vol. 9, no. 6, p. e98019, 2014.

[25] G. Rebolledo-Mendez, I. Dunwell, E. A. Martínez-Mirón, M. D. Vargas-Cerdán, S. De Freitas, F. Liarokapis, and A. R. García-Gaona, "Assessing neurosky's usability to detect attention levels in an assessment exercise," in *International Conference on Human-Computer Interaction*. Springer, 2009, pp. 149–158.

[26] K. Ullah, M. Ali, M. Rizwan, and M. Imran, "Low-cost single-channel *EEG* based communication system for people with lock-in syndrome," in *Multitopic Conference (INMIC), 2011 IEEE 14th International.* IEEE, 2011, pp. 120–125.

[27] A. Shoeb, H. Edwards, J. Connolly, B. Bourgeois, S. T. Treves, and J. Guttag, "Patient-specific seizure onset detection," *Epilepsy & Behavior*, vol. 5, no. 4, pp. 483–498, 2004.

[28] M. De Vos, W. Deburchgraeve, P. Cherian, V. Matic, R. Swarte, P. Govaert, G. H. Visser, and S. Van Huffel, "Automated artifact removal as preprocessing refines neonatal seizure detection," *Clinical Neurophysiology*, vol. 122, no. 12, pp. 2345–2354, 2011.

[29] A. Vergult, M. De Vos, P. LeVan, J. Gotman, and S. Van Huffel, "Automatic muscle artifact removal as a preprocessing technique for seizure detection," in *Proc. of the The first Annual Symposium of the IEEE/EMBS Benelux Chapter.(IEEE EMBS)*, 2006, pp. on–cdrom.

[30] M. Fatourechi, A. Bashashati, R. K. Ward, and G. E. Birch, "*EMG* and *EOG* artifacts in brain computer interface systems: A survey," *Clinical neurophysiology*, vol. 118, no. 3, pp. 480–494, 2007.

[31] A. Bashashati, B. Nouredin, R. K. Ward, P. Lawrence, and G. E. Birch, "Effect of eye-blinks on a self-paced brain interface design," *Clinical neurophysiology*, vol. 118, no. 7, pp. 1639–1647, 2007.

[32] I. I. Goncharova, D. J. McFarland, T. M. Vaughan, and J. R. Wolpaw, "*EMG* contamination of *EEG*: spectral and topographical characteristics," *Clinical neurophysiology*, vol. 114, no. 9, pp. 1580–1593, 2003.

[33] M. Saab and J. Gotman, "A system to detect the onset of epileptic seizures in scalp *EEG*," *Clinical Neurophysiology*, vol. 116, no. 2, pp. 427–442, 2005.

[34] T.-P. Jung, S. Makeig, C. Humphries, T.-W. Lee, M. J. Mckeown, V. Iragui, and T. J. Sejnowski, "Removing electroencephalographic artifacts by blind source separation," *Psychophysiology*, vol. 37, no. 2, pp. 163–178, 2000.

[35] C. A. Joyce, I. F. Gorodnitsky, and M. Kutas, "Automatic removal of eye movement and blink artifacts from *EEG* data using blind component separation," *Psychophysiology*, vol. 41, no. 2, pp. 313–325, 2004.

[36] K. Ting, P. Fung, C. Chang, and F. Chan, "Automatic correction of artifact from single-trial event-related potentials by blind source separation using second order statistics only," *Medical engineering & physics*, vol. 28, no. 8, pp. 780–794, 2006.

[37] S. Halder, M. Bensch, J. Mellinger, M. Bogdan, A. Kübler, N. Birbaumer, and W. Rosenstiel, "Online artifact removal for brain-computer interfaces using support vector machines and blind source separation," *Computational intelligence and neuroscience*, vol. 2007, 2007.

[38] R. N. Vigário, "Extraction of ocular artefacts from *EEG* using independent component analysis," *Electroencephalography and clinical neurophysiology*, vol. 103, no. 3, pp. 395–404, 1997.

[39] T. P. Jung, S. Makeig, M. Westerfield, J. Townsend, E. Courchesne, and T. J. Sejnowski, "Removal of eye activity artifacts from visual event-related potentials in normal and clinical subjects," *Clinical Neurophysiology*, vol. 111, no. 10, pp. 1745–1758, 2000.

[40] R. N. Vigário, "Extraction of ocular artefacts from *EEG* using independent component analysis," *Electroencephalography and clinical neurophysiology*, vol. 103, no. 3, pp. 395–404, 1997.

[41] M. T. Medaglia, C. Porcaro, A. S. Meyer, and A. Krott, "Removal of muscle artifacts from *EEG* recordings by *ICA* during overt speech production," in *HBM 2011-The 17th Annual Meeting of the Organization for Human Brain Mapping*, 2011.

[42] N.-Y. Bian, B. Wang, Y. Cao, and L. Zhang, "Automatic removal of artifacts from *EEG* data using *ICA* and exponential analysis," in *International Symposium on Neural Networks*. Springer, 2006, pp. 719–726.

[43] E. Urrestarazu, J. Iriarte, M. Alegre, M. Valencia, C. Viteri, and J. Artieda, "Independent component analysis removing artifacts in ictal recordings," *Epilepsia*, vol. 45, no. 9, pp. 1071–1078, 2004.

[44] J. T. Gwin, K. Gramann, S. Makeig, and D. P. Ferris, "Removal of movement artifact from high-density *EEG* recorded during walking and running," *Journal of neurophysiology*, vol. 103, no. 6, pp. 3526–3534, 2010.

[45] A. Hyv *et al.*, "Fast and robust fixed-point algorithms for independent component analysis," *IEEE Transactions on Neural Networks*, vol. 10, no. 3, pp. 626–634, 1999.

[46] V. Zarzoso and P. Comon, "Robust independent component analysis by iterative maximization of the kurtosis contrast with algebraic optimal step size," *IEEE Transactions on Neural Networks*, vol. 21, no. 2, pp. 248–261, 2010.

[47] P. Comon, "Independent component analysis, a new concept?" *Signal processing*, vol. 36, no. 3, pp. 287–314, 1994.

[48] E. Oja and A. Hyvarinen, "A fast fixed-point algorithm for independent component analysis," *Neural computation*, vol. 9, no. 7, pp. 1483–1492, 1997.

[49] D. Xu, J. C. Principe, J. Fisher, and H.-C. Wu, "A novel measure for independent component analysis (*ICA*)," in *Acoustics, Speech and Signal Processing, 1998. Proceedings of the 1998 IEEE International Conference on*, vol. 2. IEEE, 1998, pp. 1161–1164.

[50] R. Boscolo, H. Pan, and V. P. Roychowdhury, "Independent component analysis based on nonparametric density estimation," *IEEE Transactions on Neural Networks*, vol. 15, no. 1, pp. 55–65, 2004.

[51] J.-F. Cardoso *et al.*, "On the performance of orthogonal source separation algorithms," in *Proc. EUSIPCO*, vol. 94. Edinburgh, UK, 1994, pp. 776–779.

[52] J.-F. Cardoso, "High-order contrasts for independent component analysis," *Neural computation*, vol. 11, no. 1, pp. 157–192, 1999.

[53] A. Delorme and S. Makeig, "*EEGLAB*: an open source toolbox for analysis of single-trial *EEG* dynamics including independent component analysis," *Journal of neuroscience methods*, vol. 134, no. 1, pp. 9–21, 2004.

[54] H. Hotelling, "Relations between two sets of variates," *Biometrika*, vol. 28, no. 3/4, pp. 321–377, 1936.

[55] W. De Clercq, A. Vergult, B. Vanrumste, W. Van Paesschen, and S. Van Huffel, "Canonical correlation analysis applied to remove muscle artifacts from the electroencephalogram," *IEEE Transactions on Biomedical Engineering*, vol. 53, no. 12, pp. 2583–2587, 2006.

[56] M. E. Davies and C. J. James, "Source separation using single channel *ICA*," *Signal Processing*, vol. 87, no. 8, pp. 1819–1832, 2007.

[57] Z. Wu and N. E. Huang, "Ensemble empirical mode decomposition: A noise-assisted data analysis method," *Advances in Adaptive Data Analysis*, vol. 01, no. 01, pp. 1–41, 2009.

[58] Y. Liu, W. Zhou, Q. Yuan, and S. Chen, "Automatic seizure detection using wavelet transform and *SVM* in long-term intracranial *EEG*," *IEEE transactions on neural systems and rehabilitation engineering*, vol. 20, no. 6, pp. 749–755, 2012.

[59] S. Mihandoost, M. C. Amirani, and B. Z. Varghahan, "Seizure detection using wavelet transform and a new statistical feature," in *Application of Information and Communication Technologies (AICT), 2011 5th International Conference on*. IEEE, 2011, pp. 1–5.

[60] Y. Kumar, M. Dewal, and R. Anand, "Epileptic seizures detection in *EEG* using *DWT*-based *ApEn* and artificial neural network," *Signal, Image and Video Processing*, vol. 8, no. 7, pp. 1323–1334, 2014.

[61] Y. Khan and J. Gotman, "Wavelet based automatic seizure detection in intracerebral electroencephalogram," *Clinical Neurophysiology*, vol. 114, no. 5, pp. 898–908, 2003.

[62] H. Ocak, "Automatic detection of epileptic seizures in *EEG* using discrete wavelet transform and approximate entropy," *Expert Systems with Applications*, vol. 36, no. 2, pp. 2027–2036, 2009.

[63] Y. Kumar, M. Dewal, and R. Anand, "Epileptic seizure detection using *DWT* based fuzzy approximate entropy and support vector machine," *Neurocomputing*, vol. 133, pp. 271–279, 2014.

[64] V. Bajaj and R. B. Pachori, "Classification of seizure and nonseizure *EEG* signals using empirical mode decomposition," *IEEE Transactions on Information Technology in Biomedicine*, vol. 16, no. 6, pp. 1135–1142, 2012.

[65] B. Azzerboni, F. La Foresta, N. Mammone, and F. C. Morabito, "A new approach based on wavelet-*ICA* algorithms for fetal electrocardiogram extraction." in *ESANN*, 2005, pp. 193–198.

[66] B. Mijović, M. De Vos, I. Gligorijević, v. Taelman, and S. Van Huffel, "Source separation from single-channel recordings by combining empirical-mode decomposition and independent component analysis," *IEEE Transactions on Biomedical Engineering*, vol. 57, no. 9, pp. 2188–2196, Sept 2010.

[67] M. Ghil, M. Allen, M. Dettinger, K. Ide, D. Kondrashov, M. Mann, A. W. Robertson, A. Saunders, Y. Tian, F. Varadi *et al.*, "Advanced spectral methods for climatic time series," *Reviews of geophysics*, vol. 40, no. 1, 2002.

[68] N. Golyandina, V. Nekrutkin, and A. Zhigljavsky, *Analysis of Time Series Structure:* SSA *and Related Techniques*, ser. Chapman & Hall/CRC Monographs on Statistics & Applied Probability. CRC Press, 2001.

[69] A. R. Teixeira, A. M. Tomé, E. W. Lang, P. Gruber, and A. M. Da Silva, "Automatic removal of high-amplitude artefacts from single-channel electroencephalograms," *Computer methods and programs in biomedicine*, vol. 83, no. 2, pp. 125–138, 2006.

[70] A. R. Teixeira, A. M. Tomé, M. Bohm, C. G. Puntonet, and E. W. Lang, "How to apply nonlinear subspace techniques to univariate biomedical time series," *IEEE Transactions on Instrumentation and Measurement*, vol. 58, no. 8, pp. 2433–2443, 2009.

[71] S. Sanei, T. K. Lee, and V. Abolghasemi, "A new adaptive line enhancer based on singular spectrum analysis," *IEEE Transactions on Biomedical Engineering*, vol. 59, no. 2, pp. 428–434, 2012.

[72] F. Ghaderi, H. R. Mohseni, and S. Sanei, "Localizing heart sounds in respiratory signals using singular spectrum analysis," *IEEE Transactions on Biomedical Engineering*, vol. 58, no. 12, pp. 3360–3367, 2011.

[73] S. Kouchaki, S. Sanei, E. L. Arbon, and D.-J. Dijk, "Tensor based singular spectrum analysis for automatic scoring of sleep *EEG*," *IEEE Transactions on Neural Systems and Rehabilitation Engineering*, vol. 23, no. 1, pp. 1–9, 2015.

[74] S. M. Mohammadi, S. Kouchaki, M. Ghavami, and S. Sanei, "Improving time-frequency domain sleep *EEG* classification via singular spectrum analysis," *Journal of Neuroscience Methods*, vol. 273, pp. 96–106, 2016.

[75] V. Moskvina and A. Zhigljavsky, "An algorithm based on singular spectrum analysis for change-point detection," *Communications in Statistics-Simulation and Computation*, vol. 32, no. 2, pp. 319–352, 2003.

[76] M. E. F. Djellatou, D. Massicotte, and M. Boukadoum, "Adaptive block ssa based anc implementation for high performances *ECG* removal from *sEMG* signals," in *Electrical and Computer Engineering (CCECE), 2014 IEEE 27th Canadian Conference on.* IEEE, 2014, pp. 1–6.

[77] B. Widrow, J. R. Glover, J. M. McCool, J. Kaunitz, C. S. Williams, R. H. Hearn, J. R. Zeidler, J. E. Dong, and R. C. Goodlin, "Adaptive noise cancelling: Principles and applications," *Proceedings of the IEEE*, vol. 63, no. 12, pp. 1692–1716, 1975.

[78] W. Du, H. Leong, and A. Gevins, "Ocular artifact minimization by adaptive filtering," in *Statistical Signal and Array Processing., IEEE Seventh SP Workshop on.* IEEE, 1994, pp. 433–436.

[79] P. He, G. Wilson, and C. Russell, "Removal of ocular artifacts from electroencephalogram by adaptive filtering," *Medical and biological engineering and computing*, vol. 42, no. 3, pp. 407–412, 2004.

[80] M. Z. U. Rahman, R. A. Shaik, and D. R. K. Reddy, "Efficient and simplified adaptive noise cancelers for *ECG* sensor based remote health monitoring," *IEEE Sensors Journal*, vol. 12, no. 3, pp. 566–573, 2012.

[81] G. V. S. Karthik, S. Y. Fathima, M. Z. U. Rahman, S. R. Ahamed, and A. Lay-Ekuakille, "Efficient signal conditioning techniques for brain activity in remote health monitoring network," *IEEE sensors journal*, vol. 13, no. 9, pp. 3276–3283, 2013.

[82] T. Gasser, J. Möcks *et al.*, "Correction of *EOG* artifacts in event-related potentials of the *EEG*: Aspects of reliability and validity," *Psychophysiology*, vol. 19, no. 4, pp. 472–480, 1982.

[83] A. Schlögl, C. Keinrath, D. Zimmermann, R. Scherer, R. Leeb, and G. Pfurtscheller, "A fully automated correction method of *EOG* artifacts in *EEG* recordings," *Clinical neurophysiology*, vol. 118, no. 1, pp. 98–104, 2007.

[84] G. Gómez-Herrero, W. De Clercq, H. Anwar, O. Kara, K. Egiazarian, S. Van Huffel, and W. Van Paesschen, "Automatic removal of ocular artifacts in the *EEG* without an *EOG* reference channel," in *Signal Processing Symposium, 2006. NORSIG 2006. Proceedings of the 7th Nordic*. IEEE, 2006, pp. 130–133.

[85] H. Peng, B. Hu, Q. Shi, M. Ratcliffe, Q. Zhao, Y. Qi, and G. Gao, "Removal of ocular artifacts in *EEG*-an improved approach combining *DWT* and *ANC* for portable applications," *IEEE journal of biomedical and health informatics*, vol. 17, no. 3, pp. 600–607, 2013.

[86] Z. Koldovskỳ and P. Tichavskỳ, "Time-domain blind audio source separation using advanced *ICA* methods." in *Interspeech*. Citeseer, 2007, pp. 846–849.

[87] D. Mallis, T. Sgouros, and N. Mitianoudis, "Convolutive audio source separation using robust *ICA* and reduced likelihood ratio jump," in *IFIP International Conference on Artificial Intelligence Applications and Innovations*. Springer, 2016, pp. 230–241.

[88] R. Martín-Clemente and S. Hornillo-Mellado, "Image processing using *ICA*: a new perspective," in *Electrotechnical Conference, 2006. MELECON 2006. IEEE Mediterranean*. IEEE, 2006, pp. 502–505.

[89] A. Hyvärinen and E. Oja, "Independent component analysis: algorithms and applications," *Neural networks*, vol. 13, no. 4, pp. 411–430, 2000.

[90] I. Daubechies, E. Roussos, S. Takerkart, M. Benharrosh, C. Golden, K. D'ardenne, W. Richter, J. Cohen, and J. Haxby, "Independent component analysis for brain *fMRI* does not select for independence," *Proceedings of the National Academy of Sciences*, vol. 106, no. 26, pp. 10 415–10 422, 2009.

[91] O. Friman, "Adaptive analysis of functional MRI data," Ph.D. dissertation, Linköping University, Sweden, 2003, dissertation No 836, ISBN 91-7373-699-6.

[92] Y. Ou Li, T. Adali, W. Wang, and V. Calhoun, "Joint blind source separation by multiset canonical correlation analysis," *IEEE Transactions on Signal Processing*, vol. 57, no. 10, pp. 3918–3929, Oct 2009.

[93] X. Chen, C. He, and H. Peng, "Removal of muscle artifacts from single-channel *EEG* based on ensemble empirical mode decomposition and multiset canonical correlation analysis," *Journal of Applied Mathematics*, vol. 2014, 2014.

[94] A. Hyvärinen, J. Karhunen, and E. Oja, *Independent component analysis*. John Wiley & Sons, 2004, vol. 46.

[95] B. Azzerboni, M. Carpentieri, F. La Foresta, and F. Morabito, "Neural-*ICA* and wavelet transform for artifacts removal in surface *EMG*," in *IEEE International Joint Conference on Neural Networks. Proceedings. 2004.*, vol. 4, July 2004, pp. 3223–3228 vol.4.

[96] "Fastica graphical user interface," 2005. [Online]. Available: http://www.cis.hut.fi/projects/ica/fastica/code/dlcode.shtml

[97] N. E. Huang, Z. Shen, S. R. Long, M. C. Wu, H. H. Shih, Q. Zheng, N.-C. Yen, C. C. Tung, and H. H. Liu, "The empirical mode decomposition and the hilbert spectrum for nonlinear and non-stationary time series analysis," in *Proceedings of the Royal Society of London A: Mathematical, Physical and Engineering Sciences*, vol. 454, no. 1971. The Royal Society, 1998, pp. 903–995.

[98] K. Sweeney, S. McLoone, and T. Ward, "The use of ensemble empirical mode decomposition with canonical correlation analysis as a novel artifact removal technique," *Biomedical Engineering, IEEE Transactions on*, vol. 60, no. 1, pp. 97–105, Jan 2013.

[99] S. L. Netto and L. W. Biscainho, "Adaptive filters: Structures, algorithms, and applications," in *Advances in Audio and Speech Signal Processing: Technologies and Applications*. IGI Global, 2007, pp. 190–224.

[100] T. S. Alexander, *Adaptive signal processing: theory and applications*. Springer Science & Business Media, 2012.

[101] M. Bellanger, *Adaptive digital filters*. CRC Press, 2001.

[102] J. R. Treichler, C. R. Johnson Jr, and M. J. Larimore, *Theory and design of adaptive filters*. Wiley-Interscience, 1987.

[103] A. Bertrand, V. Mihajlovic, B. Grundlehner, C. Van Hoof, and M. Moonen, "Motion artifact reduction in *EEG* recordings using multi-channel contact impedance measurements," in *Biomedical Circuits and Systems Conference (BioCAS), 2013 IEEE*. IEEE, 2013, pp. 258–261.

[104] X. Chen and Z. J. Wang, "Design and implementation of a wearable, wireless *EEG* recording system," in *Bioinformatics and Biomedical Engineering,(iCBBE) 2011 5th International Conference on*. IEEE, 2011, pp. 1–4.

[105] S. D. Ridwan, R. Thompson, B. T. Jap, S. Lal, and P. Fischer, "Single channel wireless *EEG* proposed application in train drivers," in *Broadband Communications, Information Technology & Biomedical Applications, 2008 Third International Conference on*. IEEE, 2008, pp. 58–63.

[106] B. Koley and D. Dey, "An ensemble system for automatic sleep stage classification using single channel *EEG* signal," *Computers in biology and medicine*, vol. 42, no. 12, pp. 1186–1195, 2012.

[107] R. R. Vázquez, H. Velez-Perez, R. Ranta, V. L. Dorr, D. Maquin, and L. Maillard, "Blind source separation, wavelet denoising and discriminant analysis for *EEG* artefacts and noise cancelling," *Biomedical Signal Processing and Control*, vol. 7, no. 4, pp. 389–400, 2012.

[108] K. Patel, C.-P. Chua, S. Fau, and C. J. Bleakley, "Low power real-time seizure detection for ambulatory *EEG*," in *Pervasive Computing Technologies for Healthcare, 2009. PervasiveHealth 2009. 3rd International Conference on.* IEEE, 2009, pp. 1–7.

[109] M. Wax and T. Kailath, "Detection of signals by information theoretic criteria," *IEEE Transactions on Acoustics, Speech, and Signal Processing*, vol. 33, no. 2, pp. 387–392, 1985.

[110] K. Najarian and R. Splinter, *Biomedical signal and image processing.* CRC press, 2005.

[111] J.-H. Lee, S. Oh, F. A. Jolesz, H. Park, and S.-S. Yoo, "Application of independent component analysis for the data mining of simultaneous eeg–fmri: Preliminary experience on sleep onset," *International Journal of Neuroscience*, vol. 119, no. 8, pp. 1118–1136, 2009.

[112] Y.-H. Wang, C.-H. Yeh, H.-W. V. Young, K. Hu, and M.-T. Lo, "On the computational complexity of the empirical mode decomposition algorithm," *Physica A: Statistical Mechanics and its Applications*, vol. 400, pp. 159–167, 2014.

[113] D. Safieddine, A. Kachenoura, L. Albera, G. Birot, A. Karfoul, A. Pasnicu, A. Biraben, F. Wendling, L. Senhadji, and I. Merlet, "Removal of muscle artifact from *EEG* data: comparison between stochastic (*ICA* and *CCA*) and deterministic (*EMD* and wavelet-based) approaches," *EURASIP Journal on Advances in Signal Processing*, vol. 2012, no. 1, p. 127, 2012.

[114] L. A. Farwell and E. Donchin, "Talking off the top of your head: toward a mental prosthesis utilizing event-related brain potentials," *Electroencephalography and clinical Neurophysiology*, vol. 70, no. 6, pp. 510–523, 1988.

[115] P. R. Kennedy, R. A. Bakay, M. M. Moore, K. Adams, and J. Goldwaithe, "Direct control of a computer from the human central nervous system," *IEEE Transactions on rehabilitation engineering*, vol. 8, no. 2, pp. 198–202, 2000.

[116] J. R. Wolpaw, D. J. McFarland, G. W. Neat, and C. A. Forneris, "An *EEG*-based brain-computer interface for cursor control," *Electroencephalography and clinical neurophysiology*, vol. 78, no. 3, pp. 252–259, 1991.

[117] E. E. Sutter, "The brain response interface: communication through visually-induced electrical brain responses," *Journal of Microcomputer Applications*, vol. 15, no. 1, pp. 31–45, 1992.

[118] D. J. McFarland, G. W. Neat, R. F. Read, and J. R. Wolpaw, "An *EEG*-based method for graded cursor control," *Psychobiology*, vol. 21, no. 1, pp. 77–81, 1993.

[119] G. Pfurtscheller, D. Flotzinger, and J. Kalcher, "Brain-computer interface-a new communication device for handicapped persons," *Journal of Microcomputer Applications*, vol. 16, no. 3, pp. 293–299, 1993.

[120] N. Birbaumer, N. Ghanayim, T. Hinterberger, I. Iversen, B. Kotchoubey, A. Kübler, J. Perelmouter, E. Taub, and H. Flor, "A spelling device for the paralysed," *Nature*, vol. 398, no. 6725, pp. 297–298, 1999.

[121] A. Kübler, B. Kotchoubey, J. Kaiser, J. R. Wolpaw, and N. Birbaumer, "Brain-computer communication: Unlocking the locked in." *Psychological bulletin*, vol. 127, no. 3, p. 358, 2001.

[122] A. Kübler, B. Kotchoubey, T. Hinterberger, N. Ghanayim, J. Perelmouter, M. Schauer, C. Fritsch, E. Taub, and N. Birbaumer, "The thought translation device: a neurophysiological approach to communication in total motor paralysis," *Experimental brain research*, vol. 124, no. 2, pp. 223–232, 1999.

[123] D. J. McFarland, L. M. McCane, S. V. David, and J. R. Wolpaw, "Spatial filter selection for *EEG*-based communication," *Electroencephalography and clinical Neurophysiology*, vol. 103, no. 3, pp. 386–394, 1997.

[124] I. I. Goncharova, D. J. McFarland, T. M. Vaughan, and J. R. Wolpaw, "*EMG* contamination of *EEG*: spectral and topographical characteristics," *Clinical neurophysiology*, vol. 114, no. 9, pp. 1580–1593, 2003.

[125] T. Gasser, J. Möcks *et al.*, "Correction of *EOG* artifacts in event-related potentials of the *EEG*: Aspects of reliability and validity," *Psychophysiology*, vol. 19, no. 4, pp. 472–480, 1982.

[126] J. Woestenburg, M. Verbaten, and J. Slangen, "The removal of the eye-movement artifact from the *EEG* by regression analysis in the frequency domain," *Biological psychology*, vol. 16, no. 1, pp. 127–147, 1983.

[127] S. S. Haykin, *Adaptive filter theory*. Pearson Education India, 2008.

[128] C. Guerrero-Mosquera and A. Navia-Vázquez, "Automatic removal of ocular artefacts using adaptive filtering and independent component analysis for electroencephalogram data," *IET signal processing*, vol. 6, no. 2, pp. 99–106, 2012.

[129] A. Teixeira, A. Tome, E. Lang, P. Gruber, and A. M. da Silva, "On the use of clustering and local singular spectrum analysis to remove ocular artifacts from electroencephalograms," in *Neural Networks, 2005. IJCNN'05. Proceedings. 2005 IEEE International Joint Conference on*, vol. 4. IEEE, 2005, pp. 2514–2519.

[130] C. M. Bishop, *Neural networks for pattern recognition*. Oxford university press, 1995.

[131] G. Pfurtscheller and F. L. Da Silva, "Event-related *EEG/MEG* synchronization and desynchronization: basic principles," *Clinical neurophysiology*, vol. 110, no. 11, pp. 1842–1857, 1999.

[132] W. Yi, S. Qiu, H. Qi, L. Zhang, B. Wan, and D. Ming, "*EEG* feature comparison and classification of simple and compound limb motor imagery," *Journal of neuroengineering and rehabilitation*, vol. 10, no. 1, p. 106, 2013.

[133] Y. Ichimaru and G. Moody, "Development of the polysomnographic database on *CD-ROM*," *Psychiatry and Clinical Neurosciences*, vol. 53, no. 2, pp. 175–177, 1999.

[134] M. Naeem, C. Brunner, R. Leeb, B. Graimann, and G. Pfurtscheller, "Seperability of four-class motor imagery data using independent components analysis," *Journal of neural engineering*, vol. 3, no. 3, p. 208, 2006.

[135] A. Cichocki, T. Rutkowski, and K. Siwek, "Blind signal extraction of signals with specified frequency band," in *Neural Networks for Signal Processing, 2002. Proceedings of the 2002 12th IEEE Workshop on.* IEEE, 2002, pp. 515–524.

[136] S. A. Cruces-Alvarez, A. Cichocki, and S.-I. Amari, "On a new blind signal extraction algorithm: different criteria and stability analysis," *IEEE signal processing letters*, vol. 9, no. 8, pp. 233–236, 2002.

[137] B. Greene, G. Boylan, W. Marnane, G. Lightbody, and S. Connolly, "Automated single channel seizure detection in the neonate," in *Engineering in Medicine and Biology Society, 2008. EMBS 2008. 30th Annual International Conference of the IEEE.* IEEE, 2008, pp. 915–918.

[138] G. Rebolledo-Mendez, I. Dunwell, E. A. Martínez-Mirón, M. D. Vargas-Cerdán, S. De Freitas, F. Liarokapis, and A. R. García-Gaona, "Assessing neuroskys usability to detect attention levels in an assessment exercise," in *International Conference on Human-Computer Interaction.* Springer, 2009, pp. 149–158.

[139] S.-F. Liang, C.-E. Kuo, Y.-H. Hu, Y.-H. Pan, and Y.-H. Wang, "Automatic stage scoring of single-channel sleep *EEG* by using multiscale entropy and autoregressive models," *IEEE Transactions on Instrumentation and Measurement*, vol. 61, no. 6, pp. 1649–1657, 2012.

[140] S. Ge, R. Wang, and D. Yu, "Classification of four-class motor imagery employing single-channel electroencephalography," *PloS one*, vol. 9, no. 6, p. e98019, 2014.

[141] J. Lin and A. Zhang, "Fault feature separation using wavelet-*ICA* filter," *NDT & e International*, vol. 38, no. 6, pp. 421–427, 2005.

[142] P. Celka and P. Colditz, "A computer-aided detection of *EEG* seizures in infants: a singular-spectrum approach and performance comparison," *IEEE transactions on biomedical engineering*, vol. 49, no. 5, pp. 455–462, 2002.

[143] A. Wennberg and L. H. Zetterberg, "Application of a computer-based model for *EEG* analysis," *Electroencephalography and clinical neurophysiology*, vol. 31, no. 5, pp. 457–468, 1971.

[144] B. H. Jansen, J. R. Bourne, and J. W. Ward, "Autoregressive estimation of short segment spectra for computerized *EEG* analysis," *IEEE Transactions on Biomedical Engineering*, no. 9, pp. 630–638, 1981.

[145] P. C. Hansen and S. H. Jensen, "Fir filter representations of reduced-rank noise reduction," *IEEE Transactions on Signal Processing*, vol. 46, no. 6, pp. 1737–1741, 1998.

[146] A. Tomé, A. R. Teixeira, N. Figueiredo, I. Santos, P. Georgieva, and E. Lang, "Ssa of biomedical signals: A linear invariant systems approach," 2010.

[147] L. De Gennaro and M. Ferrara, "Sleep spindles: an overview," 2003.

[148] R. Rosipal, G. Dorffner, and E. Trenker, "Can *ICA* improve sleep-spindles detection?" *Neural Network World*, vol. 8, pp. 539–548, 1998.

[149] S. Devuyst, T. Dutoit, P. Stenuit, and M. Kerkhofs, "Automatic sleep spindles detection-overview and development of a standard proposal assessment method," in *Engineering in Medicine and Biology Society, EMBC, 2011 Annual International Conference of the IEEE*. IEEE, 2011, pp. 1713–1716.

[150] W. H. Organization *et al.*, "Fact sheet n 999," *Epilepsy. Geneva: World Health Organization-[Cited Feb 24, 2011]. Available from: URL: http://www. who. int/-mediacentre/factsheets/fs999/en*, 2009.

[151] R. S. Fisher, W. v. E. Boas, W. Blume, C. Elger, P. Genton, P. Lee, and J. Engel, "Epileptic seizures and epilepsy: definitions proposed by the international league against epilepsy (*ILAE*) and the international bureau for epilepsy (*IBE*)," *Epilepsia*, vol. 46, no. 4, pp. 470–472, 2005.

[152] A. T. Berg, S. F. Berkovic, M. J. Brodie, J. Buchhalter, J. H. Cross, W. van Emde Boas, J. Engel, J. French, T. A. Glauser, G. W. Mathern *et al.*, "Revised terminology and concepts for organization of seizures and epilepsies: report of the *ILAE* commission on classification and terminology, 2005–2009," *Epilepsia*, vol. 51, no. 4, pp. 676–685, 2010.

[153] N. Foldvary, G. Klem, J. Hammel, W. Bingaman, I. Najm, and H. Lüders, "The localizing value of ictal *EEG* in focal epilepsy," *Neurology*, vol. 57, no. 11, pp. 2022–2028, 2001.

[154] I. I. Goncharova, D. J. McFarland, T. M. Vaughan, and J. R. Wolpaw, "*EMG* contamination of *EEG*: spectral and topographical characteristics," *Clinical neurophysiology*, vol. 114, no. 9, pp. 1580–1593, 2003.

[155] H. Nam, T.-G. Yim, S. K. Han, J.-B. Oh, and S. K. Lee, "Independent component analysis of ictal *EEG* in medial temporal lobe epilepsy," *Epilepsia*, vol. 43, no. 2, pp. 160–164, 2002.

[156] V. Vapnik, *The Nature of Statistical Learning Theory*. Springer, Berlin, Germany, 1995.

[157] "*LIBSVM* : a library for support vector machines," 2011. [Online]. Available: http://www.csie.ntu.edu.tw/~cjlin/libsvm

[158] G. Giannakakis, V. Sakkalis, M. Pediaditis, and M. Tsiknakis, "Methods for seizure detection and prediction: an overview," *Modern Electroencephalographic Assessment Techniques: Theory and Applications*, pp. 131–157, 2015.

[159] T. N. Alotaiby, S. A. Alshebeili, T. Alshawi, I. Ahmad, and F. E. A. El-Samie, "*EEG* seizure detection and prediction algorithms: a survey," *EURASIP Journal on Advances in Signal Processing*, vol. 2014, no. 1, p. 183, 2014.

List of Publications

Published Journals

- **A. K. Maddirala** and R. A. Shaik, "Removal of EOG Artifacts From Single Channel EEG Signals Using Combined Singular Spectrum Analysis and Adaptive Noise Canceler," in *IEEE Sensors Journal*, vol. 16, no. 23, pp. 8279-8287, Dec.1, 2016. doi: 10.1109/JSEN.2016.2560219
- **Ajay Kumar Maddirala** and Rafi Ahamed Shaik, "Motion artifact removal from single channel electroencephalogram signals using singular spectrum analysis", in *Biomedical Signal Processing and Control*, vol 30, September 2016, Pages 79-85, ISSN 1746-8094.

Manuscript Submitted

- **A. K. Maddirala** and R. A. Shaik, "Separation of Sources from Single Channel EEG Signals using Independent Component Analysis", *Minor revision submitted to IEEE Transactions on Instrumentation and Measurement.*
- **A. K. Maddirala** and R. A. Shaik, "Subspace based Muscle Artifact Removal Technique as Preprocessor in Seizure Detection Systems", *Major revision submitted to Biomedical Signal Processing and Control, Major revision.*

International Conferences

- **A. K. Maddirala** and and R. A. Shaik, "Removal of EMG artifacts from single channel EEG signal using singular spectrum analysis," *2015 IEEE International Circuits and Systems Symposium (ICSyS)*, Langkawi, Malaysia, 2015, pp. 111-115. doi: 10.1109/CircuitsAndSystems.2015.7394075
- **A. K. Maddirala** and R. A. Shaik, "Separation of artifacts from electroencephalogram signal using sequential singular spectrum analysis," *Signal Processing And*

Communication Engineering Systems (SPACES), 2015 International Conference, Guntur, India, 2015, pp. 384-388.